Using Computational Models to Assess the Functional Consequences of BDNF-Induced Excitatory and Inhibitory Synapse Formation

By

Domenico Fortunato Galati

B.S. Millersville University of Pennsylvania

A thesis submitted to the

Faculty of the Graduate School of the

University of Colorado in partial fulfillment

of the requirement for the degree of

Doctor of Philosophy

Department of Molecular, Cellular, and Developmental Biology

2013

This thesis entitled:

Using Computational Models to Assess the Functional Consequences of BDNF-Induced Excitatory and Inhibitory Synapse Formation

Written by Domenico Fortunato Galati

Has been approved for the Department of Molecular, Cellular, and Developmental Biology

_____

(Dr. Kevin Jones)

Date _____

_____

(Dr. Michael Klymkowsky)

Date _____

The final copy of this thesis has been examined by the signatories, and we find that both the content and the form meet acceptable presentation standards of scholarly work in the above mentioned discipline

Abstract

Domenico Fortunato Galati (Ph.D., Molecular, Cellular, and Developmental Biology)
Using Computational Models to Assess the Functional Consequences of BDNF-Induced Excitatory and Inhibitory Synapse Formation
Thesis directed by Associate Professor Kevin R. Jones

The action potential is fundamental to the transfer of information between neurons. The generation of an action potential is influenced by the spatial distribution of dendrites and synapses around the neuronal soma where the action potential is initiated. Brain-derived neurotrophic factor (BDNF) is a secreted molecule that influences synapse density and action potential generation. In this thesis, I test the hypothesis that elevated BDNF signaling increases the rate of action potential generation by promoting a spatial distribution of synapses that is more efficient at generating action potentials. I begin by developing an algorithmic approach for constraining computational models of action potential generation with actual distributions of excitatory and inhibitory synapses obtained with confocal microscopy of individual neurons. Next, I apply this algorithm to primary cortical neurons that have been stimulated with a single acute dose of BDNF. I determine that BDNF alters the spatial distribution of excitatory and inhibitory synapses and that the resulting distribution is more adept at converting barrages of synaptic activity into action potentials. Finally, I investigate the molecular mechanisms that mediate BDNF-induced excitatory synapse formation. I determine that the established BDNF target gene Arc is required for BDNF-induced excitatory synapse and dendrite formation. Further, I determine that LRRMT1 is a BDNF target gene that displays an additive interaction with BDNF during the process of excitatory synapse formation. Collectively, these data highlight previously undocumented mechanisms by which BDNF may shape cortical circuitry.

Dedication

This thesis is dedicated to my first scientific advisor, Dr. Narayan Avadhani, and the members of his laboratory in the Animal Biology Department at the University of Pennsylvania. The Avadhani lab provided me with my first opportunity to conduct biological research, and the lab provided unwavering support in my quest to obtain this Ph.D. Without their guidance, this thesis would not have been possible. Thank you.

Acknowledgements

As most graduate students are well-aware, the process of completing a doctoral dissertation requires a tremendous amount of intellectual and emotional support. Accordingly, I would like to acknowledge the supporting cast that made this work possible.

First, I would like to thank Prof. Kevin Jones for being my guide throughout this adventure. Even during the most trying times, of which there were many, Kevin has been an outstanding mentor who has instilled within me two traits that will guide each of my future professional endeavors. Kevin is patient, and as I move on to the next stage of my career, I strive to achieve that same level of patience in my day to day interactions. Kevin is the most rational thinker that I have ever met, and my ultimate professional goal is to be able to approach scientific problems with Kevin-like sensibility. As my inclination is towards haste and emotion, which often leads to scientific failure, I cannot thank Kevin enough for showing me how to conduct scientific research in a professional manner. In addition, thank you Kevin for stepping away from your role as a "Graduate Advisor" to be a person when I needed it most. I would also like to acknowledge all members of Kevin's lab, past and present, for providing many enlightening conversations.

I would like to thank the remaining members of my thesis committee, Prof. Michael Stowell, Prof. Harald Junge and Prof. Bill Betz, while specifically acknowledging two members, Prof. Michael Klymkowksy and Prof. Corrella Detweiler. Mike Klymkowsky's support has been invaluable throughout this process. Whether it be in his office chatting about my most recent mental breakdown or over a beer talking about the future of the scientific enterprise, Mike's commitment to my training as a scientist have been a cornerstone of my graduate career. I can say with absolute certainty that without Mike's support, I would have walked away from this Ph.D., so thank you and I look forward to many enlightening conversations about what those little cilia are doing up there. Corrie Detweiler was my mentor in establishing our seminar journal club series, which developed into one of the most rewarding

endeavors of my graduate career. In addition to her encouragement in setting up our journal club, Corrie has spent a considerable amount of time helping to plan my career going forward. Thank you both for your support. I hope to one day provide a similar level of mentoring to my future students.

I would like to thank two people who came into my life as graduate student colleagues, but who have become much more than that, Dr. Ryan Henry and Dr. Brian Hiester. Ryan Henry is the most precise scientist that I have ever met, and his attention detail will serve him well on his quest to revolutionize the pharmaceutical scientific enterprise. However, as our conversations turned from the absurdities of science to the future joys of raising a family, Ryan has become one of my closest friends. His scientific insights made me a better a scientist, but his friendship got me through graduate school. Brian Hiester is the most passionate scientist to come through Boulder during my time in the department, and his passion will carry him to great heights as he endeavors to train the next generation of scientists. However, it's not just Brian's scientific acumen that will serve him well in life. Brian is, hands down, one of the most loyal people I have ever met, and it is an honor to be within his inner circle. Boys…Thank you for your friendship, for your scientific discussions and for taking me to Harpo's to talk some sense into me.

I would like to thank Dr. Alison Vigers and Dr. Massimo Buvoli. Alison has been one of my biggest advocates throughout this process, and she has been a role model as a scientist, as a teacher and as a parent. Alison, thank you for picking up the phone to ask how I'm doing, for listening to my scientific ramblings and for using your beautiful home to host my celebrations. Massimo's friendship started out as a desperate plea to preserve my Italian heritage, but over the past six years his friendship has gone beyond the silly banter that takes place in a scientific lab after the PI's have gone home. Massimo has been a sounding board for many of my crazy ideas, and he has taught me that the greatest scientists do not always take themselves too seriously.

Finally, I would like thank my family. I would like to thank my mother, Linda, and my father, Fortunato, for ensuring that I received the education that they did not. They are the two bravest people that I have ever met, and I would never have completed this process without their support. I would like to thank my sister and her family. Gina, you are a true role model and one of my personal heroes in this world. Once again, this would not have happened without your support over the last thirty-two years. I would like to thank my great friend, Jeff Dahlgren. Jeff, it has been almost twenty years since we started playing hockey together, and I cannot thank you enough for all of your support throughout those twenty years. People like you come along once in a lifetime, and I am thankful that you are still here. And last but not least, I need to thank my wife Bridget. Bridget, thank you for all the dinners, all the laughs and all the friendship. You have been my rock throughout this process, and your investment in me has made all the difference in the world. Thank you and I look forward to our life together.

Table of Contents

List of Figures

Chapter 1. Background and Significance

1.1 Introduction

Computation within the cerebral cortex is based upon the flow of electrochemical information at synaptic inputs. The cortex contains billions of neurons, each of which receives thousands of inputs, and, therefore, the static computational power of the cortex is extraordinary. However, although it is convenient to think of the cortex as a machine with a fixed amount of computational power, that is hardly the case. This is because individual synaptic inputs, and the neurons that receive them, are in a constant state of flux with synapses being added, removed and modified over time. Therefore, two major thrusts of modern cellular neuroscience are: 1) to describe how individual neurons change over time and 2) to understand how these changes influence the generation of action potentials by individual neurons.

In this dissertation, I present my investigations describing how the neurotrophin brain-derived neurotrophic factor (BDNF) simultaneously alters action potential generation as well as the number of synaptic inputs. I propose that BDNF rapidly augments the population of excitatory inputs and inhibitory inputs, resulting in a synaptic configuration that is particularly adept at generating action potentials. In this first chapter, I will present a literature review that distinguishes excitatory synaptic inputs from inhibitory synaptic inputs and provides a general background on BDNF expression and function. In the second chapter, I will present a computational approach to predict how the location of excitatory and inhibitory synapses influences action potential generation. In the third chapter, I will present my conclusion that BDNF increases cortical neuron action potential generation by promoting a spatial distribution of excitatory and inhibitory synapses that has greater intrinsic excitability. In the fourth chapter, I will present evidence that activity-regulated cytoskeletal protein (Arc) and leucine-rich repeat transmembrane protein (LRRTM1) mediate BDNF's ability to augment excitatory synaptic inputs. In the

fifth and final chapter, I will critically discuss the significance of my work within the broad context of cellular neuroscience.

1.2 Overview: The Cellular Anatomy of the Cerebral Cortex

The Cortex Consists of Glia and Neurons

The mammalian cerebral cortex consists of two basic cell types, glia and neurons (Figure 1.1). Glia are not electrically excitable and they are the most numerous cells within the brain (Herculano-Houzel, 2011). Glia can be subdivided into three major classes: oligodendrocytes, astrocytes and microglia. Oligodendrocytes are responsible for bestowing axons with a myelin sheath that facilitates the conduction of electrical impulses (Simons and Lyons, 2013). Astrocytes are a structurally and functionally diverse class of cells that play an important role in modulating synapse function as well as facilitating the flow of nutrients away from cerebral blood vessels (Clarke and Barres, 2013; Rajkowska et al., 2013). Microglia, which are derived from the macrophage lineage, are the primary immune cells of the cortex, though they also participate in synapse elimination (Kettenmann et al., 2013). Although clearly important for aspects of central nervous system (CNS) function, this dissertation is focused on the location of synapses on individual neurons, and, thus, the potential contribution of non-neuronal cells will not be discussed further. If the reader is interested, I recommend the recent reviews mentioned above as a broad survey of glia's role in nervous system function.

The Basic Anatomy of a Cortical Projection Neuron

Cortical neurons are electrically excitable cells that can be divided into two major classes, projection neurons and interneurons (Figure 1.2) (DeFelipe, 2011). Projection neurons, also called principal neurons or pyramidal neurons, constitute the majority (~70-80%) of cortical neurons and they are defined by the course of their axons, which project distally to other areas of the cortex or to subcortical regions (Mérot et al., 2009). Interneurons represent a smaller subpopulation of cortical neurons that are defined by their axons, which project locally, typically contacting neighboring neurons

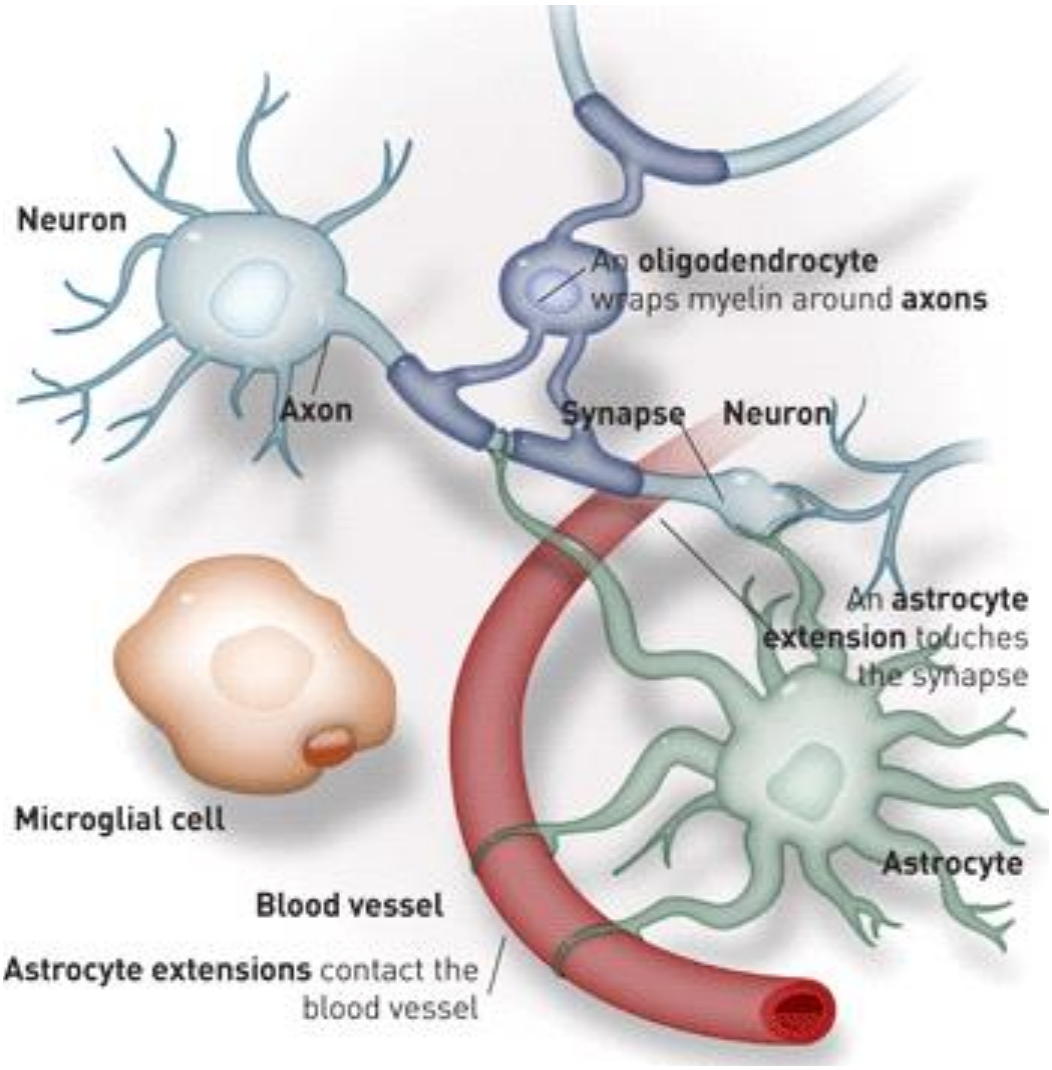

Figure 1.1 Schematic of the major cell types within the cortex. A simple neuron is depicted within a framework of non neuronal cells. Oligodendrocytes are depicted providing myelin sheaths. Astrocytes are depicted in close contact with blood vessels as well as unmyelinated portions of the axon. Microglial cells are depicted in their surveillance role. Reproduced from Clark and Barres, 2013 without permission.

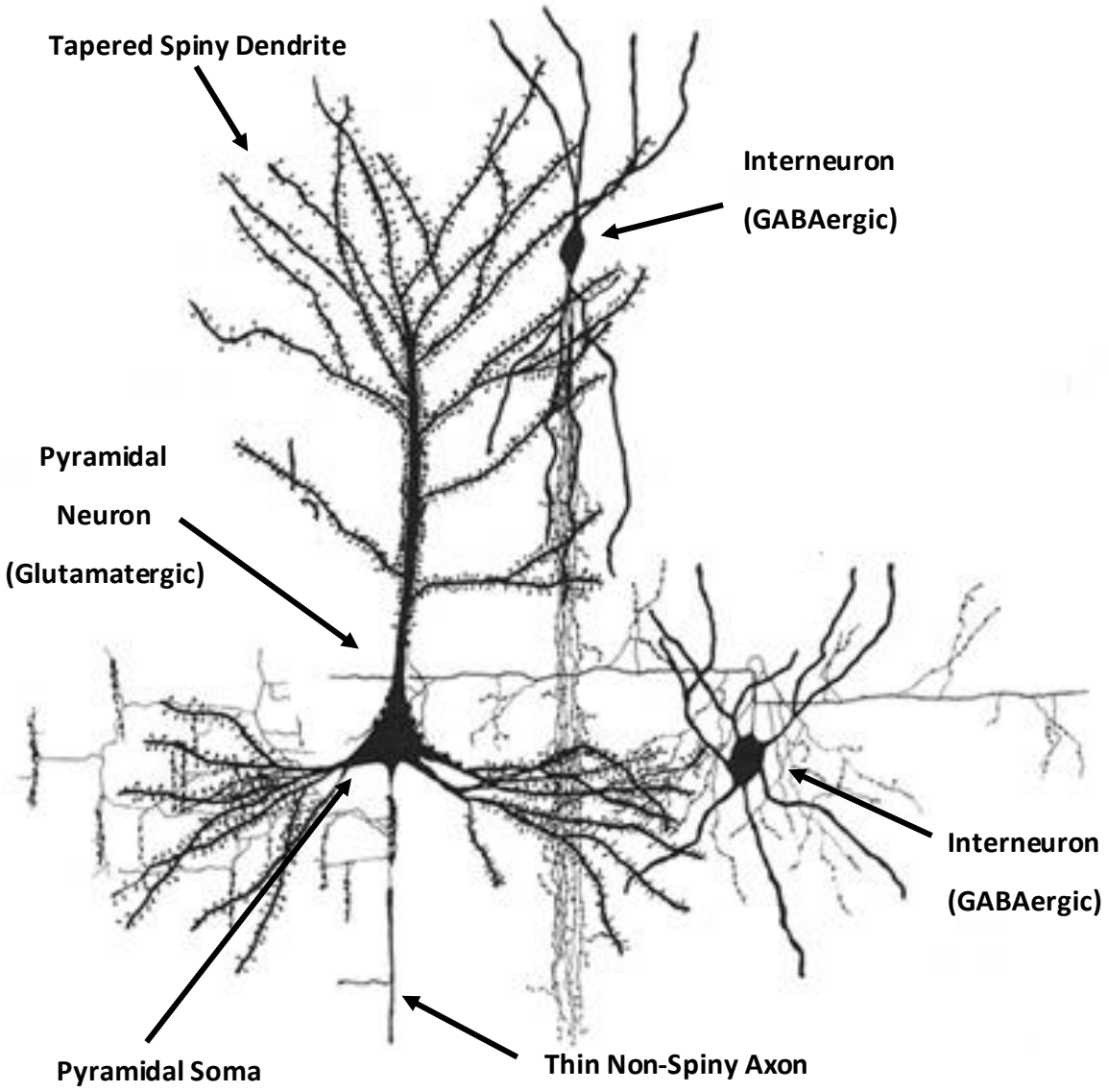

Figure 1.2. Schematic representing the general structural properties of cortical neurons. GABAergic interneurons generally display aspiny, smooth dendrites, radially symmetric dendritic arbors and axons that project locally. Glutamatergic pyramidal neurons display spiny dendrites that exhibit tapering, distinct apical and basal arbors and an axon that projects outside of the cortex. Reproduced from Defelipe, 2011 without permission.

(Markram et al., 2004). In addition to the ultimate destination of their axons, cortical neurons can be demarcated biochemically. Nearly all cortical projection neurons utilize the neurotransmitter glutamate and are excitatory neurons. In contrast, nearly all cortical interneurons utilize the neurotransmitter γ aminobutyric acid (GABA) and are inhibitory neurons. Therefore, pyramidal neurons lack the additional biosynthetic enzymes necessary to catalyze the conversion of glutamate into GABA (Le Magueresse and Monyer, 2013), although it should be noted that a sub-population of spiny interneurons, the spiny stellate cells (SSC), are excitatory (Feldmeyer et al., 2002). As they represent the majority of neuronal cells in the cultured cortical preparations used in this dissertation, I will now describe the basic cellular anatomy of the cortical pyramidal neuron. However, it will be important to remember that in primary cortical cultures inhibitory synapses onto pyramidal neurons arise from the axonal projections of inhibitory interneurons, while excitatory synapses onto pyramidal neurons arise from the axonal projections of other pyramidal neurons.

First described in fine anatomical detail by the great neuroanatomists Camilo Golgi and Santiago Ramon y Cajal (for review, see (DeFelipe, 2013), the cortical projection neuron is a multi-polar cell that is consists of three basic compartments: a single axon, a collection of dendrites and a cell soma (Figure 1.2). The axon is a smooth, tortuous and highly-branched structure that emanates from the cell soma and projects to other neurons. As the axon projects to its final destination, it forms specialized hemi-structures with other neurons, called pre-synapses (Simons and Lyons, 2013). The dendrites, collectively known as the dendritic arbor, are an assembly of highly branched structures that also emanate from the cell soma. However, in contrast to the axon, which is generally smooth and of a single diameter, dendrites are decorated with numerous protrusions, called dendritic spines, and the dendritic shaft displays a gradual taper as its distance from the cell soma increases (Jan and Jan, 2001). In addition, the dendritic shaft and dendritic spines harbor specialized clusters of receptors and scaffolding molecules, called post-synapses, that directly oppose the presynaptic structures of passing axons (Koleske, 2013).

Finally, between the axon and the dendrites, conceptually but not always physically, is a pyramidal-shaped cell soma that contains the nucleus and biosynthetic organelles (Purves et al., 2001). In addition to structural differences, neuronal compartments have functional differences, which will be discussed below with respect to the electrochemical synapse. Because the electrical synapse, or gap junction, will not be discussed in this dissertation, hereafter the electrochemical synapse will simply be referred to as the synapse.

Within cortical networks, the vast majority of fast (millisecond time scale) information transfer takes place at synapses. Although there is a tremendous amount of molecular diversity across individual synapses, each cortical synapse has a similar structural and functional footprint. Specifically, presynaptic terminals contain fusion-competent vesicles, which are filled with neurotransmitter, and a post-synaptic plasma membrane that contains neurotransmitter-gated ion channels (Harris and Weinberg, 2012). During the process of synaptic transmission, the axon undergoes a rapid and transient depolarization, which increases the conductance of voltage-gated calcium channels and thus elevates the cytoplasmic calcium concentration within the presynaptic terminal. Neurotransmitter vesicle fusion is calcium dependent. Therefore, depolarization of the presynaptic terminal causes the axon to release neurotransmitter into the synaptic cleft. Subsequently, neurotransmitter diffuses from its axonal source and some fraction activates post-synaptic neurotransmitter receptors. As neurotransmitter receptors are ion channels, the binding of neurotransmitter initiates a local change in the dendritic, or post-synaptic, membrane potential. It is through this remarkable process that the axon of one neuron transmits electrochemical information to another neuron (Alabi and Tsien, 2012).

1.3 Excitatory and Inhibitory Synapses: Composition and Function

In the mammalian cortex, the primary excitatory neurotransmitter is the amino acid glutamate, while the primary inhibitory neurotransmitter is GABA. The excitatory or inhibitory actions of a neurotransmitter result from the ionic conductance of post-synaptic receptors and are dependent on

neurotransmitter release from presynaptic terminals into the synaptic cleft (Attwell and Gibb, 2005; Belelli and Lambert, 2005). In the following section, I will compare basic structural and functional aspects of the post-synaptic and presynaptic machineries that are essential for excitatory and inhibitory synaptic transmission (Figure 1.3).

Fast post-synaptic transmission is mediated by ligand gated ion channels, termed ionotropic neurotransmitter receptors. Ionotropic glutamate receptors (iGluRs) are non-selective cation channels, which primarily conduct sodium and potassium currents and have an equilibrium potential close to 0 mV (Traynelis et al., 2010). Therefore, iGluR activation initiates an influx of sodium ions and an efflux of potassium ions that persists until the channel closes or the membrane potential reaches 0 mV causing an excitatory post-synaptic potential (EPSP). In general, ionotropic GABA receptors conduct chloride ions, which, in adult neurons, have a reversal potential close to resting potential (~-70 mV) and a high extracellular to low intracellular concentration gradient (Sigel and Steinmann, 2012). Therefore, GABA-mediated activation of ionotropic GABA receptors initiates an inward flux of chloride ions which hyperpolarizes, or inhibits the post-synaptic neuron causing an inhibitory post-synaptic potential (IPSP). Assuming a resting membrane potential of -70 mV, it should be noted that the hyperpolarizing effect of GABA receptor activation requires that the membrane potential be depolarized, as is the case when the neuron has recently received excitatory input. In addition to the ionotropic receptors, there are also slow, or metabotropic, glutamate (mGluRs) and GABA ($GABA_B$) receptors, which activate g-protein coupled receptors (reviewed in, (Gassmann and Bettler, 2012; Niswender and Conn, 2010)).

iGluRs are tetrameric assemblies of transmembrane proteins. The iGluRs are divided into three families depending on their subunit composition: AMPA receptors (GluA1-GluA4) (Anggono and Huganir, 2012), NMDA receptors (GluN1, GluN2A-GluN2D, GluN3A and GluN3B) (Paoletti et al., 2013) and kainate receptors (GluK1-GluK5) (Copits and Swanson, 2012). AMPA-type glutamate receptors primarily conduct fast cation currents (< 2 ms) (Traynelis et al., 2010), although heterodimers lacking GluA2 display

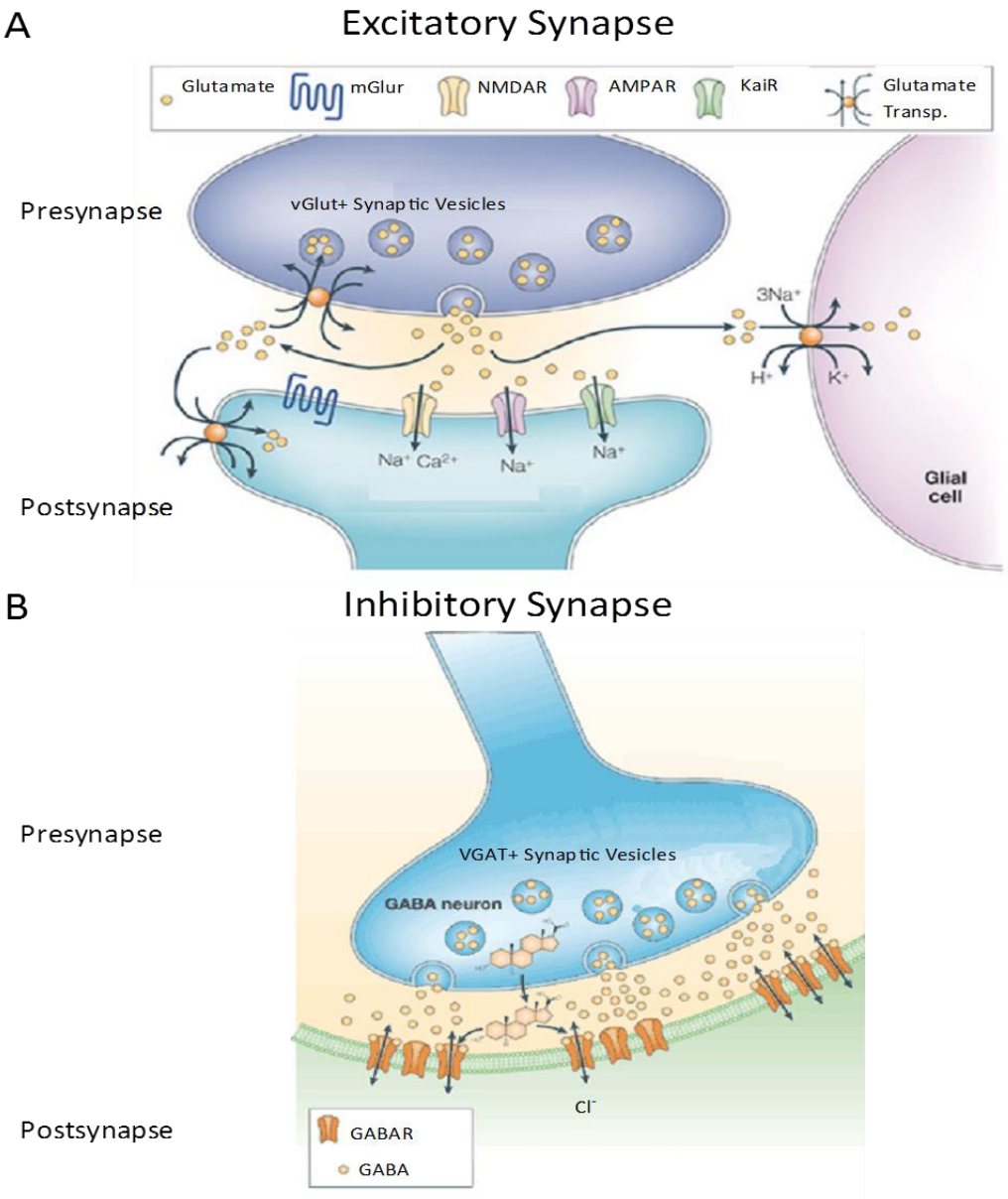

Figure 1.3 Schematic representing the general architecture of excitatory and inhibitory synapses. A) Excitatory synapses contain vGlut positive presynaptic vesicles filled with glutamate along with AMPA, NMDA and Kainate postsynaptic glutamate receptors. Adapted from Atwell and Gibb, 2005. B) Inhibitory synapses contain vGAT positive presynaptic vesicles filled with GABA along with $GABA_A$ postsynaptic receptors. The glial cell is pictured to represent the tripartite synapse, as many synapses are functionally associated with non-neuronal cells. Reproduced from Belelli and Lambert, 2005 without permission.

significant calcium conductance, which allows AMPA receptors to directly activate calcium-dependent second messenger signaling (Man, 2011). Similar to AMPA receptors, kainate receptors primarily conduct cation currents. However, whereas AMPA-mediated synaptic conductance is extremely rapid (~2 ms) and produces a relatively large depolarizing post-synaptic potential, kainate-mediated synaptic conductance is up to 50 fold slower (~100 ms) and has a much more modest depolarizing effect on the post-synaptic neuron (Contractor et al., 2011). NMDA-type glutamate receptors conduct sodium and calcium currents, although at resting membrane potential the pore conducting channel of NMDA receptors is sterically blocked by magnesium ions. The magnesium block is relieved by AMPA receptor mediated membrane depolarization. Therefore, a primary role of NMDA receptors may be to link AMPA-mediated synaptic activation to intracellular calcium signaling cascades (Paoletti et al., 2013). In addition to the core glutamate receptors, post-synaptic specializations also contain a dense collection of accessory proteins, which are collectively called the post-synaptic density (Butko et al., 2013). The primary components of the post-synaptic density include cytoplasmic scaffolding molecules (PSD-95, SAP97, etc.), growth factor receptors (TrkB, FGFR, IGFR, etc.), cell adhesion molecules (N-Cadherin, Neuroligins, and LRRTMs) and glutamate receptor regulatory proteins (TARPs, NETO, etc.). As each post-synaptic density component can modulate synaptic transmission to some extent and each synapse contains these molecules in distinct stoichiometries (Sheng and Hoogenraad, 2007), there is an almost unlimited repertoire of molecularly distinct post-synaptic specializations.

Ionotropic GABA receptors are tetrameric assemblies of transmembrane proteins that are commonly referred to as the $GABA_A$ receptors. In total there are 19 different GABA subunits encoded by 19 different genes (Sigel and Steinmann, 2012). Many of these subunits display overlapping expression within the brain, and reconstitution studies using recombinant receptor subunits expressed in *Xenopus* oocytes and/or mammalian tissue culture lines have documented that a wide array of hetero-oligomeric and homo-oligomeric assemblies conduct chloride current (Sigel and Steinmann, 2012). Therefore, the

mammalian nervous system has the potential to generate an enormous collection of unique functional $GABA_A$ receptors. Regardless of the subunit composition, upon binding GABA, $GABA_A$ receptors mediate a fast chloride conductance (~ 10-50 ms) (Banks and Pearce, 2000). Similar to excitatory synapses, $GABA_A$ receptors do not exist in isolation within the post-synaptic membrane. Notably, the post-synaptic density of inhibitory synapses contains the cytoplasmic scaffolding molecule gephyrin, the g-protein signaling regulatory molecule collybistin as well as the cell-adhesion molecule Neuroligin-2. Similar to excitatory synapses, inhibitory synapses can form a diverse repertoire of post-synaptic assemblies due to the numerous proteins present at the post-synaptic membrane (Fritschy et al., 2012).

While a clear delineation can be made between excitatory and inhibitory post-synapses, the presynaptic machineries that facilitate neurotransmitter release are quite similar. At the plasma membrane of a presynaptic specialization is the active zone, which serves as the primary site for synaptic vesicle fusion with the plasma membrane. The active zone is enriched with the evolutionarily conserved proteins RIM and RIM-BP and it contains vesicle fusion machinery, such as syntaxin and SNAP-25. However, rather than being specifically enriched at the plasma membrane of active zones, the ubiquitous fusion machinery is present throughout the neuronal plasma membrane and in other cell types (Südhof, 2012). There are also a number of highly-conserved proteins that decorate the surface of neurotransmitter vesicles, including VAMP/Synaptobrevin and synaptotagmin (Takamori et al., 2006). During the process of synaptic transmission, a concerted series of protein-protein interactions occurs between these factors. As an action potential depolarizes the presynaptic terminal, it opens voltage-gated calcium channels, which are anchored into the active zone via physical interactions with RIM and RIM-BP proteins. As calcium enters the presynaptic terminal, it binds to synaptotagmin and facilitates the physical interaction between the vesicular SNARE synaptobrevin and the plasma membrane SNAREs syntaxin and SNAP-25 resulting in a trans-snare complex, which primes the vesicle for plasma membrane fusion and eventual pore formation (Südhof, 2012). Upon pore formation, the neurotransmitter vesicle

releases its contents into the synaptic cleft, the trans-snare complex disassembles and the neurotransmitter vesicle returns to the reserve or recycling vesicle pool, where its neurotransmitter contents are restored (Rizzoli and Betz, 2005).

The mechanism of neurotransmitter release is nearly identical for every synapse. How then are excitatory presynaptic terminals distinct from inhibitory presynaptic terminals? Biochemically, they are differentiated by the cytoplasmic pool of neurotransmitter and the neurotransmitter transporters that pump neurotransmitter into synaptic vesicles. Excitatory presynaptic terminals contain glutamate-filled vesicles, which are loaded by a family of vesicular glutamate transporters (VGlut1-3). In the excitatory presynaptic terminal, high concentrations of cytoplasmic glutamate are achieved via a phosphate activated glutaminase which converts glutamine to glutamate (Takamori, 2006). Glutamate is then concentrated within presynaptic vesicles by the VGlut transporter which relies upon a strong vesicular membrane potential and a relatively low concentration of chloride ions (Omote et al., 2011). Inhibitory presynaptic terminals contain GABA-filled vesicles, which are loaded with GABA by a single vesicular GABA transporter (VGAT) (Chaudhry et al., 1998). In the inhibitory presynaptic terminal, GABA is synthesized by glutamic acid decarboxylase (GAD), which is a vesicular membrane associated enzyme. GABA is then concentrated within presynaptic vesicles by VGAT, which requires the activity of a vesicular ATPase and acts as a glycine/GABA/Cl^- co-transporter (Buddhala et al., 2009; Juge et al., 2009). The three VGlut transporters display differential expression within the rodent brain, with VGlut1 being the prominent glutamate transporter within the cortex, while rodents express only a single GABA transporter that is expressed in a variety of brain structures.

In addition to their unique pre and post-synaptic proteomes, excitatory and inhibitory synapses can be differentiated by their ultra-structural characteristics. Excitatory synapses are of the Type I, or asymmetric, variety. They are characterized by a presynaptic axonal bouton that contains a pool of spherical vesicles and a thin electron dense active zone. On the post-synaptic side, they are

characterized by a more prominent electron density, which is typically located at the tip of dendritic spine (Harris and Weinberg, 2012). Inhibitory synapses are of the Type II, or symmetric, variety. Similar to excitatory synapses, inhibitory synapses have an axonal bouton filled with individual vesicles. However, rather than being spherical, many of the vesicles have a flattened or compressed appearance. In addition, whereas the post-synaptic density is most prominent at excitatory synapses, the inhibitory pre and post-synaptic densities are roughly similar in size (Harris and Weinberg, 2012; Klemann and Roubos, 2011). These ultra-structural differences have been used in countless studies to differentiate excitatory from inhibitory synapses.

The ultimate function of the synapse is to provide a means for information transfer between two nerve cells. However, synaptic communication is not a binary process. In other words, the release of neurotransmitter from a presynaptic neuron does not necessarily elicit an action potential in the post-synaptic neuron. To fire an action potential, the post-synaptic neuron must receive tens to hundreds of individual excitatory inputs within a relatively short window of time because individual synaptic inputs do not produce sufficient depolarization to drive the neuron to its action potential threshold (Magee, 2000; Spruston, 2008). Therefore, the post-synaptic neuron sums the thousands of synaptic inputs throughout its dendritic arbor, but it only fires an action potential when it receives a sequence of synaptic inputs that is sufficient to drive the membrane potential of the axon initial segment beyond the action potential threshold. This concept will be explored in greater detail in Chapter 2.

1.4 An Introduction to BDNF Expression and Signaling

The neurotrophic hypothesis states that neurons compete for a limited supply of neurotrophin, and, ultimately, neurons that receive a sufficient quantity of neurotrophin survive and differentiate (Snider and Lichtman, 1996). This hypothesis was put forth to explain the observation that excessive synaptic connections between neurons and muscle cells are reduced and refined over time. In mammals, the neurotrophin family is highly conserved and consists of nerve growth factor (NGF), brain-

derived neurotrophic factor (BDNF) neurotrophin-3 (NT-3) and neurotrophin-4 (NT-4) (Park and Poo, 2013). Neurotrophins bind to one of three tropomyosin related kinase receptors (Trks). NGF binds to TrkA, BDNF and NT-4 bind to TrkB and NT-3 binds to TrkC (Huang and Reichardt, 2003). In addition, each neurotrophin binds to the low-affinity pan neurotrophin receptor, p75. The neurotrophins and their receptors display overlapping expression within the CNS. However, BDNF is the most abundantly expressed neurotrophin within the cortex (Maisonpierre et al., 1990), and an explosion of evidence in the past 2 decades has identified BDNF as a critical mediator of cortical neuron structure and function.

BDNF transcription is regulated by nine distinct promoters (I-IX) and two poly-adenylation sites allowing the BDNF locus to produce at least 18 potential transcripts (Pruunsild et al., 2007). However, as the BDNF coding region is contained entirely within a single exon, these transcripts vary solely in their 5' and 3' untranslated regions (UTRs) (Pruunsild et al., 2007). Of the promoters, the best studied has been promoter IV, which is regulated by neuronal activity. Specifically, promoter IV contains multiple CaRF and CREB binding elements (Hong et al., 2008; Lyons and West, 2011). Intracellular calcium and cAMP signaling are elevated when neurons fire action potentials. Thus, promoter IV couples BDNF transcription to strong neuronal stimulation (Greer and Greenberg, 2008). Beyond promoter IV, much less is understood about the neuronal conditions that activate the other promoters. However, UTRs can influence mRNA localization and mRNA translation, and it has been hypothesized that distinct 5' and 3' UTRs allow BDNF mRNA to localize to distinct locations within the cell depending on the nature of the stimulation that caused its production. This notion is supported by analysis of BDNF transcripts harboring distinct 3' UTRs. In this case, it appears that long 3' UTR transcripts specifically localize to and are translated within dendrites, while short 3' UTR transcripts are restricted to the soma (Orefice et al., 2013).

The BDNF coding region contains a single exon, and, thus, the BDNF protein that is translated from each BDNF mRNA is identical. Like other secreted proteins, BDNF is produced as a precursor

protein within the endoplasmic reticulum, where its signal sequence is cleaved to yield 32 kDa pro-BDNF (Carvalho et al., 2008). Pro-BDNF is then packaged into dense core vesicles allowing it to be secreted. Similar to BDNF transcription from promoter IV, BDNF secretion is enhanced by neural activity. Both high-frequency stimulation (>100 Hz) and theta-burst stimulation (TBS) increase BDNF secretion from presynaptic terminals, while evidence suggests that lower frequency stimulation (<10 Hz) increases BDNF secretion from dendrites (Balkowiec and Katz, 2002; Matsuda et al., 2009). Although BDNF mRNA has been localized to dendrites and tagged BDNF appears to be secreted from dendrites, a recent study utilizing in vivo hippocampal preparations has suggested that BDNF and its pro-peptide are localized exclusively to presynaptic terminals (Dieni et al., 2012; Tongiorgi, 2008). At some point during the secretory process, pro-BDNF is again cleaved, yielding the mature 14 kDa mature BDNF protein. However, the precise cellular location where pro-BDNF cleavage occurs is an intensely investigated topic and a clear consensus has not been reached. In primary culture studies, significant amounts of tagged pro-BDNF accumulated within the culture media, suggesting that pro-BDNF can be secreted without being cleaved (Yang et al., 2009). The secretion of pro-BDNF could play a significant role in shaping nervous system development, as pro-BDNF preferentially binds p75, which is a canonical death receptor (Dechant and Barde, 2002). My work utilizes recombinant mature BDNF, thus the possible role of pro-BDNF/p75 signaling will not be discussed further.

Mature BDNF is a low-abundance, positively charged growth-factor that functions as a homo-dimer (Lu et al., 2013) (Figure 1.4). Dimerized BDNF activates the canonical receptor tyrosine kinase, TrkB. BDNF binding causes TrkB homo-dimerization and subsequent tyrosine phosphorylation within TrkB's cytoplasmic tail (Huang and Reichardt, 2003). Upon activation, TrkB initiates common growth factor-induced intracellular signaling cascades, including the phospholipase Cγ (PLCγ) pathway, the mitogen activated protein kinase (MAPK) pathway and the phosphatidylinositol 3-kinase (PI3K) pathway. Activated PLCγ catalyzes the hydrolysis of phosphatidyl-inositol-4,5 bisphosphate into diacylglycerol

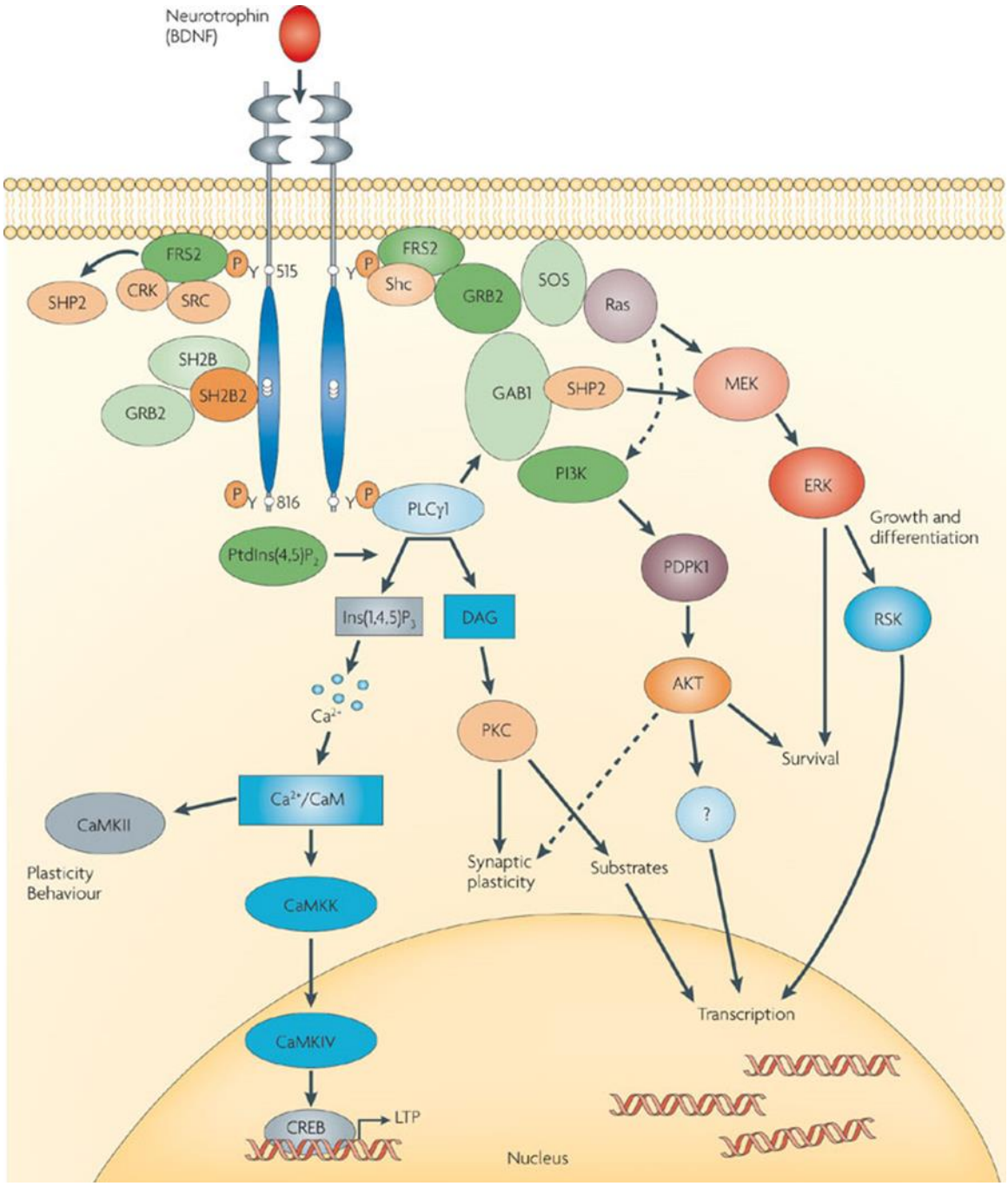

Figure 1.4. Schematic diagramming the intracellular consequences of BDNF/TrkB signaling. BDNF induces thedimerization and phosphorylation of TrkB receptors on their cytoplasmic tails. Phosphorylated TrkB initiates the PLCγ, PI3K/AKT and MEK/ERK intracellular signaling cascades. The activation of these signaling cascades has a wide range of overlapping cellular effects, ultimately, many of these effects are mediated by changes in gene expression within the nucleus. Reproduced from Park and Poo, 2013 without permission.

(DAG) and inositol triphosphate-1,4,5 (IP3). DAG activates protein kinase C, while IP3 activates the IP3 receptor within the endoplasmic reticulum, which elevates cytoplasmic calcium levels and influences calcium-mediated gene expression. TrkB phosphorylation also activates Ras signaling, which ultimately activates the MAPK pathway. Once activated, the MAPK pathway regulates transcription factors and the translational machinery, which allows BDNF to indirectly regulate the expression of many genes simultaneously. In addition to the MAPK pathway, Ras signaling also activates the phosphatidylinositol-3 kinase (PI3K) pathway which alters the lipid composition of the plasma membrane inner leaflet and ultimately results in the activation of Akt, which increases mTOR-dependent translation (Huang and Reichardt, 2003). Although it is convenient to separate TrkB signal transduction into distinct outcomes, it is becoming increasingly clear that there is significant convergence amongst each of the individual TrkB signaling cascades (Yoshii and Constantine-Paton, 2010). Therefore, teasing apart the contribution of individual TrkB signaling cascades to specific neuronal phenotypes is extremely challenging. In addition, TrkB undergoes alternative splicing which results in the production of a truncated protein (TrkB.T1) that lacks the cytoplasmic tail required for BDNF/TrkB signaling. By acting as a dominant-negative, TrkB.T1 is thought to negatively regulate BDNF/TrkB signaling by sequestering BDNF away from functional TrkB receptors (Fenner, 2012). However, TrkB.T1 also participate in intracellular signaling within CNS glia (Ohira, 2005). Since glia outnumber neurons within the CNS, TrkB.T1's role within glia may explain why TrkB.T1 displays higher expression than TrkB within the adult central nervous system.

Mature BDNF is positively charged at physiological pH and displays significant non-specific interactions with negatively charged components of the phospholipid bilayer and the extracellular matrix, which limits BDNF diffusion. BDNF is secreted from pre and/or post-synaptic sites, and limited BDNF diffusion is thought to restrict BDNF/TrkB signaling near the site of secretion. Accordingly, TrkB has been localized to the post-synaptic density and presynaptic axonal boutons of excitatory synapses within the cortex and the hippocampus, which would allow BDNF secreted at the synapse to initiate

TrkB signaling (Gomes et al., 2006; Huang et al., 2013). TrkB is associated with presynaptic structures throughout axon development, while post-synaptic TrkB appears to accumulate within post-synaptic structures as dendrites mature (Gomes et al., 2006), which suggests that BDNF could signal at the synapse throughout development. Similar to other growth factor/receptor signaling complexes, it appears that a fraction of BDNF/TrkB complexes are endocytosed and continue signaling at intracellular endosomes (Zhou et al., 2012). TrkB is not exclusively localized to excitatory synapses. Full-length TrkB has been localized to interneurons, oligodendrocytes, astrocytes and microglia, suggesting that BDNF/TrkB signaling may play an important role in a multitude of cells (Colombo et al., 2012; Ferrini and De Koninck, 2013; Liot et al., 2013; Wong et al., 2013). Although TrkB is produced by non-neuronal cells and interneurons, BDNF expression is largely restricted to excitatory neurons within the neocortex (Wetmore et al., 1994). Therefore, BDNF derived from pyramidal neurons initiates TrkB signaling in a wide range of cells, allowing BDNF to have a broad influence on CNS function.

1.5 BDNF Influences Cognition during Development and in Disease

BDNF signaling appears to be essential for learning and memory. In rodents, learning and memory can be tested using behavioral assays, such as contextual-conditioning and spatial learning. BDNF mRNA is up-regulated within the hippocampus of rodents during both contextual fear conditioning and the Morris water maze, suggesting that BDNF may be involved in hippocampal dependent learning (Hall et al., 2000; Mizuno et al., 2000). Conversely, mutant mice with a targeted disruption of the BDNF gene within the neocortex, display impaired contextual learning (Gorski et al., 2003a; Vigers et al., 2012). Long-term potentiation (LTP) is the process by which stimulation of synaptic connections at a specific frequency strengthens the connections such that subsequent stimulations elicit a stronger response. LTP is thought to be an electrophysiological correlate of learning memory (Minichiello, 2009). BDNF is required for LTP at hippocampal synapses, and BDNF application is sufficient to induce a form of LTP (BDNF-LTP) (Kang and Schuman, 1995; Korte et al., 1995; Messaoudi et al., 2007;

Patterson et al., 1996). Finally, a naturally occurring Val to Met polymorphism in the BDNF gene, which impairs BDNF secretion, is associated with reduced episodic memory, altered hippocampal activity and reduced hippocampal volume (Hariri et al., 2003; Pezawas et al., 2004). Collectively, these results suggest that the BDNF plays an important role in regulating learning and memory and its potential electrophysiological correlate, LTP.

BDNF signaling is disrupted in many human neurodegenerative and psychiatric disorders that are characterized by reduced CNS volume and impaired cognitive abilities, suggesting that BDNF may influence neurodegenerative processes (Lu et al., 2013; Nagahara and Tuszynski, 2011). The earliest insights into BNDF's role in neurodegeneration came from post-mortem studies that analyzed BDNF levels in diseased human brains. In Alzheimer's, Parkinson's, and Huntington's diseases, BDNF expression is reduced within degenerating areas of the brain, including the cortex, the hippocampus, the striatum and the substantia nigra (Connor et al., 1997; Mogi et al., 1999; Zuccato et al., 2001). BDNF also appears to be important in depressive psychiatric disorders as well (Autry and Monteggia, 2012). Depressed human patients have reduced hippocampal volume and reduced serum and hippocampal BDNF levels. In addition, polymorphisms within the human BDNF gene are associated with various mood disorders including bipolar and unipolar depression (Nagahara and Tuszynski, 2011). Schizophrenic patients have reduced prefrontal cortical volume, and post-mortem studies have identified reduced BDNF levels within the prefrontal cortex of patients who died while suffering from schizophrenia (Buckley et al., 2011). Therefore reduced BDNF levels and BDNF polymorphisms are correlated with negative outcomes in multiple human neurodegenerative and psychiatric illnesses.

Evidence from mouse models indicates that reduced BDNF expression may be a causative event that leads to neurodegeneration. Genetic deletion of BDNF results in perinatal lethality that is accompanied by brain and sensory neuron deficits (Jones et al., 1994). To circumvent the perinatal lethality, conditional BDNF mutants were created that lack the BDNF gene specifically within the

forebrain during early embryogenesis (Gorski et al., 2003b). These mice display impaired learning and memory as well as cortical compaction due to cortical neuron shrinkage, which is reminiscent of structural and functional deficits observed in Alzheimer's disease patients (Gorski et al., 2003a, 2003b). Huntington's disease causes neurodegeneration within the striatum, which is a brain region that receives the majority of its BDNF from anterograde projections emanating from the cortex. BDNF conditional mice display significant striatal degeneration that results from a reduction in medium spiny neuron numbers and dendritic complexity (Baquet et al., 2004). Interestingly, gene expression analysis of the brains from forebrain-restricted BDNF knockout mice indicates that the pattern of gene expression that results from BDNF deprivation is more similar to human Huntington's disease patients than disease-specific mouse models (Strand et al., 2007). Conditional mice in which BDNF was specifically deleted within the mid-hindbrain region display impaired motor coordination and dopaminergic cell loss that is reminiscent of human Parkinson's disease (Baquet et al., 2005). Finally, conditional deletion of BDNF within the forebrain of adult animals results in reduced brain size, dendritic spine loss and increased depressive-like behavior, suggesting that cortical neurons require BDNF for their maintenance (Vigers et al., 2012). Collectively, these results indicate that reduced BDNF expression within various brain regions is sufficient to induce neurodegenerative phenotypes that are similar to human neurodegeneration.

Clinical evidence supports the notion that restoring BDNF expression may have a therapeutic effect in many neurodegenerative disorders (Lu et al., 2013; Nagahara and Tuszynski, 2011). In rodent and primate models of Alzheimer's disease, viral delivery of BDNF enhanced cognitive ability and increased neocortical volume and synapse formation (Nagahara et al., 2009). In a primate model of Parkinson's disease, BDNF protein infusion reduced cell death and enhanced striatal innervation from the substantia nigra (Tsukahara et al., 1995). In rodent models of Huntington's disease, BDNF protein infusion improved motor ability and enhanced the survival of a population of neuropeptide producing

neurons (Canals et al., 2004). Finally, improvements of depressive symptoms can be brought about by antidepressant compounds as well as simple exercise. Interestingly, long-term and short-term treatment with antidepressant compounds, including selective serotonin reuptake inhibitors (SSRIs) and ketamine, along with voluntary exercise elevate hippocampal BDNF levels in rodents (Duman and Li, 2012; Waterhouse and Xu, 2013). Although BDNF appears to be a promising target for restorative therapies, it should also be noted that BDNF signaling may have a causative role in some neurological disorders as well. For example, excessive BDNF/TrkB signaling is thought to contribute to mossy fiber sprouting and general hyperexcitability within the hippocampus that leads to epileptic seizures (Liu et al., 2013).

BDNF is emerging as an important therapeutic target for a number of neurological disorders, and with the exception of epileptic seizures, the desired therapeutic outcome is an elevation of BDNF signaling. BDNF intervention is highly desirable in neurodegenerative disorders, which, increasingly, are being seen as disorders that result from an inability to maintain synapses (Marcello et al., 2012; Picconi et al., 2012). Accordingly, therapeutic BDNF infusion has been evaluated in 5 clinical trials (4 for ALS and 1 for diabetic neuropathy)(Lu et al., 2013). Although each of these trials ultimately failed, they were generally considered to be unsuccessful because of the difficulty in delivering the highly basic BDNF molecule to the correct location (Molina-Holgado et al., 2008). In fact, rather than abandoning direct BDNF infusion therapy, there is an increased interest in developing clever BDNF delivery vehicles, including osmotic pumps (Mantilla et al., 2013), hydrogels (Bertram et al., 2010), nanoparticles (Pilakka-Kanthikeel et al., 2013) and nasal sprays (Vaka et al., 2012). However, there is also intense interest in small molecule compounds that could augment endogenous BDNF/TrkB signaling, obviating the need for direct BDNF delivery (Lu et al., 2013). Regardless, direct BDNF infusion is currently being investigated as a disease modifying therapeutic to reverse synapse loss, and it is important to have a complete and mechanistic understanding of how direct BDNF application influences neuronal circuitry.

1.6 Summary and Aims of the Thesis

The goal of this introductory chapter was two-fold. First, I hope that I have provided sufficient information to allow the reader to appreciate the structural and functional distinctions between excitatory and inhibitory synapses and how synapses contribute to the flow of information between neurons. Second, I hope that I have presented adequate evidence to support the notion that BDNF plays a prominent role in shaping the structure and the function of the mammalian central nervous system, and that studying the neuronal response to BDNF stimulation is therapeutically relevant.

Throughout the remainder of this thesis, I will present my research documenting novel aspects of the relationship between BDNF, excitatory and inhibitory synapses, and action potential generation. In chapter 2, I will introduce the complex interactions that take place between excitatory and inhibitory synapses and how computational modeling provides a means to analyze these interactions. This will be followed by a novel method to computationally model the outcome of excitatory/inhibitory interactions based on morphological data. In chapter 3, I will introduce the reader to some of the known mechanisms that allow BDNF signaling to regulate action potential generation within the neocortex. This will be followed by my research documenting that BDNF simultaneously stimulates the addition of excitatory synapses, inhibitory synapses, and dendrites and that the resulting configuration of synaptic inputs is more efficient at generating action potentials. In chapter 4, I will introduce the reader to the process of synapse formation and examples of how BDNF-induced expression of synaptic proteins mediates BDNF-induced synapse formation. This will be followed by my research documenting that two specific BDNF target genes, activity-regulated cytoskeletal protein (Arc) and leucine-rich repeat transmembrane protein (LRRTM1), facilitate aspects of BDNF-induced synapse addition. Finally, in Chapter 5, I will integrate my findings into the scientific literature at large and present speculations that may invite future inquiry.

Chapter 2. Modeling Excitation and Inhibition in Individual Neurons

2.1 Introduction

Neuroscience is a multi-disciplinary field. In addition to biologists, our current understanding of circuits, neurons and synapses is indebted to physiologists, engineers, mathematicians, psychologists and philosophers, amongst many others. Although it is unnecessary to rank contributions according to their absolute importance, certainly two of the more influential offerings were the pioneering work of Hodgkin and Huxley and that of Wilifrid Rall. In the late 1940's and early 1950's using the squid giant axon as a model system, Hodgkin and Huxley identified the voltage-gated interplay between sodium and potassium ions that underlies the generation of the action potential (HODGKIN and HUXLEY, 1952). In the 1960's Rall established the cable theory of dendrite function in which he derived a set of differential equations that described how Hodgkin-Huxley conductance would behave in a leaky cable such as a dendrite (Rall, 1969). Together, these contributions laid the foundation for computational models that describe the non-linear summation of synaptic inputs. In this chapter, I provide a brief background on our current understanding of the non-linear interactions between synaptic inputs and how computational models can help us predict the functional consequences of these interactions. I will then describe an algorithmic approach to creating computational models of action potential generation based upon confocal images of neurons and their synaptic inputs.

2.2 Interactions between Excitatory and Inhibitory Synaptic Inputs Take Place within Dendrites

Excitatory and inhibitory synaptic inputs antagonize one another. Excitatory inputs depolarize the post-synaptic neuron and bring its membrane potential closer to the threshold for firing an action potential. Inhibitory synaptic inputs prevent the post-synaptic neuron from reaching the action potential threshold. Therefore, the transfer of information from a collection of presynaptic neurons through a post-synaptic neuron results from the summation of excitatory and inhibitory synaptic inputs within the post-synaptic neuron. However, this process of summation, also known as synaptic integration, is not

linear. In fact, the process is highly non-linear and it is influenced by the absolute proximity of the inputs from the physical site of action potential generation as well as the relative spatial and temporal proximity of the inputs from one another.

The dendritic arbor largely behaves as though it were a collection of leaky electrical cables (Meunier and Lamotte d'Incamps, 2008). Excitatory synaptic inputs transiently depolarize the post-synaptic membrane potential causing an EPSP. However, because the neuronal membrane is porous and the dendritic membrane displays capacitance, EPSPs are filtered, or attenuated, as they spread away from the site of generation (Gulledge et al., 2005). The primary consequences of filtering are that EPSPs exhibit a decreased amplitude and prolonged kinetic time course as they travel towards the site of integration (Magee, 2000). Attenuation is enhanced by basic aspects of cortical dendrite geometry. Pyramidal neuron dendrites are successively branched and they get thicker closer to the soma. Therefore, as a post-synaptic potential travels down a dendritic branch towards the soma, the membrane surface area expands causing further attenuation (Ferrante et al., 2013). Initially, dendritic filtering was examined using computational approaches that drew heavily from Rall's influential cable theory. However, as dual recording techniques were developed, experimentalists were able to directly determine the extent of dendritic filtering in different classes of neurons by simultaneously recording from the site of synaptic conductance as well as the neuronal soma (Magee and Cook, 2000; Williams, 2002).

Attenuation has been examined in multiple neuron types. In hippocampal CA1 pyramidal neurons, the effect of attenuation appears to be minimal because distal synapses are stronger than proximal synapses. Therefore, although distal EPSPs are filtered, the effect of filtering is minimized in part because distal synapses produce EPSPSs with larger amplitudes than proximal EPSPs (Magee and Cook, 2000). However, in layer V cortical neurons, although the amplitude of distal EPSPs was larger than proximal EPSPs, attenuation was marked with the most distal EPSPs attenuating up to 40 fold by

the time they reached the neuronal soma (Williams, 2002). It should be noted that although layer V neurons exhibited significant attenuation, distal synapses were still able to generate action potentials by initiating dendritic spikes, a process facilitated by the activation of non-synaptic ion channels (Smith et al., 2013; Williams, 2002). These observations suggest that filtering does indeed take place within the dendrites of pyramidal neurons, but the extent of filtering is largely dependent on neuron type. In addition, because pyramidal neuron dendrites are decorated with an assortment of voltage-gated ion channels, the active properties of dendrites may be able to counterbalance attenuation by initiating dendritic spikes or facilitating the backpropagation of action potentials (Segev and London, 2000; Waters et al., 2005). These studies provide experimental support for the notion that individual synaptic inputs are not equally efficient at generating somatic action potentials and that the location of a synapse can dictate how it is summed in the post-synaptic neuron.

EPSPs initiate local membrane depolarization within dendrites and to fire an action potential a post-synaptic neuron must sum multiple EPSPs within a sufficiently small temporal window. As discussed above, the somatic depolarization initiated by an EPSP is dependent upon the absolute distance of the input from the neuronal soma. However, summation is also influenced by the location of inputs relative to one another. The driving force for an excitatory synaptic input is the difference between the membrane potential (~-70 mV) and the equilibrium potential for a combined sodium/potassium cationic current (Häusser and Roth, 1997). However, while the reversal potential for sodium ions is a relatively constant 0 mV, the instantaneous membrane potential for a given patch of dendritic membrane can vary considerably. For example, if two neighboring synapses of identical strength (equal quantal size and post-synaptic receptor densities) fire in succession, the driving force for the first synaptic input will be greater than that of the second input. This is because the local membrane potential will be elevated closer to the reversal potential for sodium by the time the second synapse fires. Theoretically, the above scenario, where excitatory synaptic inputs are clustered in time and

space, results in sublinear summation of two EPSPs (Bush and Sejnowski, 1994). As mentioned above, dendrites contain an assortment of voltage-gated ion channels, which can facilitate supralinear summation. By activating nonsynaptic ion channels, two relatively weak excitatory inputs have the potential to initiate dendritic spikes, which amplify dendritic membrane depolarization and result in supralinear summation (Nettleton and Spain, 2000). Importantly, these theoretical interactions are beginning to be borne out experimentally. In cortical slice cultures, individual synapses on individual dendrites of layer V pyramidal neurons were sequentially activated by glutamate uncaging while recording from the soma. In these experiments, it was shown that simultaneous activation of multiple excitatory inputs on the same branch display a wide range of nonlinear interactions that depend on the order of activation as well as the distance of the inputs from the cell soma (Behabadi et al., 2012).

In addition to interactions between concurrent EPSPs, significant interactions also take place between EPSPs that arrive concurrent with IPSPs (Figure 2.1). The reversal potential of chloride is close to the resting potential of the dendritic membrane, so the activation of an inhibitory synapse causes a minimal change in membrane potential. In other words, whereas a typical AMPA-mediated EPSP on a thin distal dendrite can, in theory, cause a local depolarization on the order of 15 mV, a typical $GABA_A$-mediated IPSP on that same dendrite would cause no local change in membrane potential (Qian and Sejnowski, 1990). How then do inhibitory synapses inhibit the post-synaptic neuron? First, although inhibitory inputs may not hyperpolarize a resting neuronal membrane, they decrease the overall input resistance of the neuron by creating temporary pores in the membrane (Prescott and Koninck, 2003). Following Ohm's law, this temporary decrease in input resistance will reduce the magnitude of depolarization caused by simultaneous excitatory inputs in what is known as shunting inhibition (Koch et al., 1983; Mo et al., 2004). Second, if the membrane is already depolarized due to concurrent excitatory synaptic activity, the opening of $GABA_A$ chloride channels will have a hyperpolarizing effect that brings the membrane potential back towards its resting state. In this scenario, EPSPs that are on the same

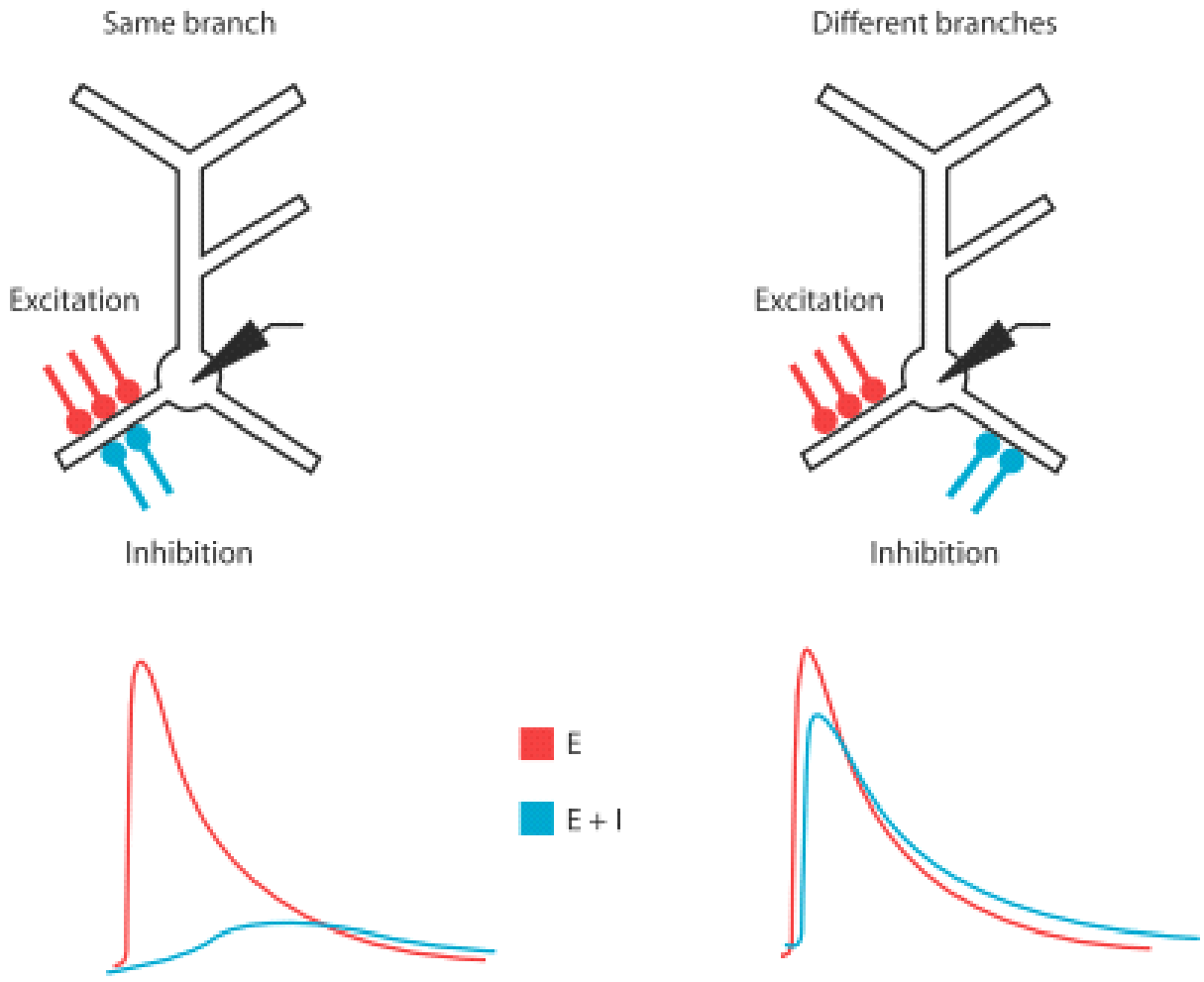

Figure 2.1. A diagram depicting the location dependent nature of interactions between excitatory and inhibitory synaptic inputs. Left) When excitatory synapses are activated in the absence of concurrent inhibitory synapse activation (red), the electrode within the soma records a strong depolarization. When excitatory synapses are activated with concurrent inhibitory synapse activation on the same branch (blue), the inhibitory synapses effectively veto the excitatory postsynaptic potential at the soma. Right) However, when excitatory synapses are activated with concurrent inhibitory synapse activation on different branches, the inhibitory synapses are less effective at blocking the excitatory postsynaptic potential. The ability of an inhibitory synapse to inhibit the neuron depends on its location relative to excitatory inputs. Reproduced from Mel and Schiller, 2004 without permission.

dendritic path can be vetoed by inhibitory synaptic inputs (Andersen, 1990). An elegant study utilizing precise iontophoretic application of glutamate and GABA to individual dendritic branches provided direct experimental support for localized interactions between excitatory and inhibitory inputs. In this study, activation of inhibitory synaptic inputs on the same branch as excitatory inputs reduced the magnitude of somatic EPSPs, while activation of inhibitory inputs on different branches had a much smaller impact on the magnitude of somatic EPSPs (Liu, 2004).

The ability of excitatory synaptic inputs to depolarize the somatic compartment is influenced by the location of other synaptic inputs as described above. In addition, the structure of the dendritic arbor itself impacts the summation of excitatory inputs as well (Brown et al., 2008; London and Häusser, 2005; Segev and London, 2000). Mathematical models have demonstrated that neurons with identical passive properties, but different dendrite geometries, produce distinct firing patterns in response to synaptic stimulation (van Elburg and van Ooyen, 2010; Mainen and Sejnowski, 1996). The ability of an individual synaptic input to drive a neuron past the action potential threshold is dependent upon the dendritic arbor morphology where the input resides (Behabadi et al., 2012; Komendantov and Ascoli, 2009). It has even been shown that subtle alterations in the fine structure of individual dendritic branch points may account for differences in neuronal output (Ferrante et al., 2013). Finally, in primate cortex, a recent study utilizing 3-D neuronal reconstructions, electrophysiology and mathematical modeling confirmed that dendrite morphology alone is predictive of some, but not all, aspects of cortical neuron output (Amatrudo et al., 2012).

The relative locations of excitatory and inhibitory synaptic inputs within the dendritic arbor can have a significant influence on the ability of an individual synaptic input to depolarize the somatic membrane. Therefore, it is not surprising that the balance of excitatory and inhibitory balances is tightly regulated. In the hippocampus, interneurons and CA1 pyramidal neurons displayed distinct spatial profiles with respect to the number and distribution of symmetric (excitatory) and asymmetric

(inhibitory) synapses, with the general trend being that the E/I ratio increases with increasing distance from the soma (Gulyás et al., 1999; Megías et al., 2001). In cultured hippocampal neurons, the balance between protein markers for E/I synapses (specific pre- and post-synaptic components) is similar on individual dendritic branches of the same neuron and the overall E/I ratio increased during development (Liu, 2004). In retinal ganglion cells, although the overall balance was coordinated throughout the majority of postnatal development, the distance-dependence of the E/I ratio was minimal (Bleckert et al., 2013; Johnson et al., 2003; Soto et al., 2011).

2.3 Compartmental Modeling: Testing Complex Interactions between Thousands of Inputs

The concepts discussed above provide a framework for thinking about how the relative location of a synapse can influence synaptic integration. However, a neuron can harbor thousands of individual synaptic inputs, which begs the question: How does one tease apart the functional consequences of these myriad interactions? Although iontophoretic application of neurotransmitter is becoming more accessible, the preferred method for studying complex interactions between more than a handful of synaptic inputs is the computational model. Currently, the majority of computational models utilize the compartmental approach, which reduces a neuron to a series of electrical circuits, or compartments (Brette et al., 2007). In this section, I provide a basic introduction to compartmental modeling before moving on to an algorithmic approach I developed to convert immunostained images of labeled neurons into compartmental models that produce action potentials.

Compartmental modeling is a computational method that reduces the complex electrophysiology of real neurons into a matrix of differential equations that describe neuronal processes in the terms of electrical circuits (Brette et al., 2007). Although the output of a computational model is a numerical solution, the process of creating a computational model is a subjective one that requires considerable judgment and revision (Bower, 1998; Carnevale and Hines, 2006). The creation of a computational model can be broken down into three stages: conceptualization, implementation and

simulation. During conceptualization, the modeler must determine the question to be addressed by the computational model and must devise a strategy to constrain the model with actual data. In this thesis, I am investigating whether the distribution of excitatory and inhibitory synapses that results from BDNF stimulation is sufficient to explain BDNF's ability to increase action potential generation. Once the model has been conceptualized, the next step is to implement the model as a series of mathematical relationships that use the actual data as variables. In this thesis, I have developed a novel image analysis algorithm that calculates the spatial relationship between synapses and dendrites and I have used these relationships to construct compartmental models using the NEURON simulator (Carnevale and Hines, 2006). Finally, after implementation, the model is simulated and the results are analyzed, and, if necessary, the model is refined. In this thesis, the results of my simulation will be presented in Chapter 3, while the approach used to create the simulation will be presented in this chapter.

Before the advent of simulation packages such as NEURON, computational modeling was restricted to those who could derive the necessary differential equations and create computer programs to solve them. However, with NEURON the differential equations necessary to perform compartmental modeling are built in to the simulator, and they are controlled via a graphical user interface or a simple scripting language (Carnevale and Hines, 2006). The fundamental unit of a compartmental model is a single combination circuit that describes the electrical properties of a small isopotential patch of membrane (Bower, 1998) (Figure 2.2). Although the actual number of components that compose the circuit depends on the constraints of the model, the most basic circuit has four components. There is a voltage source in parallel with a resistor to create the membrane potential and to represent the passive conductance of the membrane. There are one or more variable voltage sources in series with one or more resistors to represent the potential and the conductance of non-synaptic ion channels. There is a capacitor in parallel with the aforementioned voltage sources, which represents the capacity of the membrane to store a charge. Finally, the entire circuit is connected to adjacent circuits in series with a

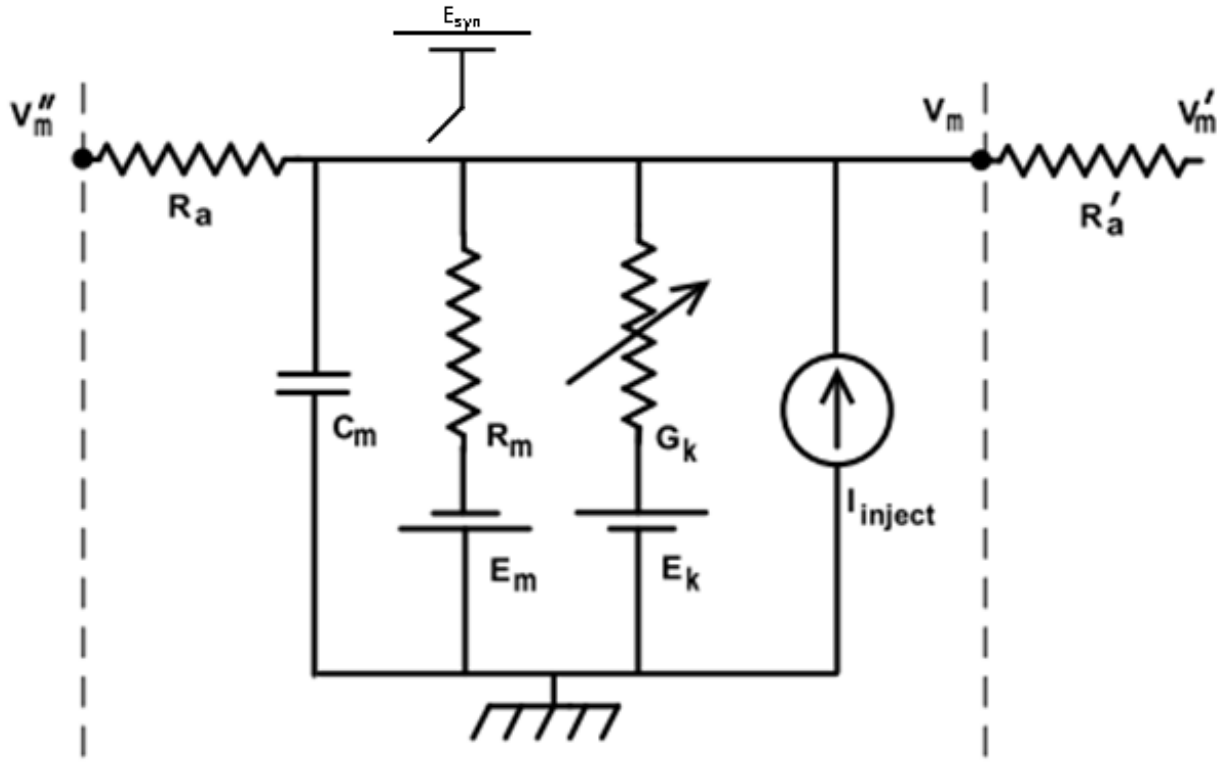

Figure 2.2. An electrical circuit representing a patch of neuronal membrane. V_m represents the membrane potential with respect to ground. C_m is a capacitor which represents the ability of the phospholipid bilayer to store a charge. E_m represents the ionic driving force that creates the membrane potential and it is connected in series with the resistor R_m which represents the fixed conductance of passive membrane channels. E_k in series with G_k represents the combined effect of variable conductance channels (voltage-gated, ligand-gated, etc) present within the neuronal membrane. E_{syn} represents the driving force for a synapse that is connected to the membrane via a switch. R_a and R_a' represent resistors that connect the circuit to adjacent circuits, which are designed to model the adjacent patches of membrane. At rest V_m is isopotential with V_m' and V_m''. V_m can become isopotential with V_m' and V_m'' by the discharging of the synaptic battery or via the variable conductance of E_k. Adapted from Bower, 1998 without permission.

resistor which represents the axial resistance created by the cytoplasm (Magee, 2000). At rest, each connected circuit is isopotential and there is no voltage difference across any of the circuits. However, neurons are decorated with synaptic inputs, and, therefore, an additional component can be added to the circuit and that is the synaptic battery. In compartmental modeling, synapses are integrated as voltage sources connected to the circuit via a switch that activates a conductance. When a depolarizing synaptic input is activated, the switch is closed, the battery discharges and positive charge (sodium cations) flows into the circuit via the synaptic conductance. When a hyperpolarizing synaptic input is activated, the switch is closed and the battery discharges and negative charge (chloride anions) flows into the circuit via the synaptic conductance. Therefore, synaptic batteries are the means by which an individual circuit can become anisopotential. When the circuit's potential is greater (it is depolarized) than that of its neighbors, current flows into the adjacent circuits. When the circuit's potential is less (it is hyperpolarized) than that of its neighbors, current flows from the adjacent circuits (Koch and Segev, 1989).

Interactions between excitatory and inhibitory synapses take place within dendrites. These interactions are non-linear, and assessing the functional consequences of the interactions between more than a few synapses on an individual neuron is technically challenging. Compartmental modeling provides a computational means to circumvent these inherent difficulties. However, compartmental models themselves are limited by the data that is used to constrain them. In the next section, I will present an algorithmic method that identifies synaptic features within confocal images of immunostained neurons and uses these features to constrain computational models that fire action potentials.

2.4 Results: Creating Compartmental Models from Morphological Data

Estimating the distribution of excitatory and inhibitory synapse distribution across large regions of individual neurons is a difficult endeavor (Bleckert et al., 2013) that has been overcome using a

number of approaches. Freund and colleagues used serial-section electron microscopy to characterize the location of symmetric and asymmetric synapses on individual neurons within the hippocampus (Gulyás et al., 1999; Megías et al., 2001). Wong and colleagues co-expressed fluorescently-tagged PSD-95 (excitatory) and $GABA_A$ receptors (inhibitory) to visualize excitatory and inhibitory post-synaptic sites, respectively, on individual retinal ganglion cells (Bleckert et al., 2013). Finally, Liu tracked glutamatergic and GABAergic presynaptic terminals by immunostaining for VGlut1 and GAD65, respectively, on individual neocortical neurons in culture (Liu, 2004). Furthermore, Liu provided direct electrophysiological evidence that the ratio of immunostained glutamatergic and GABAergic presynaptic terminals reflects the E/I synapse ratio. Thus, I used this approach to assess the E/I balance in rat cortical cultures, immunostaining for VGlut1 to detect excitatory presynaptic terminals and VGAT to detect GABAergic presynaptic terminals. It must be noted that the most rigorous method for detecting synapses with immunocytochemistry relies upon the colocalization of pre-synaptic components with post-synaptic components on individual neuritis. Therefore, my approach will undoubtedly falsely identify non-synaptic vesicular structures as bona fide pre-synaptic terminals.

To identify excitatory and inhibitory synapses within the dendritic arbors of individual neurons, I transfected primary cortical cultures with GFP and performed triple immunofluorescence against GFP, VGAT and VGlut1 (Figure 2.3; Raw Data). Primary cortical cultures contain a mixture of excitatory and inhibitory neurons. To distinguish between these two classes of neurons, I restricted my analysis to neurons that had a well-defined apical dendrite as well as dendritic spines. These morphological features are typically found on excitatory pyramidal neurons of the cortex. As cultures were grown at a fairly high density, each individual field of view contained a large number of VGlut1 and VGAT presynaptic terminals. Visual inspection of GFP labeled neurons revealed VGlut1 punctae present at the tips of dendritic spines and VGAT punctae on the cell soma. However, I also observed excitatory and inhibitory synapses on the dendritic shaft, which has been detected at the resolution of electron

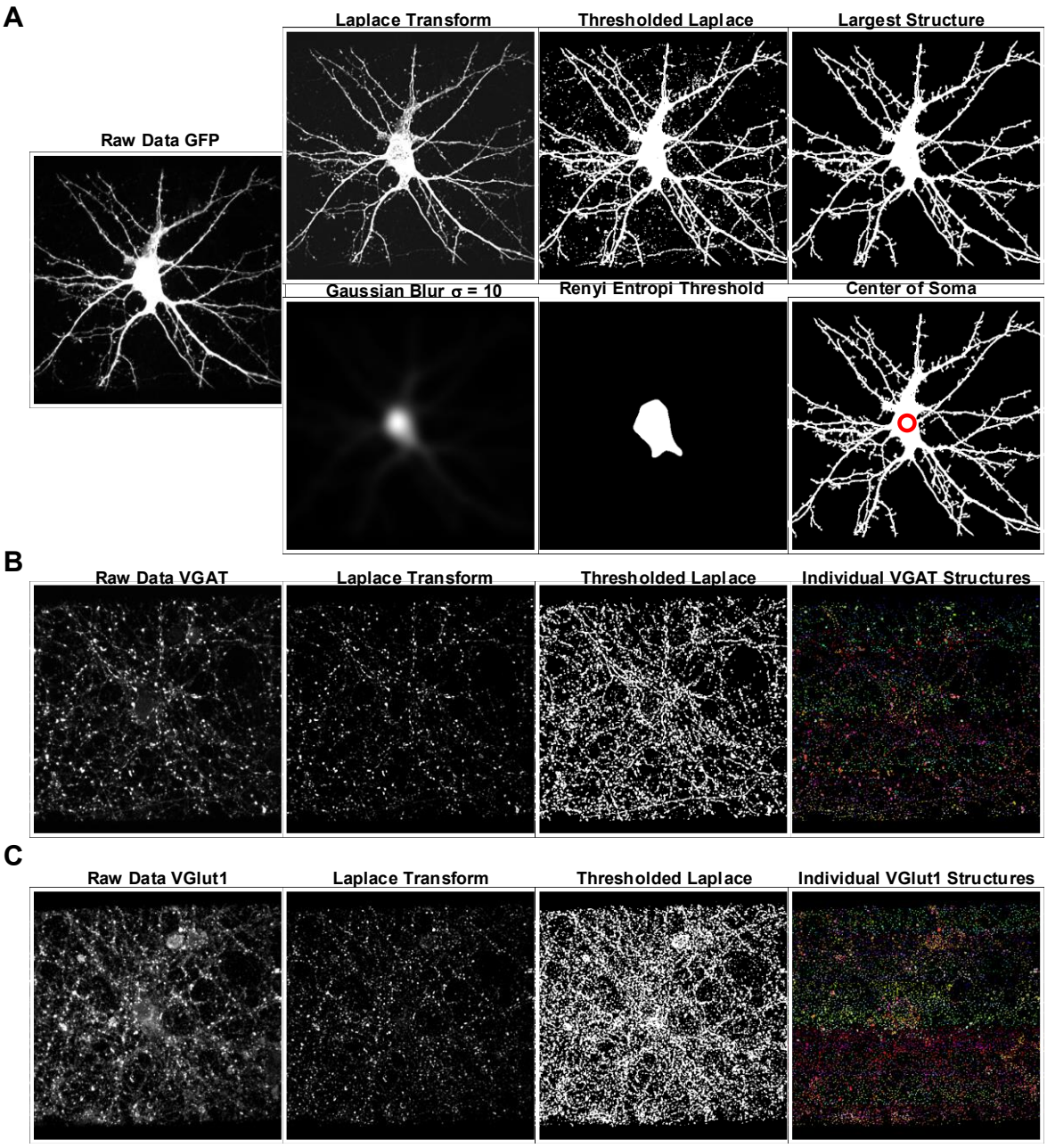

Figure 2.3. An overview of the image thresholding algorithms used to segment images. (A Top) The algorithm used to segment the GFP labeled neuron away from background signal. The raw data are convolved with a L.O.G. (left). The L.O.G. convolution is thresholded (middle) and the thresholded data are treated with a connectedness filter to remove all but the largest connected object. (A Bottom) The algorithm used to find the center of the cell soma. The raw data are convolved with a high-radius Gaussian filter (left). A Renyi entropy threshold is applied to the Gaussian image to identify the soma (middle). The centroid of the soma is calculated and used as the center of the neuronal soma (right). (B and C) The algorithm used to segment synaptic puncta. The raw data are convolved with a L.O.G. (left). The L.O.G. is thresholded (middle) and each individual feature is assigned a unique identifier (right). The right hand images utilizes a lookup table where each feature is shaded with a different color.

microscopy. In addition, each field of view displayed a high number of background presynaptic terminals that were presumably synapsing with untransfected neurons. As expected, presynaptic punctae displayed a wide range of distinct shapes and intensities. Collectively, this qualitative analysis of VGlut1 and VGAT distribution on individual GFP labeled neurons is consistent with many other reports of high density cortical cultures.

In order to reliably quantify synaptic puncta in high density cultures, the criteria used to score immunolabeled punctae must be objective and imposed reproducibly to avoid bias. To enable the quantification of large numbers of presynaptic punctae, I developed an automated image analysis procedure based upon previous work by (Ollion et al., 2013). The cornerstone of the analysis revolves around convolution with a Laplacian of Gaussian (L.O.G.) isotropic kernel to enhance the edges of presynaptic structures and dendrites. L.O.G. convolution approximates the second spatial derivative of an image, and thus converts areas with a strong intensity gradient (i.e. edges) into zero crossings (Figure 2.4). The primary benefit of utilizing L.O.G. convolution, rather than strict intensity thresholding, lies in the fact that L.O.G. convolution is relatively insensitive to the absolute intensity of the structure. Further, when the appropriate kernel size is used (typically, full-width at half-maximum for the structure of interest), L.O.G. convolution is also relatively insensitive to salt and pepper noise as well as the shape of the structure (Figure 2.4).

Primary cortical cultures are transfected with approximately 10% efficiency, which leads to isolated GFP-positive cells in a field of untransfected cells. Although individual neurons tend to be well isolated, individual fields of view can still be contaminated by significant GFP signal that is not continuous with the centered neuron. Therefore, to automate image analysis of an individual neuron it is essential to segment GFP signal continuous with the neuron of interest away from contaminating GFP signal. To accomplish this, I developed an algorithm that implements a low-radius L.O.G. convolution followed by a connectedness filter which segments continuous cluster of voxels that are connected by at

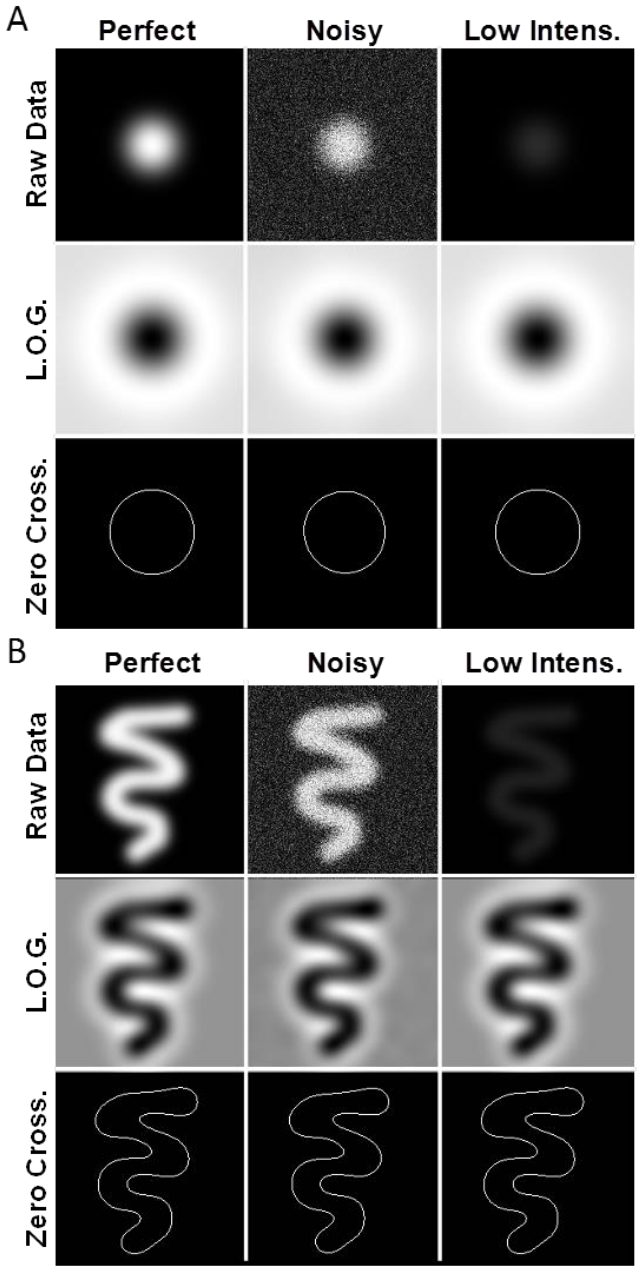

Figure 2.4. Laplacian of Gaussian (L.O.G.) convolution as an edge detector. A) L.O.G. convolution of a perfect puncta (left), a perfect puncta with extreme noise (middle), and a perfect puncta with low intensity (right). The top row is the raw data; the middle row is the L.O.G. convolution with a radius of full width at half maximum (FWHM); the bottom row are the zero crossings of the L.O.G. convolution. B) Identical to A) except the convolution was performed on a perfect curved-line. The L.O.G. convolution is insensitive to noise, low-intensity and the shape of the underlying feature.

least 1 voxel. Finally, I performed a size analysis on the segmented clusters and removed all but the largest cluster. The result is a binary confocal stack in which the largest continuous cluster of voxels represents the fine features of the neuron of interest (Figure 2.3; Top).

As described in the introduction, the location of synaptic inputs relative to one another and relative the cell soma influences how those inputs are integrated. Therefore, to accurately constrain computational models it is essential to identify the center of the soma and to use this point in 3-dimensional space to serve as the reference point for all other features (synapses and dendrites). To accomplish this, I developed an algorithm that can be used on grey level images of GFP -labeled neurons. To flatten the fine dendritic features and convert the broad cell soma into a smooth spheroid, the entire image is blurred with a high-radius Gaussian filter. To define the boundaries of the smooth spheroid, the blurred image is segmented with Renyi's entropy threshold, and the centroid of the resulting 3-dimensional polygon is calculated. Finally, a Euclidean distance transformation is applied to the single pixel centroid, which creates an image in which the intensity values of a given pixel represent the distance of that pixel from the center of the cell soma (Figure 2.3, Top and Figure 2.5).

The axonal boutons of cultured neocortical neurons have an average volume of 0.122 μm^3 +/- 0.106 μm^3 (S.D.), which is supraresolution with respect to light microscopy. However, the average synaptic vesicle has a volume of 0.0000228 μm^3, which is well below the limit of resolution with a light microscope (Schikorski and Stevens, 1997). With a 63X 1.4 N.A. objective, our confocal optics produce digital images with an X-Y pixel size of 0.24 μm and Z resolution of 0.5 μm, which results in a voxel volume of 0.03125 μm^3. Therefore, a collection of VGlut1 or VGAT vesicles localized to an axonal bouton and detected with immunofluorescence, would be expected to produce clusters of voxels with variable intensity that range in size from less than 1 voxel to 7.3 voxels. To identify clusters of voxels, I developed an algorithm that can be used on grey level images of synaptic puncta. To isolate presynaptic punctae, the image is convolved with a low radius L.O.G. kernel. The resulting image is further convolved with an

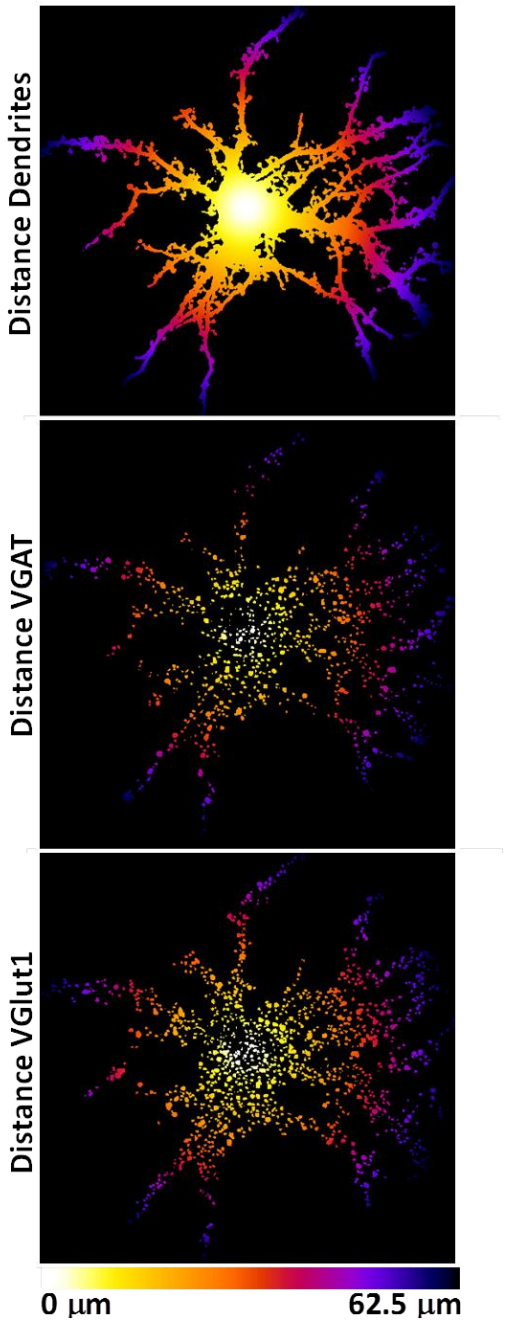

Figure 2.5. Euclidean distance transformation of neuronal features. A heat map representation documenting the relative distance of dendrties (top), VGAT punctae (middle) and VGlut1 punctae (bottom) from the center of the neuronal soma. The features were isolated using the approach outlined in Figure 8. Background VGAT and VGlut1 punctae were excluded using object-based colocalization with the GFP signal.

isotropic local maximum kernel to identify the peak intensity points for each individual presynaptic feature. Finally, the local maxima are used as seeds for seed-based region growing within the L.O.G. convolved image to cluster up to 5 continuous voxels. Seed-based region growing was required to separate closely apposed presynaptic clusters that were not separated with L.O.G. convolution alone (Figure 2.3; Middle and Bottom).

Having developed algorithms to segment each of the features within 3 channel images, next I developed a final algorithm that quantifies the distribution of each feature with respect to the center of the cell soma. The synaptic cleft is approximately 20 nm in width, which is well below the resolution of light microscopy, and, thus, presynaptic terminals should display partial colocalization with the post-synaptic neuron. To segment presynaptic terminals that synapse with the GFP-labeled neuron away from presynaptic terminals that synapse with unlabeled background neurons, the algorithm analyzes the GFP intensity (from the binary GFP image) within the volume of each of the presynaptic punctae. If the intensity is greater than 0, the puncta displays object-colocalization with the labeled neuron and it is retained, otherwise it is omitted. To map the location of presynaptic terminals, the algorithm analyzes the intensity of the Euclidean distance transform, which represents the distance from the neuronal soma. The output of the image analysis procedure is a map that describes the relative location of each dendritic and synaptic feature with respect to the center of the neuronal soma (Figure 2.5).

The goal of this research was to predict and understand how a given arrangement of dendrites and synapses influences action potential generation. Therefore, I devised a strategy for converting the features from the morphological maps into compartmental model topologies using the NEURON simulator (Figure 2.6). Dendrite topology was specified using a deterministic approach where individual Sholl crossings were directly converted into isopotential dendrite sections (Figure 2.6A). The diameter of the dendrite sections was calculated by dividing the total GFP volume between two consecutive Sholl radii by the number of sections within the Sholl radius and solving for the diameter of the resulting

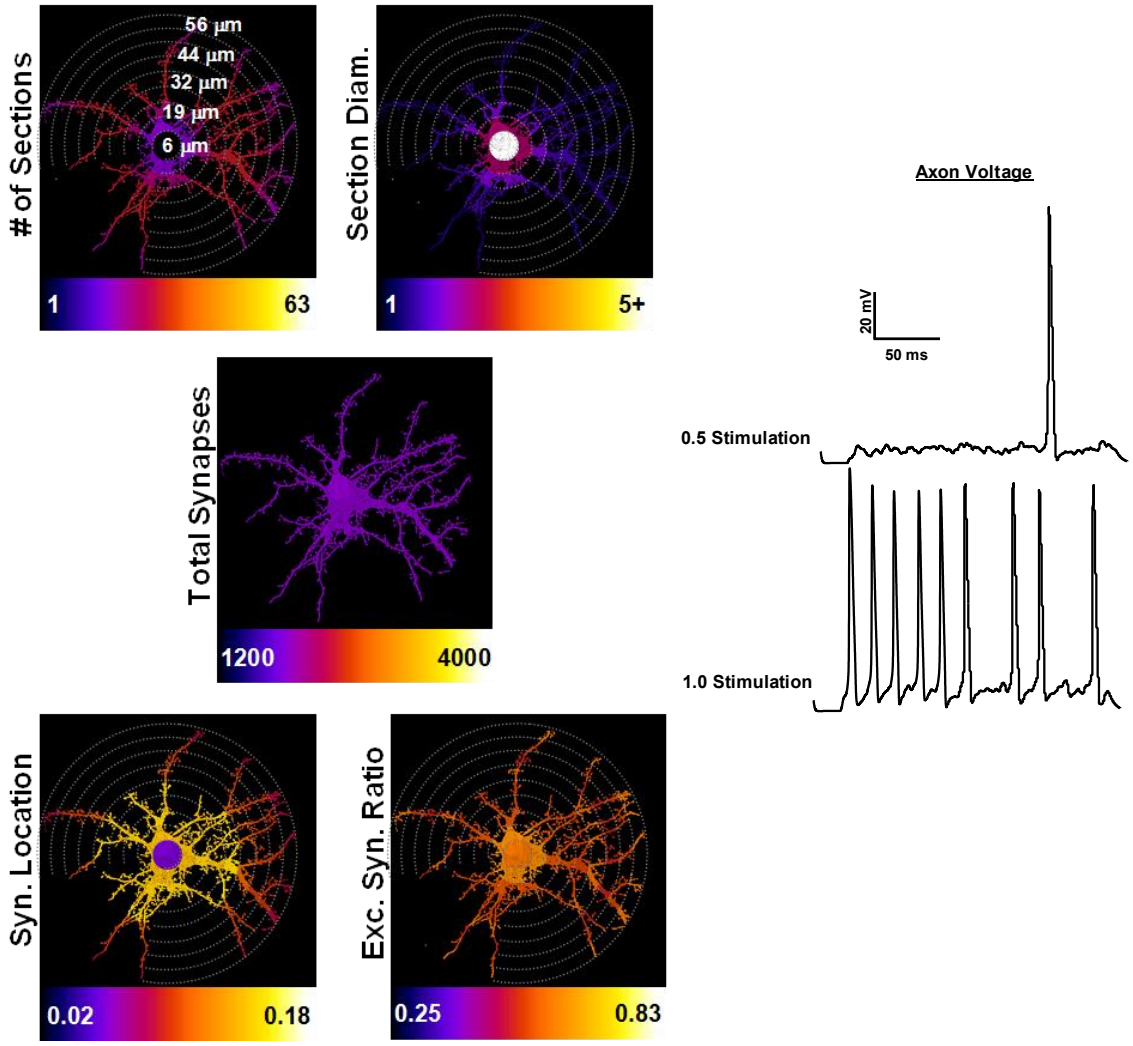

Figure 2.6. Creating a compartmental model constrained by morphological data. A graphical representation of the process used to constrain compartmental models. A) The number of Sholl crossings within each 6.25 µm bins are directly converted to individual dendrite sections 6.25 µm in length. B) The diameter of each section is calculated by dividing the total neuronal volume within a Sholl radius by the number of crossings within the Sholl radius and solving for the diameter of the resulting cylinder. C) The total number of synapses on the individual neuron. D) The probability of an active synapse being located within a particular Sholl radius. E) The probability of an active synapse having an excitatory reversal potential. The heat maps below each image represent the range parameters as determined for the data set described in Chapter 3. F) A representative model neuron firing action potentials in response to having 20% and 100% of its synapses stimulated in a stochastic fashion.

cylinder (Figure 2.6B). Synapse placement within the arbor was specified based on the number of synapses within a given Sholl radius divided by the total number of synapses on the neuron (Figure 2.6D). Individual synaptic reversal potentials (-70 mV for inhibitory or 0 mV for excitatory) were specified based upon the ratio of VGlut1/VGAT punctae within a given Sholl radius (Figure 2.6E). Finally, synaptic conductance was based upon the distribution of normalized puncta intensities, where 1 normalized A.F.U equals 1 nS of conductance.

Despite our best efforts, compartmental models are always under-constrained. Within the post-synaptic density of a single synapse alone there are hundreds to thousands of different proteins which can influence the function of that synapse. Therefore, an important aspect of compartmental modeling is to identify unconstrained parameters that may influence the modeled solution and to develop a strategy to incorporate them into the model. I identified five parameters that are especially likely to influence the outcome of the model, but for which I had no constraints. These parameters were the size of the apical arbor, the decay kinetics of excitatory and inhibitory synaptic conductance, the length of time in which synapses were activated (integration window), the membrane excitability of the dendritic arbor and the fraction of active synapses during a stimulation. I began by using reasonable baseline values for each of these parameters. I chose a simple 250 μm apical dendritic arbor, based on Sholl analysis of 14 DIV cortical cultures (Hiester et al., 2013); a matched synapse decay constant of 4 ms, which is roughly twice the typical AMPA-type excitatory synapse decay constant and half the typical fast component of $GABA_A$-type inhibitory synapse decay (Banks and Pearce, 2000; Roth); a 100 ms synaptic integration window based on the bursting behavior of high-density cortical cultures (Wagenaar et al., 2006); and I set dendritic Hodgkin Huxley channel conductance to 25% of the somatic value, based on the approach used in (Komendantov and Ascoli, 2009). Finally, to test the effect of stimulation strength, I devised a stimulation scheme where the fraction of active synapses was increased from 0.2 to 1 (in 0.2 increments). I then systematically varied each parameter value by 2 and 4 fold in both directions (except

for stimulation strength which was increased linearly) while keeping all other parameter values at baseline. Figure 2.6F documents that this model building approach yields a computational model that fires action potentials at a physiologically relevant rate and that the rate increases as the percentage of active synapses increases.

2.4 Conclusions

I have developed an algorithmic approach to quantify excitatory and inhibitory synapses as well as dendritic arbor morphology on individual GFP-labeled primary cortical neurons. Further, I have developed an approach to convert this morphological data into compartmental models using the NEURON simulation environment. I implemented L.O.G. convolution as a means to identify punctate and dendritic features within multi-channel images. Further, I used a combination of high-radius Gaussian convolution in conjunction with Renyi entropy thresholding to approximate the geometrical center of the neuronal soma. Finally, Euclidean distance transformation was used to map the distance of each synaptic and dendritic feature with respect to the center of the cell soma. The output of this image analysis procedure was then used to constrain a computational multi-compartmental model that fired action potentials at physiologically relevant rates. Further, I developed a way to systematically manipulate unconstrained parameters within the model, which allows for the robustness of the model to be assessed under a wide range of conditions. Collectively, this methodology represents a novel way to create realistic neuron models and to assess how a given distribution of excitatory and inhibitory synapses influence the generation of action potentials.

2.5 Detailed Methods

Primary Neuron Cultures

The entire cerebral cortex was isolated from postnatal day 0 (P0) Sprague-Dawley rats, which were anesthetized on wet ice prior to decapitation according to IACUC recommendations, dissociated and maintained in a 36.5^{o} Celsius, 5% CO2 and 75% humidity environment (Huettner and Baughman,

1986). Briefly, three cerebral cortices (both hemispheres) were pooled, chopped using a sterile scalpel and digested for 45 minutes in 200 Units of Papain. Tissue chunks were washed three times with DMEM containing 10% FBS, 100 U/mL penicillin and 100 U/ml streptomycin before being dissociated using a series of fire polished pipets. Following dissociation, the total number of Trypan Blue negative cells was estimated using a hemocytometer, and 215,000 viable cells were plated onto acid washed, Poly-D-Lysine coated (1 mg/ml in 0.15 mM Borate Buffer, pH 8.5) 12 mm glass coverslips in 24 well plates with a final media volume of 500 μl. Twenty-four hours after plating (day in vitro, DIV, 1), DMEM media was replaced with 500 μl Neurobasal-A culture media supplemented with 1X B-27, 1X Glutamax, 100 U/ml penicillin and 100 U/ml streptomycin. Seventy-two hours after plating (DIV 3), glial proliferation was inhibited with 1 mM AraC. While monitoring evaporation during preliminary experiments, we observed approximately 5% evaporation for every seven days of culture. Therefore, every seven days 25 μl of 18 Ω–Ohm Milli-Q water was added to the cultures.

DNA Transfection

Plasmid DNA transfections were performed using Lipofectamine 2000 according to the manufacturer's instructions. Briefly, 0.700 μg of plasmid DNA was mixed with 2.1 μl of Lipofectamine (3:1 Lipofectamine to DNA ratio) in 100 μl of supplement-free Neurobasal-A and incubated for 30 minutes at room temperature. During the 30 minute incubation, 250 μl of conditioned Neurobasal-A was removed from each 24 well and pooled with 250 ml of fresh supplemented Neurobasal A (1:1 Conditioned to Fresh). After the 30 minute incubation, 100 μl of the DNA/Lipofectamine mixture was added to each well and incubated for 2-4 hours at which point the transfection media was rapidly removed and replaced with 1:1 conditioned/fresh media. Transfections were performed 12-24 hours before the start of drug treatments (11-12 DIV).

Immunocytochemistry

Unless otherwise noted, all solutions were freshly prepared in 1X PBS, pH 7.4 and all steps were performed at room temperature. Cultures were fixed with 4% PFA for 15-20 minutes, and, immediately permeabilized with 0.1% Triton-X-100 for 10 minutes. Following permeabilization, cultures were blocked in a solution of 10% normal goat serum/0.2% Tween-20 for 1 hour and immunostained with a cocktail of primary antibodies diluted in 1% normal goat serum/0.2% Tween-20 (guinea pig anti-VGlut1, SySy,1:3000; rabbit anti-VGAT, SySy, 1:2000; chicken anti-GFP, Abcam, 1:2000) for 3 hours. Secondary antibody labeling was performed with a cocktail of fluorophore conjugated antibodies diluted in 1% normal goat serum/0.2% Tween-20 (goat anti-Guinea Pig-Alexa-647; goat anti-Rabbit-Alexa-555; goat anti-Chicken-Alexa-488) for 1 hour. After every incubation, cultures were rinsed three times with 1X PBS/0.2% Tween-20. Coverslips were mounted in Fluormount G and stored in the dark at 4 degrees until imaging.

Confocal Microscopy

Confocal microscopy of fixed cells was performed on a Leica spinning disk confocal microscope equipped with a 63X 1.4 N.A. objective and a 512x512 pixel EM-CCD camera (XY resolution: 0.25 μm/pixel; Z resolution: 0.5 μm/pixel). Alexa-488 was excited with a 488 nm laser. Alexa-555 was excited with a 568 nm laser. Alexa-647 was excited with a 647 nm laser. Image acquisition was controlled with MetaMorph software and acquisition parameters were optimized to produce limited pixel saturation (<0.5%) during preliminary experiments. Acquisition settings were kept constant throughout the remaining imaging sessions. In order to limit artifacts caused by time-dependent fluctuations in laser intensity, each imaging session was equally divided between coverslips for each experimental condition. Digital images were acquired as 16-bit TIFF files.

Digital Image Processing and Synapse Quantification

Image processing was performed using a series of custom ImageJ macros. The workflow consists of three sub-streams. The first sub-stream segments the GFP labeled neuron and creates a Euclidean

distance map of the neuron, the second sub-stream segments synaptic puncta, and the final sub-stream performs object based colocalization between the segmented GFP signal and the segmented puncta signals.

The largest continuous cluster of GFP voxels is identified. GFP stacks are convolved with a Laplacian of Gaussian (L.O.G.; smoothing radius of 1 voxel). The resulting 32-bit transform is duplicated and converted into a maximum Z projection and the mode and standard deviation pixel intensities for the projection are calculated. The 32-bit L.O.G. stack is then converted into a binary 8-bit image by setting the upper and lower threshold to the mode plus $1/10^{th}$ of the standard deviation. Continuous clusters of voxels in the 8-bit image are then segmented and the largest cluster (corresponding to the soma and all continuous dendrites) is retained, while all other clusters (corresponding to GFP signal not continuous with the most massive object) are discarded. For the purpose of dendrite length determination, a skeleton of the largest structure is created using the 3D skeletonization plugin. Sholl analysis is performed on the skeleton using the Sholl analysis plugin using a high-resolution Sholl radius of 6.25 μm.

The center of the soma is defined and a Euclidean distance map is created. Contrast within the original 16-bit image stack is saturated at 0.4% and converted to an 8-bit image. The saturated 8-bit image stack is then convolved with a heavy Gaussian (smoothing radius 10 pixels), to smooth away all but the largest features, and converted to a maximum Z projection. The projection is thresholded using the Renyi entropy function and the threshold values are applied to the saturated 8-bit image stack to create a binary 8-bit image of the largest features. The largest continuous cluster of voxels (the somato-dendritic region) is retained, while all other clusters are discarded. Finally, the center of mass for the remaining object is determined and used as the reference point for a Euclidean distance transform. By mapping feature coordinates back to the Euclidean distance map, each feature's distance from the center of the cell soma is determined.

Synaptic puncta are segmented. Puncta stacks are convolved with an L.O.G. (smoothing radius of 1 voxel) to sharpen puncta boundaries. The resulting 32-bit transforms are convolved with a Local Maximum filter (x and y radius of 2 pixels; z radius of 1 pixel (isotropic with respect to absolute size) and a new 8-bit image corresponding to single pixels at each local maxima is created. The local maxima are then used as "seeds" and the L.O.G. image is used as "spots" for seed based region growing (SRG). SRG is constrained so that only the 5 most intense voxels are clustered and an additional watershed algorithm is applied to prevent the merging of spots in close spatial proximity.

Object-based colocalization is performed on the segmented objects. Synaptic puncta are considered to be synapsing on the GFP labeled neuron if they contain at least one voxel overlap with the segmented GFP signal. Each feature (GFP, VGlut1 and VGAT) is then redirected to the Euclidean distance transform in order to determine its distance from the cell soma. In addition, intensity measurements are made by redirecting the VGlut1 and VGAT features to their original, unprocessed 16-bit images. For analysis purposes, the absolute distance of each feature is binned using the same 6.25 μm radius used for Sholl analysis. For intensity comparisons, all puncta intensities were normalized to the average puncta intensity for the vehicle treated neurons and are presented as fold change relative to vehicle.

Computer Simulations

Mathematical models were implemented with the NEURON simulation environment (version 7.3) on an Intel Core i7 workstation. Simplified, multi-compartmental model topologies were constructed for individual neurons (63 vehicle; 63 BDNF) based on their distanced-binned neuron volumes and their corresponding Sholl profiles. For a given Sholl radius (6.25 μm), the number of sections and the diameter of each section was as follows:

$$Crossings = Sections$$

$$Section_{Length} = 6.25\ \mu m$$

$$Section_{Diameter} = 2\sqrt{(\frac{V}{\pi 6.25})}$$

where V is the total volume of all voxels in that particular Sholl radius. The first Sholl radius was designated as the somatic compartment, the remaining Sholl radii were designated dendrites. Individual sections were connected in a manner that maximized their even distribution throughout the dendritic arbor. In addition, each model received an identical axon ($Length = 100\ \mu m$; $Diameter = 1\ \mu m$) and an identical apical dendrite whose electrotonic potential was varied in different simulations. The number of segments for each section was computed using the d-lambda rule (Hines and Carnevale, 1997), with d-lambda equal to 0.1. The passive biophysical parameters for the model were as follows: R_i=105 Ω cm, C_m = 1 μF cm^{-2}, gPas=0.001 S cm^{-2}, E_{Na}= 50 mV, E_K= -87 mV, E_{Leak}= -70 mV. In addition, Hodgkin-Huxley sodium and potassium conductances were inserted into the model as follows: axon (g_{Nabar} = 360 mS cm^{-2}, g_{Kbar} = 10.8 mS cm^{-2}), soma (g_{Nabar} = 120 mS cm^{-2}, g_{Kbar} = 3.6 mS cm^{-2}), dendrites (g_{Nabar} = 1.2 mS cm^{-2}, g_{Kbar} = 0.36 mS cm^{-2}). The integration time step for all simulations was 0.025 ms.

Synapses were modeled using the following paradigm. The kinetics for fast synaptic transmission were modeled as a point conductance with an instantaneous rise time (t=0.2 ms) and a slow decay that varied in different simulations. Excitatory synapses had a reversal potential of 0 mV, while inhibitory synapses had a reversal potential of -70 mV. The conductance for each synapse was chosen from the actual distribution of normalized fluorescent intensities for each population of cells, where 1 normalized arbitrary fluorescence unit (a.f.u.) = 1 nS of conductance. Synaptic conductance was capped at 4 nS as ~ 99% of the normalized a.f.u. values fell below 4. Stimulation intensities ranged from 0% to 100%, where the intensity corresponded to the percentage of total synapses that were active for a given neuron. For example, neuron A has 1800 synapses, so when it is stimulated at 50%, it will have 900 active synapses. The location of the active synapses was chosen according to a weighted distribution based on the actual location of synapses within the cell. For example, neuron A has 200 synapses in each of its 9 Sholl radii (1800 total), so for a given active synapse there is a 0.11 probability (200/1800) it will be located in a particular Sholl radius. The decision to model the synapse as excitatory

or inhibitory was based on the ratio of excitatory to inhibitory synapses for that given Sholl radius. For example, neuron A has a 1:1 excitatory to inhibitory ratio in Sholl radii 12.5 μm, so there is a 0.50 probability that a synapse in Sholl radii 12.5 μm will be excitatory. After choosing active synapses, each synapse was randomly activated within an integration window that varied between simulations and the resulting number of action potentials (axon voltage crosses 0 mV) during this window was recorded.

Chapter 3. Characterizing and Modeling BDNF's Influence on Synapse Distribution

3.1 Introduction

Location-dependent interactions between synaptic inputs influence the generation of action potentials. Therefore, in theory, two neurons with identical synapse densities can have dramatically different firing properties depending on the location of their synaptic inputs within the dendritic arbor. Alternatively, two neurons with different synapse densities can have similar firing patterns. In the previous chapter I developed a mathematical model of action potential generation that is constrained by the distribution of excitatory and inhibitory synaptic inputs on real neurons. In this chapter, I will use the aforementioned modeling scheme to test whether BDNF stimulation causes a spatial distribution of synaptic inputs that is more efficient at producing action potentials.

3.1 Known Mechanisms that Link BDNF Signaling to Increased Action Potential Generation

Substantial evidence indicates that BDNF influences the generation of action potentials. In dissociated hippocampal and cortical cultures, BDNF application increased the frequency of tetrodotoxin-sensitive EPSPs (Levine et al., 1995a; Taniguchi et al., 2000). Similarly, BDNF application increased the frequency of spontaneous EPSPs in slice cultures prepared from both visual cortex and hippocampus (Carmignoto et al., 1997; Scharfman, 1997). Hippocampal slices from BDNF knockout animals display reduced presynaptic fiber volley amplitude, which are multi-unit field potentials recorded from a collection of presynaptic axons where the amplitude indirectly reflects the number of action potentials being propagated within the axons (Patterson et al., 1996). Importantly, both recombinant BDNF and viral-mediated BDNF delivery were sufficient to rescue the synaptic deficits in BDNF knockout animals, indicating the deficits were not general developmental defects arising from BDNF deletion (Korte et al., 1996; Patterson et al., 1996). While acute elevation of BDNF signaling enhances the rate of spontaneous action potential generation in cultured neurons, the effects of chronic BDNF augmentation on excitatory neuron firing may be under homeostatic control (Turrigiano, 2011).

Specifically, by preferentially increasing the firing rate of inhibitory neurons, which dampens culture-wide activity, BDNF may act as a modulatory signal that facilitates the adaptation to an optimal culture-wide firing rate (Rutherford et al., 1997, 1998). However, chronic BDNF administration has resulted in sustained elevated firing in some laboratories, suggesting that homeostatic mechanisms are not always active (Bolton et al., 2000; Tyler and Pozzo-Miller, 2001). Therefore, unaccounted for differences in culture preparation may actually determine BNDF's ultimate functional consequences.

Numerous mechanisms have been proposed to explain BDNF's ability to increase action potential generation. The majority of these mechanisms invoke BDNF's ability to: enhance excitatory synapse strength, to increase the number of excitatory synapses and to increase intrinsic neuronal excitability. In hippocampal slice cultures, extracellular BDNF application caused a rapid and lasting enhancement in the strength of Schaffer collateral-CA1 synapses as measured via extracellular field recording (Kang and Schuman, 1995). Further, the increase in field EPSPs was insensitive to BDNF washout (both in the presence or absence of the TrkB inhibitors), suggesting that a single dose of BDNF induces a lasting modification of excitatory synapse strength (Kang and Schuman, 1995). Subsequent studies, which reproduced and extended this initial finding, have revealed both pre and post-synaptic mechanisms that can explain the increase in excitatory synapse strength. In hippocampal slice cultures, BDNF application increased the number of docked presynaptic vesicles at spinous excitatory synapses without altering the size of the active zone or the pool of reserve vesicles (Tyler and Pozzo-Miller, 2001). From the post-synaptic perspective, BDNF increases the abundance of synaptic AMPA receptors, NMDA receptors and scaffolding molecules, such as PSD-95 (Caldeira et al., 2007a, 2007b; Carvalho et al., 2008; Yoshii and Constantine-Paton, 2007, 2010). In addition, during spike timing dependent plasticity, BDNF is required for activity-induced spine head enlargement, which is a morphological correlate of increased excitatory synapse strength (Tanaka et al., 2008). These studies provide structural evidence that BDNF increases the abundance of excitatory synapse machinery, which is correlated with numerous functional

studies showing that BDNF increases the amplitude and the frequency of mEPSPs. Therefore, it seems likely that some fraction of BDNF's ability to increase spontaneous action potential generation is the result of its ability to strengthen excitatory synapses.

BDNF has a well-documented role in modulating the number of excitatory synapses. In organotypic slices from CA1 of the hippocampus, BDNF infusion increased the density of dendritic spines on the apical dendrites of pyramidal neurons as well as the number of asymmetric synapses as observed with electron microscopy (Amaral and Pozzo-Miller, 2007). BDNF infusion and/or overexpression has produced similar results on the density of excitatory synapses in other systems as well, including *Xenopus* optic tectum, dissociated cortical cultures and dissociated hippocampal cultures (Hiester et al., 2013; Lesiak et al., 2013; Sanchez et al., 2006; Taniguchi et al., 2006). Conversely, BDNF removal has a negative effect on excitatory synapse density. In the rodent striatum, conditional deletion of the BDNF gene from cortical afferents results in decreased dendritic spine density on striatal medium spiny neurons (Baquet et al., 2004). Similarly, conditional deletion of BDNF within the adult visual cortex leads to an eventual reduction in spine density (Vigers et al., 2012). Finally, mosaic analysis utilizing viral-mediated recombination revealed that BDNF is cell autonomously required for the maintenance of dendritic spines (English et al., 2012). Collectively, these results provide strong evidence that BDNF signaling regulates the number of excitatory synapses onto individual neurons.

Intrinsic excitability refers to the tendency of a neuron to a fire an action potential. For example, consider two neurons that have identical shapes and identical complements of synaptic inputs. Ignoring stochastic differences that result from the diffusion of ions and neurotransmitters, if these two neurons are subjected to the same pattern of stimulation they should produce identical trains of action potentials. However, in the same theoretical experiment, if one neuron responds by producing more action potentials, that neuron is said to have increased intrinsic excitability. Although numerous factors influence intrinsic excitability, including the distance of the axon initial segment (AIS) from the cell soma

and the capacitance of the neuronal membrane (Helmstaedter et al., 2009; Qu and Myhr, 2011), intrinsic excitability is strongly influenced by the collection of non-synaptic ion channels that contribute to neuronal membrane potential (Beck and Yaari, 2008). In CA1 hippocampal pyramidal neurons, BDNF stimulation activates a TRPC channel non-selective cationic current that leads to sustained membrane depolarization and increased spontaneous activity (Amaral and Pozzo-Miller, 2007). However, in dissociated cortical cultures, BDNF actually prevents increased intrinsic excitability that arises due to chronic activity blockade (Desai et al., 1999). Similarly, BDNF/TrkB signaling negatively regulates voltage gated sodium channels subunits via Fyn-mediated phosphorylation of the current conducting pore, which leads to accelerated fast inactivation and overall decreased sodium current (Ahn et al., 2007). In embryonic cortical neurons, BDNF had a similar negative effect on the conductance of high-voltage gated calcium channels, while in cultured cortical neurons chronic BDNF exposure had no effect on calcium channel currents (Bouron et al., 2006; Levine et al., 1995b). Therefore, BDNF is able to influence intrinsic neuronal excitability in either direction by causing differential effects on distinct ion channels.

3.2 Mechanisms that Could Allow BDNF to Negatively Regulate Action Potentials

BDNF clearly has the ability to increase action potential generation by increasing the number and strength of excitatory synapses as well as intrinsic excitability. However, as noted above, BDNF is also capable of negatively regulating activity via its effects on voltage gated sodium and calcium channels. In addition, BDNF has other well-documented effects that would be predicted to decrease neuronal activity, and these will be discussed below.

Similar to its effects on excitatory synapses, BDNF modulates the number and strength of inhibitory synapses. In dissociated hippocampal cultures bath BDNF application increased both the amplitude and frequency of mIPSCs, suggesting that BDNF increases both the quantal size of inhibitory synaptic transmission as well as the inhibitory release probability (Bolton et al., 2000). In agreement with these results, long term BDNF application has also been shown to increase the number of $GABA_A$

receptor clusters (Elmariah et al., 2004). In the visual cortex, BDNF heterozygous mice display reduced mIPSC frequency and amplitude (Abidin et al., 2008; Gottmann et al., 2009), while transgenic BDNF over-expression increases the density of GAD+ presynaptic terminals as well as mIPSC amplitude (Huang et al., 1999). However, it should also be noted that there is evidence that BDNF negatively regulates inhibitory synapses, particularly in the short term. In CA1, acute BDNF application reduced the amplitude and frequency of evoked and spontaneous IPSCs (Tanaka et al., 1997). In dissociated hippocampal cultures, BDNF initially reduced the number of $GABA_A$ receptor clusters and BDNF over-expression reduced the number of VGAT+ presynaptic terminals on the dendrites of BDNF null neurons (Elmariah et al., 2004; Singh et al., 2006). Therefore, BDNF has the ability to augment inhibitory synapses as well as excitatory synapses, though these effects may be time-dependent.

Some of BDNF's most well-documented effects relate to its ability to influence the shape of the dendritic arbor. In ferret visual cortex, BDNF infusion enhances apical and basal dendritic arbors of layer IV and layer V cortical pyramidal neurons (McAllister et al., 1995, 1996). Similarly BDNF overexpression from single neurons within ferret visual cortex enhances dendritic arborization in both an autocrine and paracrine manner (Horch and Katz, 2002; Wilson Horch et al., 1999). Conversely, genetic deletion of BDNF reduces the complexity of pyramidal neuron dendrites, while genetic deletion of BDNF from single cells reduces the number of primary dendrites in a cell autonomous fashion (English et al., 2012; Gorski et al., 2003b). Collectively, these studies, and many others (for review, see (Cohen-Cory et al., 2010)), have clearly defined a role for BDNF signaling as a positive regulator of the size and shape of the dendritic arbor. However, from an electrophysiological and modeling standpoint, expansion of the dendritic arbor actually serves to decrease action potential generation. This is because adding to the dendritic arbor increases the total surface area of the neuron, which, in turn, increases the overall capacitance. Ultimately, the addition of dendrites effectively reduces the ability of synaptic current to depolarize the axonal membrane as more of the current is utilized to charge the membrane capacitance

(Komendantov and Ascoli, 2009; Weaver and Wearne, 2008). However, it should also be noted that this effect could be counterbalanced by the addition of synaptic inputs on to newly formed dendrites. Overall, because of the relationship between dendrite surface area and membrane capacitance, BDNF's substantial effects on the dendritic arbor could severely limit BDNF's ability to increase spontaneous action potential generation.

Homeostatic adaptation presents an additional mechanism which may limit BDNF's impact on pyramidal neuron action potential generation. In neuronal circuits, intrinsic homeostatic mechanisms function to restrict the activity of a neural circuit within a specific range while maintaining the relative strength of individual synaptic inputs within the circuit (Turrigiano, 2008). These mechanisms were first discovered in cultured cortical neurons in which voltage-gated sodium channels were chronically blocked with tetrodotoxin (TTX), which prevents action potential firing but does not impact spontaneous miniature synaptic transmission (Turrigiano et al., 1998). In mature cultures that were grown in the presence of TTX for 48 hours, action potential firing ceased but the amplitude of mEPSCs recorded from pyramidal neurons but not interneurons increased, which was partially the result of post-synaptic mechanisms that increased the neuronal responsiveness to glutamate. When released from TTX blockade, cultures displayed dramatically elevated firing rates, which was correlated with a reduction in GABAergic drive that results from decreased activity-dependent BDNF signaling (Rutherford et al., 1997; Turrigiano et al., 1998). Further, it was shown that co-application of BDNF and TTX abolishes the increase in mEPSC amplitude onto pyramidal neurons, while exogenous application of BDNF alone increased mEPSC onto bipolar interneurons (a well-defined class of inhibitory neurons) (Desai et al., 1999; Rutherford et al., 1998). Collectively, these results suggest that BDNF may function as a signal that fine tunes the activity level of cortical circuits. When activity is low, and hence BDNF expression is low, the strength of excitatory inputs onto inhibitory neurons is reduced while the strength of excitatory inputs onto excitatory neurons is enhanced, which serves to elevate global firing. Conversely, when

activity is high, and hence BDNF expression is high, the strength of excitatory inputs onto inhibitory neurons is enhanced while the strength of excitatory inputs onto excitatory neurons is reduced, which serves to reduce global firing.

BDNF is a context-dependent signal that is capable of modulating both excitatory and inhibitory synapses. Further there is abundant evidence that BDNF's modulation of excitatory and inhibitory synapses contributes to BDNF's ability to regulate action potential generation. As discussed in Chapter 2, the location of excitatory and inhibitory synapses within the dendritic arbor influences synaptic integration and could therefore have a significant impact on action potential generation. In the next section, I provide a detailed characterization of the cumulative effects of elevated BDNF signaling on the distribution of excitatory and inhibitory synaptic inputs within the proximal dendritic arbor of cultured cortical neurons. In conjunction with the mathematical model described in Chapter 2, I then use these characterizations to test whether BDNF promotes a spatial distribution of excitatory and inhibitory synapses that has elevated intrinsic excitability.

3.2 Results: BDNF Enhances Action Potential Generation by Promoting a Favorable Distribution of Excitatory and Inhibitory Synapses

Although the effects of BDNF on cortical neuron morphology have been extensively studied, most studies have been performed using fixed tissue and less is known about the effects of BDNF on dendrite dynamics, particularly at low doses (Ji et al., 2010; McAllister et al., 1995, 1996; Wilson Horch et al., 1999). I determined whether a low dose of BDNF induces structural plasticity at dendrites in dissociated primary cortical neuron cultures using time-lapse microscopy. Individual GFP-transfected neurons were treated with vehicle (complete Neurobasal-A) or BDNF (5 ng/ml) and imaged every 2 hours for 10 hours (Figure 3.1A through 3.1D). Over the course of the experiment, both vehicle (Figure 3.1A and 3.1B) and BDNF-stimulated (Figure 3.1C and 3.1D) neurons displayed dynamic dendritic

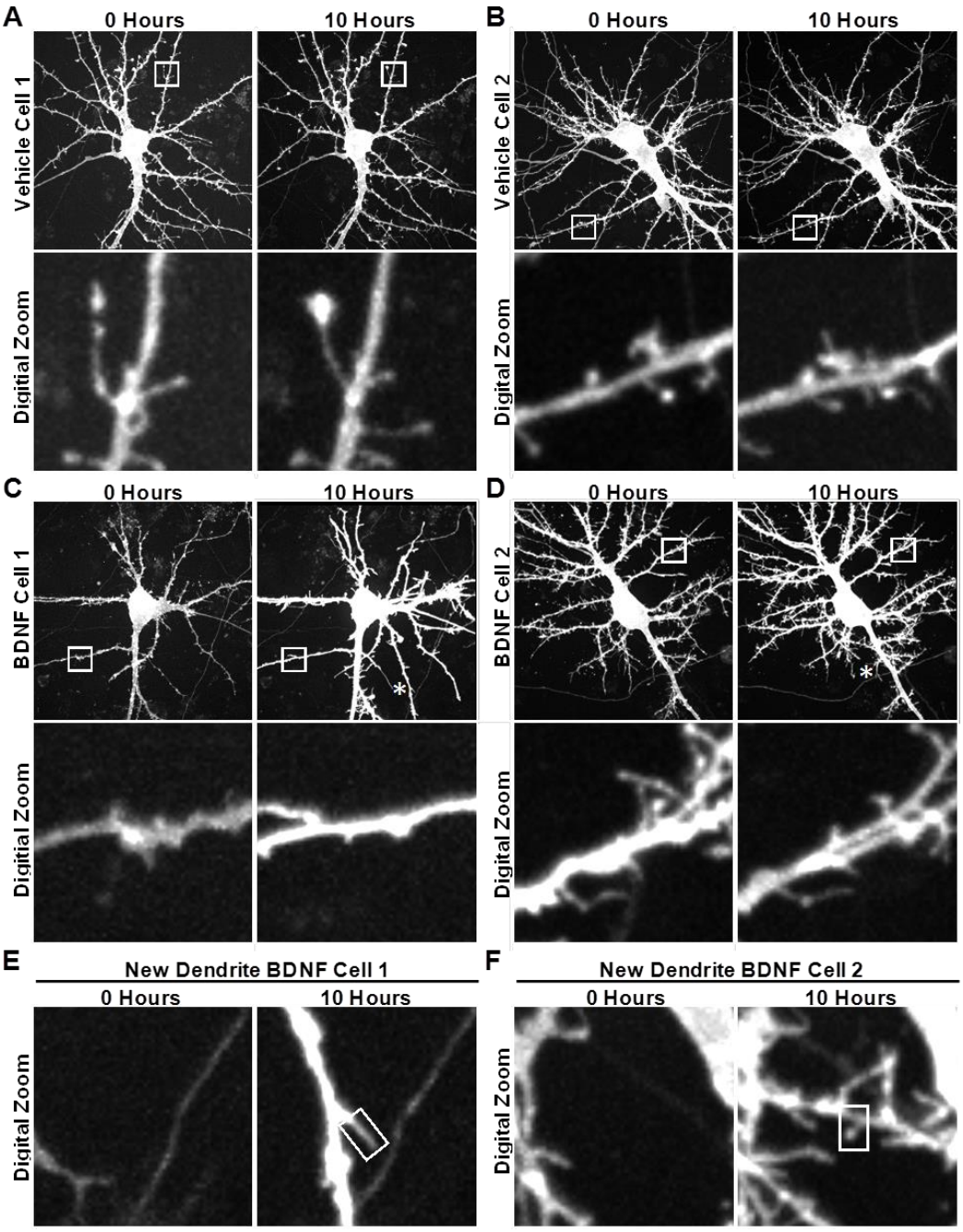

Figure 3.1. Visualizing BDNF-stimulated neurons with time-lapse microscopy. (A-D) Time lapse images (maximum intensity projections (MIPs)) of 12 DIV GFP transfected neurons treated with vehicle (A and B) or 5 ng/ml BDNF (C and D) and imaged every 2 hours. The MIPs are from the 0 hour and 10 hour time points. Upper panels are the entire field of view and lower panels are digitally enlarged (with bicubic interpolation) MIPs of the boxed region documenting dynamic behavior at filopodia. In C and D, the asterisk signifies the enlarged MIPs in E and F, respectively. (E and F) Digitally enlarged MIPs documenting the de novo emergence of "new" dendrites on BDNF-stimulated neurons. The boxed regions in the 10 hour MIPs highlight the presence of filopodia on "new" dendrites. The scale bar equals 5 μm in the zoomed-out images and 1 μm in the zoomed-in images.

filopodia. However, BDNF-stimulated neurons also exhibited *de novo* dendrite branch formation, something that was rarely seen with controls (Figure 3.1E and 3.1F). I quantified these observations by scoring each neuron based upon whether it added one or more dendritic branches (>7.5 μm) by the end of the imaging session. I determined that 89.7% (26/29) of the BDNF-treated neurons added at least one dendrite branch compared to only 17.9% (5/28) of vehicle treated neurons. In addition, while vehicle-treated neurons typically added no branches or only a single branch, the majority of BDNF-treated neurons added two or more branches. Interestingly, many BDNF-induced dendritic branches were decorated with filopodia (Figure 3.1E and 3.1F), and often these filopodia exhibited the thin neck and bulbous head characteristic of dendritic spines having presynaptic input (Figure 3.1F), suggesting that the nascent dendrite branches were undergoing excitatory synapse formation.

Having established that BDNF acutely induces dendrite and dendritic spine formation, next I determined whether these structural changes were associated with global changes in culture-wide activity. To accomplish this, I recorded the spontaneous network activity of cultures grown on two-dimensional multi-electrode arrays (Figure 3.2A (phase contrast)). I recorded from sister cultures (i.e., cultures plated from the same pool of dissociated cortex) over a 14 hour period in which the first 2 hours constituted a pre-treatment baseline. After the baseline, cultures were stimulated with vehicle or 5ng/ml BDNF and their activity was monitored after 2 hours and again after 12 hours. As previously reported (Wagenaar et al., 2006), individual cultures exhibited a range of activity patterns (Figure 3.2B1 and 3.2C1). However, while vehicle-stimulated cultures displayed a non-significant 5% increase in activity after 2 hours and a significant 32% increase in total spontaneous activity after 12 hours (Figures 3.2B and 3.2D), BDNF stimulation led to a 102% increase by 2 hours and a 534% increase by 12 hours (Figures 3.2C and 3.2D). These results indicate that a single low dose of 5ng/ml BDNF increases spontaneous network activity, and in conjunction with the time lapse imaging data, that this increase correlates with the formation of new dendrites and dendritic spines.

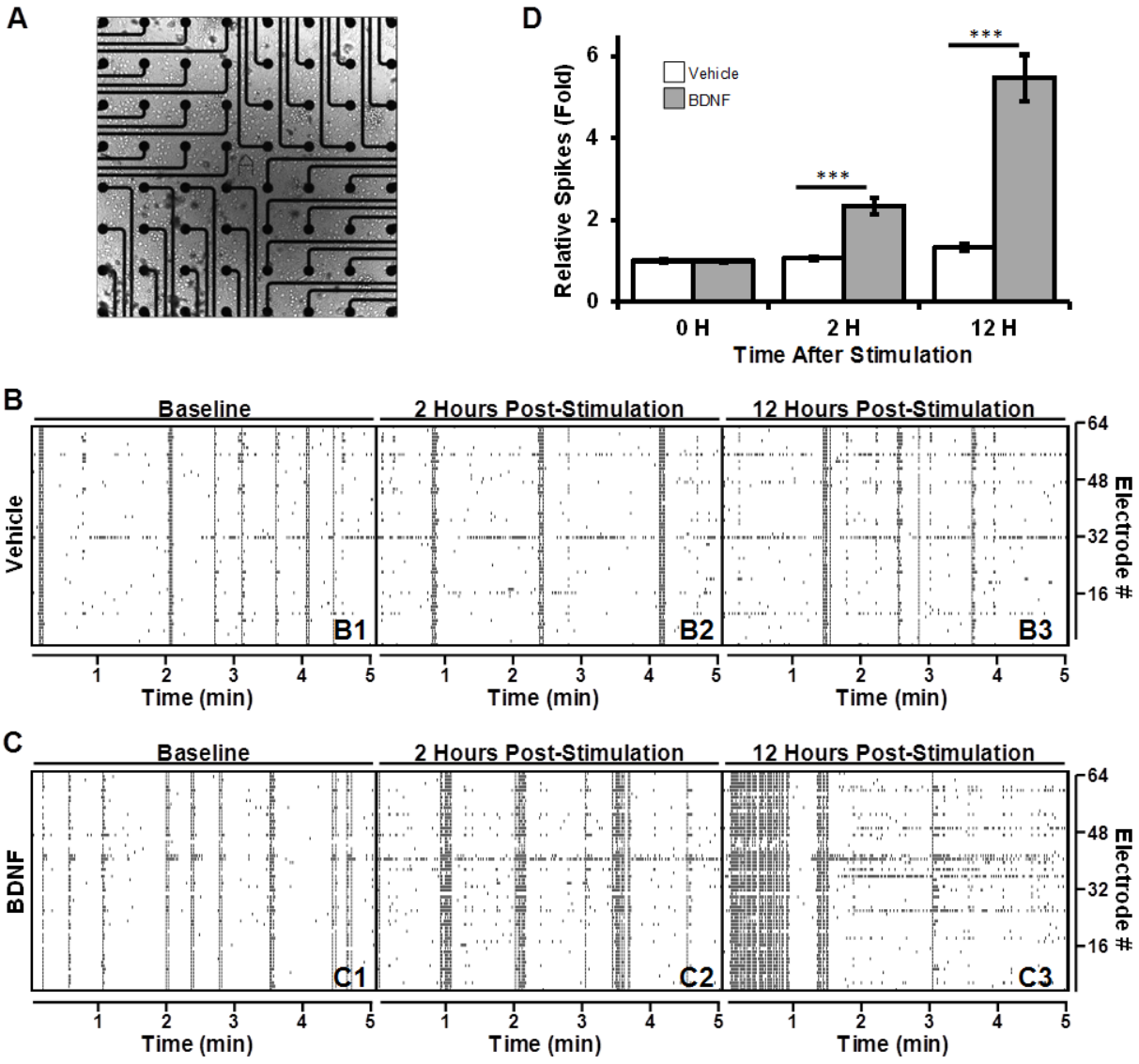

Figure 3.2. Assessing culture-wide activity patterns with multi-electrode arrays. (A) A bright-filed image of a representative culture at 14 DIV plated on a multi-electrode array. Scale bar equals 200 μm. (B and C) Raster plots from vehicle-stimulated (B) and BDNF-stimulated (C) sister cultures. Black tick marks indicate supra-threshold activity at a given electrode. Each plot represents 5 minutes of continuous recording with activity summed across 1 second intervals. The left plots (B1 and C1) are from the pre-stimulation recording. The middle plots (B2 and C2) are from the 2 hours post-stimulation recording. The right plots (B3 and C3) are from the 12 hours post-stimulation recording. (D) Normalized array-wide spike densities (ASDs) at the indicated time represented as fold change relative to the pre-drug baseline period (0 H). N = 36 (12 recordings per time point from 3 pairs of independent sister cultures). All recording were made in a 2 hour window ending at the indicated time. Vehicle or 5 ng/ml BDNF was added after the 0 H recordings. Error bars represent SEM. ***$p<0.0001$ assessed with a student's T-test (two tails, unpaired, equal variance) comparing the means of vehicle and BDNF treated neurons.

BDNF increases the level of spontaneous network activity, which indirectly reflects action potential generation. The goal of this study was to use computational models to determine whether BDNF-induced increases in action potential generation could be explained by the distribution of dendrites and synapses that is the result of BDNF stimulation. Therefore, I used the methodology developed in Chapter 2 to thoroughly characterize the morphology of BDNF stimulated neurons (Figure 3.3). I first quantified BDNF's effect on proximal dendritic arbor morphology. As expected based on our time-lapse imaging data, BDNF increased the amount of dendritic material within the proximal arbor. Specifically, BDNF stimulation led to a 24.6% increase in total dendrite length and a 30.1% increase in dendrite complexity (Figure 3.4A). This increase resulted from the addition of dendritic material from 19 μm to 60 μm from the neuronal soma for both dendrite length (Figure 3.4C) and dendrite complexity (Figure 3.4D). Long-term elevation of BDNF signaling (>= 48 hours) has been reported to alter synapse density (Bamji et al., 2006; Hiester et al., 2013; Singh et al., 2006; Taniguchi et al., 2006). BDNF induced dendrite elongation (Figure 3.4C). Therefore, synapse formation would have to be enhanced beyond dendrite elongation to increase synapse density. On the other hand, if synapse formation lags behind dendrite formation, BDNF could actually increase the total number of synapses while decreasing synapse density. To determine the relationship between synapses and dendrites with and without added BDNF, I quantified synapse distribution using two approaches. First, I calculated the total number of synapses within the entire proximal dendritic arbor. Second, I calculated synapse density per dendrite length, which provides insight into how synapse formation is coupled to dendrite formation. Similar to what has been reported for rat hippocampal cultures at 14 DIV (Liu, 2004), our cortical cultures displayed an excitatory/inhibitory ratio of 3.1 to 2 and I detected a strong correlation between the number of excitatory and inhibitory synapses on individual neurons (vehicle, R^2=0.77; BDNF, R^2=0.71; Figure 3.4B).

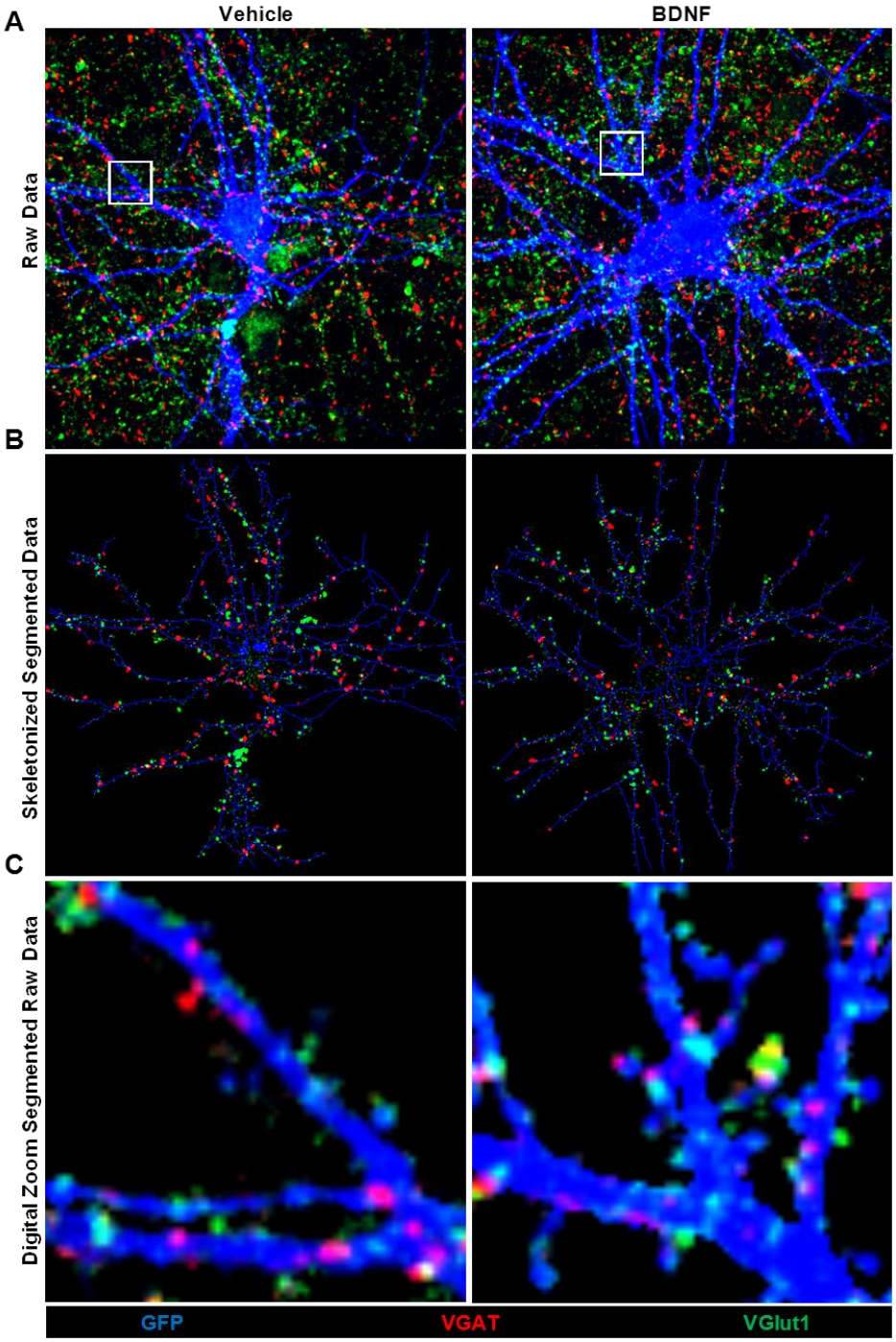

Figure 3.3. Representative images of primary cortical neurons labeled with GFP, VGAT and VGlut1. (A) Representative raw images of a vehicle-treated (left) and a BDNF-treated (right) cortical neuron that have been transfected with GFP (blue) and immunostained for VGAT (red) and VGlut1 (green). The raw data consists of three individual 7 mm Z-stacks (0.5 mm Z spacing) that have been merged and flattened into a MIP. (B) Skeletonization of the raw GFP data in (A) highlighting the distribution of VGAT and VGlut1 puncta throughout the entire proximal dendritic arbor. (C) Digitally enlarged MIPs documenting the raw data from the boxed region in (A) documenting the ability of our image analysis procedure to segment puncta based on their colocalization with GFP.

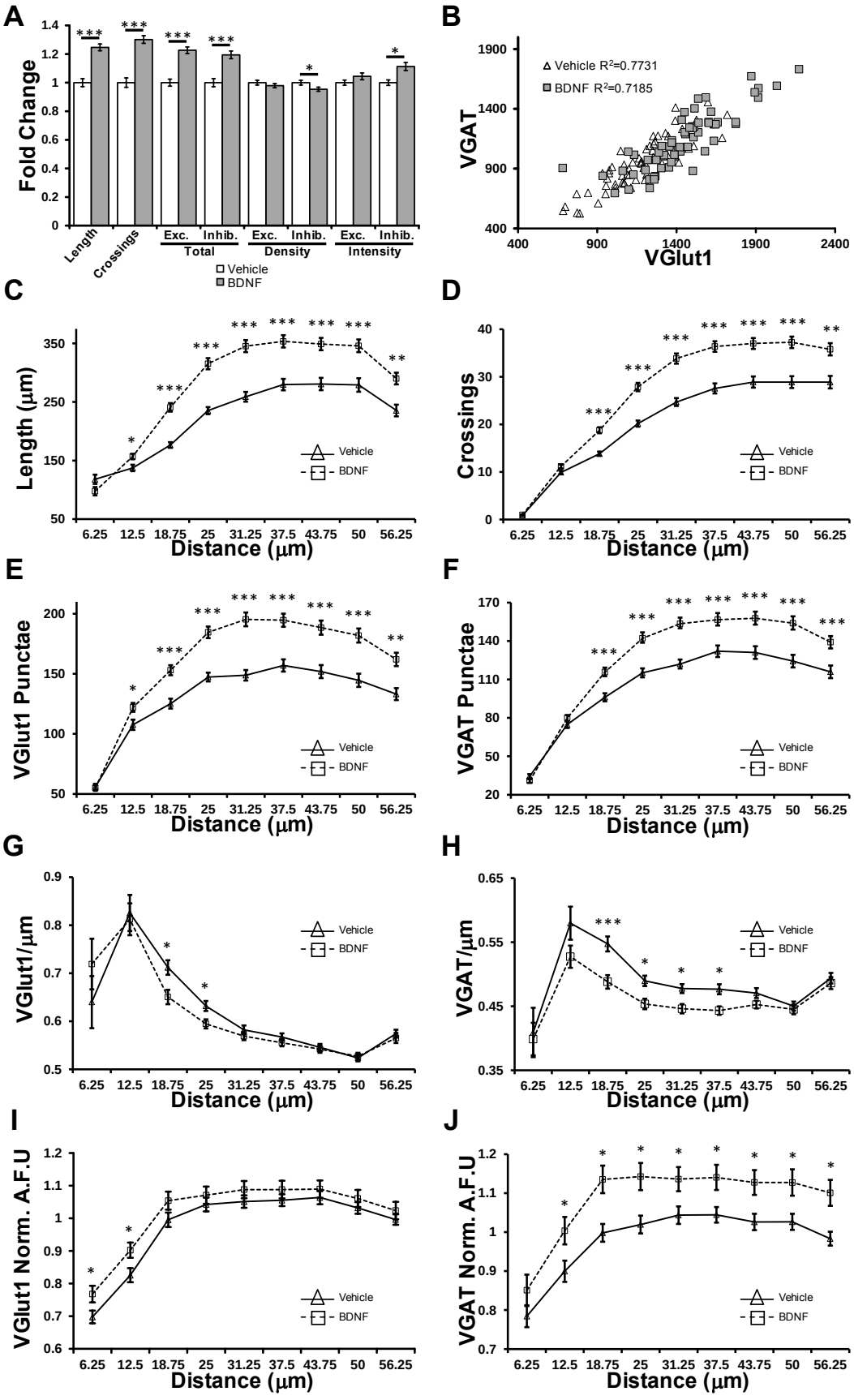
A
Fold Change
Length
Crossings
Exc.
Inhib.
Total
Density
Intensity
Vehicle
BDNF
B
Vehicle R²=0.7731
BDNF R²=0.7185
VGAT
VGlut1
C
Length (μm)
D
Crossings
E
VGlut1 Punctae
F
VGAT Punctae
G
VGlut1/μm
H
VGAT/μm
I
VGlut1 Norm. A.F.U
J
VGAT Norm. A.F.U
Distance (μm)

Figure 3.4. Quantifying BDNF's effect on synapses and dendrites throughout the proximal arbor (A) A bar graph representing the BDNF-induced alteration of the indicated parameters across the entire proximal dendritic arbor. These values represent the global change irrespective of distance from the soma. Each bar represents the average value (BDNF, grey bars; vehicle, white bars) normalized to vehicle. N=63 neurons from 3 independent cultures for both vehicle and BDNF. Error bars represent SEM. (B) Scatter plot representing the total number of VGAT punctae plotted against the total number of VGlut1 punctae for every neuron in the study (BDNF, grey squares; vehicle, white triangles). (C-J) Line plots representing the average value for the indicated parameters averaged across 6.25 μm bins (BDNF, dashed lines; vehicle, solid lines). The distance plotted along the x-axis is relative to the center of the neuronal soma. The individual plots are (C) total dendrite length, (D) dendrite crossings, (E) total number of VGlut1 punctae, (F) total number of VGAT punctae (G) VGlut1 puncta density per μm (H) VGAT puncta density per μm (I) normalized VGlut1 puncta intensity and (J) normalized VGAT puncta intensity. ***p<0.0001; **p<0.001; *p<0.05 assessed with a student's T-test (two tails, unpaired, equal variance) comparing the means of vehicle and BDNF treated neurons.

Next I evaluated BDNF's influence on excitatory synapse distribution throughout the proximal arbor. I found that BDNF increased the number of VGlut1 punctae per arbor (Figure 3.4A). This increase was due to the addition of VGlut1 punctae within 19-60 μm from the neuronal soma (Figure 3.4E). However, when normalized to dendrite length, BDNF had no effect on total VGlut1 density (Figure 3.4A) and BDNF actually decreased VGlut1 density in the 19 and 25 μm bins (Figure 3.4G). The intensity of VGlut1 punctae should be a reasonable estimate of presynaptic strength, as the amplitude of evoked excitatory post-synaptic currents (EPSC) and miniature EPSCs are proportional to the amount of VGlut1 in individual nerve terminals (Jong et al., 2012; Wilson et al., 2005). Therefore, I estimated BDNF's influence on excitatory synapse strength by summing the pixel intensities of the VGlut1 immunofluorescence signal within individual punctae. I determined that, while BDNF did not increase the overall intensity of VGlut1 punctae (Figure 3.4A), it did specifically enhance the intensity of those within the first 12.5 μm of the neuronal soma (Figure 3.4I). Collectively, these results suggest that BDNF increases the number and strength of excitatory synapses within the proximal arbor. However, BDNF-induced excitatory synapse formation is slightly uncoupled from dendrite formation, which creates a reduction in excitatory synapse density within the proximal arbor where most BDNF-induced dendrite

growth occurs. An increase in excitatory synapse strength in this region may counteract the reduction of excitatory synapse density.

Next, I assessed BDNF's influence on inhibitory synapse distribution within the proximal dendritic arbor. I found that BDNF increased the total number of VGAT punctae per arbor (Figure 3.4A) by stimulating the addition of VGAT punctae within 19-56 μm of the neuronal soma (Figure 3.4F), again indicating new synapse formation within the proximal arbor where new dendrite growth and excitatory synapses are added. However, when normalized to dendrite length, BDNF significantly decreased the overall density of VGAT punctae (Figure 3.4A), due to a reduction 19-38 μm from the soma (Figure 3.4H), a region larger than that over which the reduction in excitatory synapse density occurred (Figure 3.4G). There is a strong correlation between VGAT punctae intensity and evoked inhibitory post-synaptic currents in acute layer 2/3 cortical slices (Tabuchi et al., 2007), indicating that VGAT punctae intensity can be used as an estimate of presynaptic inhibitory synapse strength (Jong et al., 2012). Unlike VGlut1, BDNF increased the overall strength of VGAT punctae (Figure 3.4A), and this resulted in increased VGAT puncta intensity throughout the majority of the proximal arbor (Figure 3.4J), suggesting that BDNF stimulation causes the formation and strengthening of inhibitory synapses. However, inhibitory synapse formation lagged behind dendrite addition more than excitatory synapse formation, leading to a larger reduction in inhibitory synapse density.

BDNF significantly altered the complexity and length of the dendritic arbor as well as the intensity and density of excitatory and inhibitory synapses in a distance-dependent fashion. To determine whether the BDNF-induced distribution of synapses and dendrites is more efficient at generating action potentials, I developed compartmental models using the approach outlined in Chapter 2. In total, I created two sub-models (vehicle and BDNF) (Figure 3.5), with each sub-model representing the 63 individual arbor morphologies analyzed above (for a total of 126 individual models). I then analyzed the average firing rate of each sub-model across unconstrained parameter space. I first

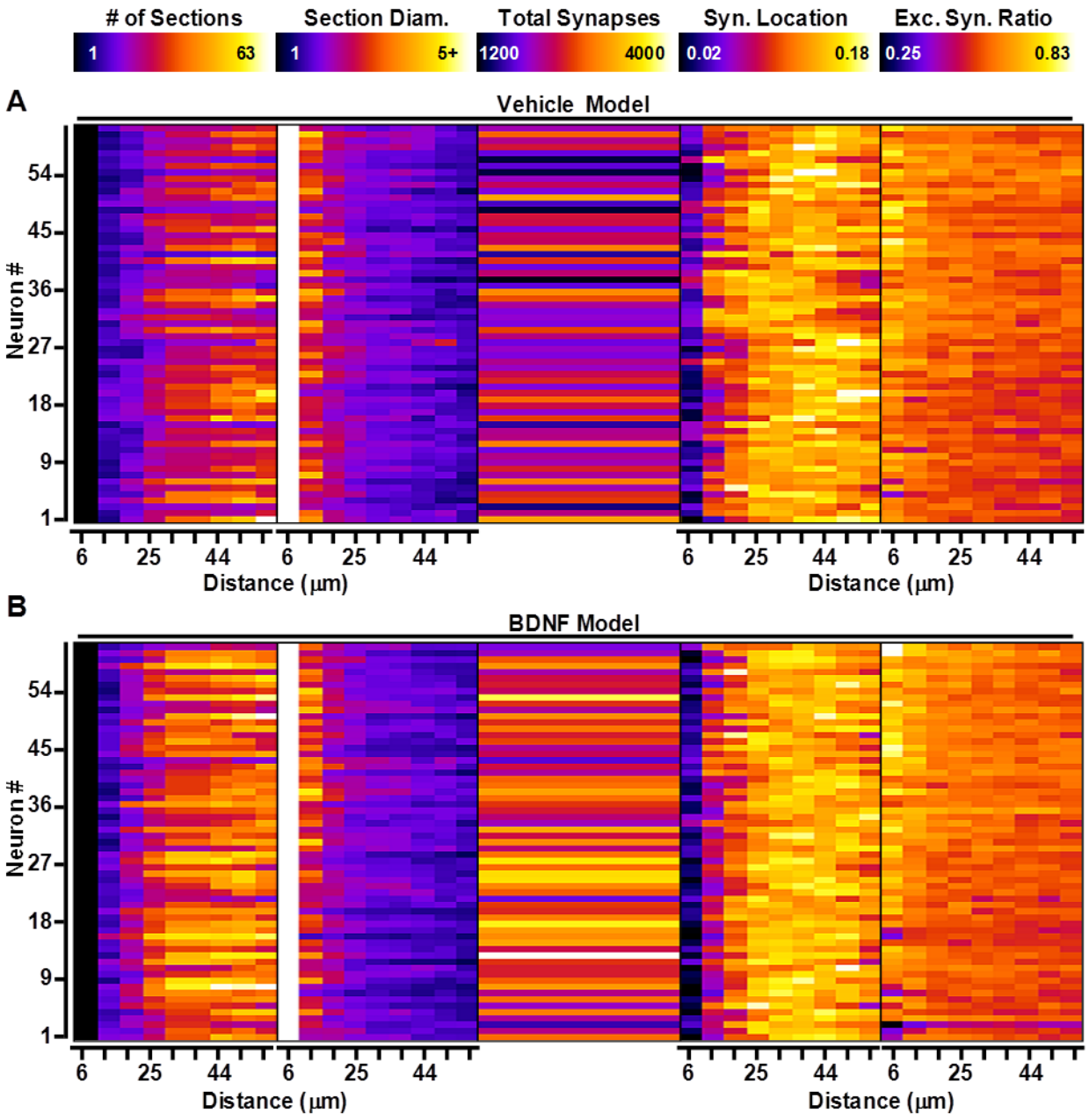

Figure 3.5. Visual representation of individual compartmental models. Heat maps representing the specific combination of sections, section diameters, synapses, synapse locations and synapse types across the first 56 μm for each of the 126 individual neurons that were morphologically characterized in this study. The text files used to generate these heat maps were directly imported into NEURON during numerical simulations. A) represents the vehicle model. B) represent the BDNF model.

determined the firing properties of the vehicle model. In general, the highest firing rates were achieved at the maximum stimulation intensity (Figure 3.6A and 3.6C-6E). An exception to this general trend was observed in the excitatory synapse decay subspace (Figure 3.6B), where maximal firing occurred at 0.6 stimulation strength because long excitatory synapse decay constants actually suppressed firing at higher stimulation strength. Within each subspace specific trends regarding the effect of individual parameter values were apparent. Decreasing the size of the apical arbor (Figure 3.6A), increasing the excitatory synapse decay constant (Figure 3.6B), decreasing the inhibitory synapse decay constant (Figure 3.6C) and shortening the synaptic integration window (Figure 3.6D) all increased the firing rate across a range of stimulation intensities. I observed that dendritic membrane excitability had little effect on firing at any of the stimulation strengths tested. Collectively, these results suggest that our model produces action potential firing in a physiological frequency range (Roxin et al., 2011) and across a wide range of physiologically representative parameter space.

Next, I evaluated the performance of the post-BDNF addition model relative to the vehicle model. Within each subspace, the response of the BDNF model paralleled that of the vehicle model. Generally, firing rates increased with increasing stimulation intensity and the same parameter values that caused fluctuations in the vehicle model also caused fluctuations in the same direction within the BDNF model (Figure 3.6A2-6E2). However, there were notable differences in the overall firing rate between the models within each parameter subspace, with the BDNF model producing higher firing rates. With respect to the apical dendrite, the BDNF model outperformed the vehicle model by ~2-10% in 20 of the 21 tested apical dendrite size/stimulation combinations (Figure 3.6F). The only exception was the smallest size tested (62.5 mm) at the lowest stimulation intensity, where the vehicle model displayed superior performance. In general, the relative firing of the BDNF model increased as the size of the apical dendrite increased and at the more moderate stimulation intensities. With respect to synapse decay kinetics, the BDNF model outperformed the vehicle model by ~2-25% in 17 of the 19 tested

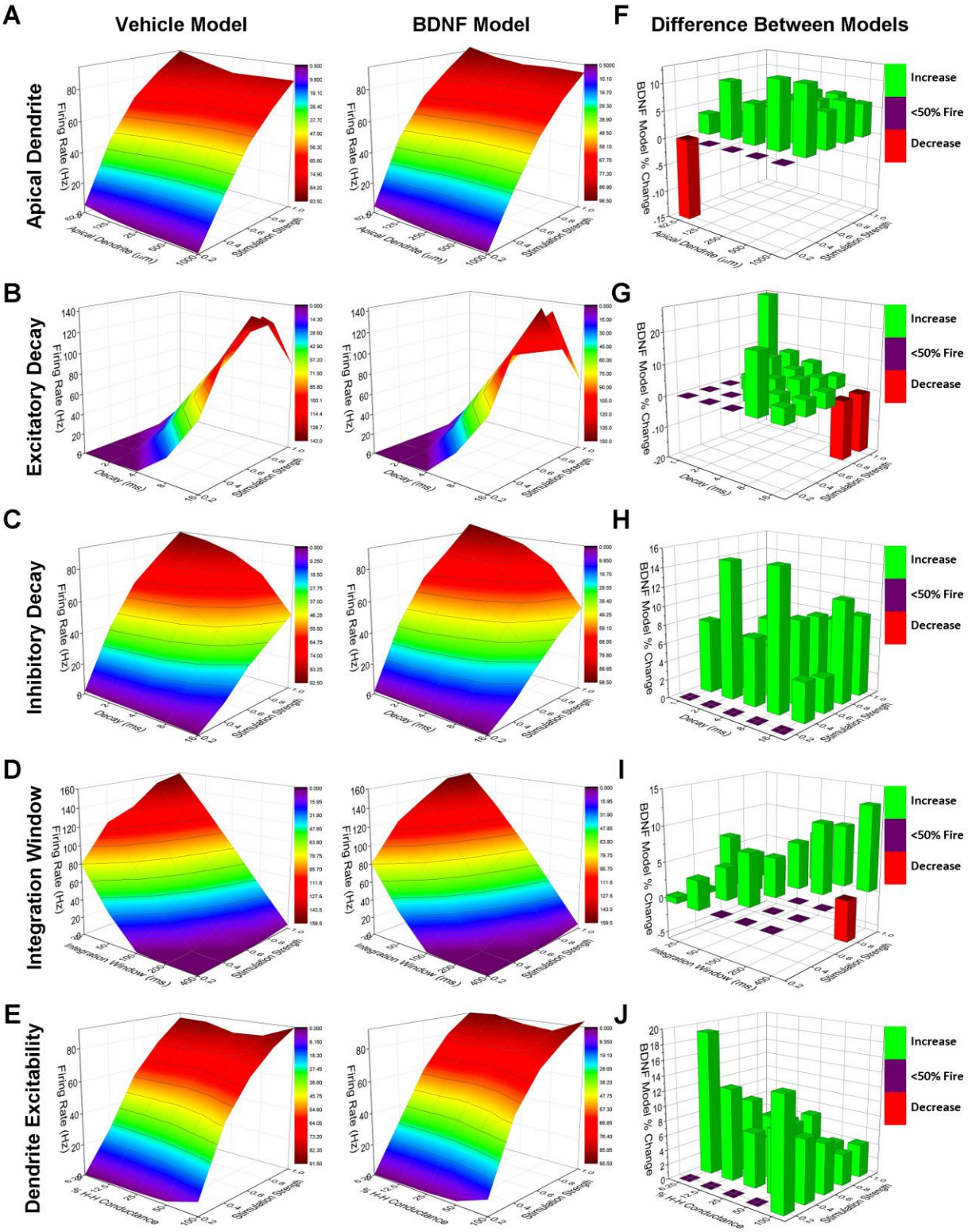
A
Vehicle Model
BDNF Model
F
Difference Between Models
Apical Dendrite
B
Excitatory Decay
C
Inhibitory Decay
D
Integration Window
E
Dendrite Excitability
Firing Rate (Hz)
BDNF Model % Change
Increase
<50% Fire
Decrease
Apical Dendrite (µm)
Decay (ms)
Integration Window (ms)
% HH Conductance
Stimulation Strength

Figure 3.6. Evaluating vehide and BDNF models across a broad range of parameter space. (A-E) Contoured color maps representing the firing rate of vehicle (left) and BDNF (right) models across 5 model subspaces. (A) Represents the apical dendrite subspace with a baseline size of 250 μm. (B) Represents the excitatory synapse decay constant subspace with a baseline value of 4 ms. (C) Represents the inhibitory synapse decay constant subspace with a baseline value of 4 ms. (D) Represents the integration window subspace with a baseline window of 100 ms. (E) Represents the dendritic membrane excitability subspace with a baseline value set to 25% of the somatic H-H parameters. Each subspace is comprised of a single parameter value varied from its baseline value 2 and 4 fold in each direction while stimulation was linearly increased from 0.2 to 1 in 0.2 increments (1 = each synapse being stimulated once). For each plot, the x-axis represents parameter values, the y-axis represents stimulation strength and the z-axis represents the average firing rate for each of the 63 model neurons in Hz. Each individual neuron was modeled in each region of subspace until the SEM of its firing rate dropped below 2% of its average firing rate. (F-J) 3-D bar graphs depicting the percent difference between the vehicle and BDNF model in each region of subspace. Green bars indicate spaces where the BDNF model outperformed the vehicle model. Red bars indicate spaces where the BDNF model underperformed the vehicle model. Purple squares represent spaces where fewer than 50% of the vehicle neurons fired and, thus, no comparison was made.

excitatory decay combinations (Figure 3.6G) and by ~2-15% in 20 of the 20 inhibitory decay combinations (Figure 3.6H). The BDNF model had the most striking advantage in producing action potentials when extremely fast excitatory decay times (1 ms) were paired with the highest stimulation intensity. Conversely, the BDNF model was at a clear disadvantage when long excitatory decay times (16 ms) were paired with the highest stimulation intensities. Regarding the window for synaptic integration, we noticed that neither model produced robust firing at low stimulation intensities when the length of stimulation was increased to 200 ms and beyond. Nonetheless, in 17 of the 18 combinations that displayed robust firing, BDNF outperformed the vehicle model by ~1-13% (Figure 3.6I). Finally, with respect to dendritic membrane excitability, altering the H-H conductance of the dendritic arbor did not by itself alter the firing properties of individual models. However, dendritic membrane excitability did influence the relative performance of the BDNF model in 21 of the 21 tested combinations, with the most striking differences occurring when low stimulation intensities were paired with either minimal (6.25% of somatic) or maximal (100% of somatic) dendritic H-H conductance (Figure 3.6H). Collectively, these results argue that the spatial distribution of dendrites and synapses throughout the proximal

arbor of BDNF-stimulated neurons is intrinsically more excitable when compared to control neurons across a broad range of parameter space.

Interactions between excitatory and inhibitory synaptic potentials are influenced by dendritic structure. To tease apart the relative contributions of dendritic structure versus excitatory and inhibitory synapse distribution, I constructed hybrid models. Specifically, I mapped the average vehicle and BDNF synapse profiles on to the globally averaged (vehicle plus BDNF models) dendrite morphology. This allowed me to test the precise contribution of synapse distribution on the same dendrite topology. I also mapped the globally averaged synapse profile onto the average vehicle and BDNF dendrite morphologies, which allowed me to test the precise contribution of dendrite topology using the same synapse distribution. I then subjected these hybrid models to the same systematic manipulation of parameter space while evaluating action potentials. Each hybrid model displayed the same general firing landscape as the original models, suggesting that the process of averaging did not fundamentally alter the response to an input barrage of synaptic activity. Assessment of the relative performance of the models revealed that the average BDNF synapse distribution is more likely than the average vehicle synapse distribution to produce action potentials across a wide range of parameter space (Figures 3.7A-E right). Conversely, the average BDNF dendrite morphology is much less excitable than the average vehicle dendrite morphology across the majority of parameter space (Figures 3.7A-E left). These results suggest that, although the BDNF model outperforms the vehicle model, the expansion of the proximal dendritic arbor antagonizes BDNF-induced synapse addition to limit BDNF's overall impact on neuronal firing.

3.3 Conclusion

I have assessed acute low dose BDNF-induced structural plasticity at dendrites, excitatory synapses and inhibitory synapses simultaneously throughout the proximal arbor of individual neurons, and I have correlated this structural response with elevated network activity. I found that excitatory and

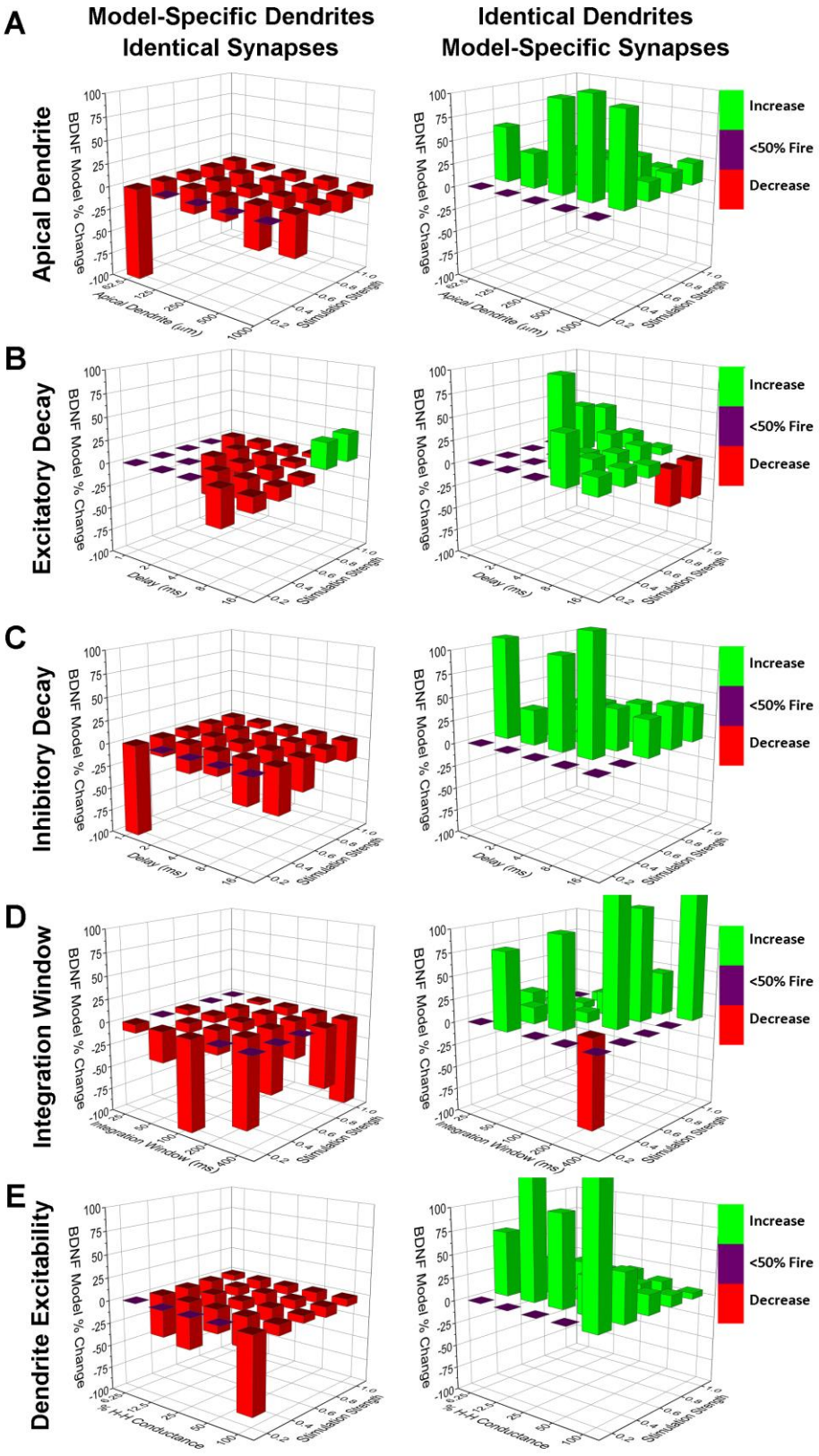
A
Model-Specific Dendrites
Identical Synapses
Identical Dendrites
Model-Specific Synapses
Apical Dendrite
B
Excitatory Decay
C
Inhibitory Decay
D
Integration Window
E
Dendrite Excitability
BDNF Model % Change
Apical Dendrite (µm)
Delay (ms)
Integration Window (ms)
% H-H Conductance
Stimulation Strength
Increase
<50% Fire
Decrease

Figure 3.7. Using hybrid models to assess the specific contributions of dendrite topologies versus synapse distributions. (A-E) 3-D bar graphs depicting the percent difference between vehicle and BDNF hybrid models across model subspace. The arrangement of axes and the color coding of individual bars is identical to Figure 6. The graphs on the left represent hybrid models where identical synapse distributions were mapped onto the average vehicle and BDNF dendrite topologies. The graphs on the right represent hybrid models where the average vehicle and BDNF synapse distributions were mapped onto identical dendrite topologies. The z-axis of each graph was truncated at -100% and +100% to preserve the scale amongst all of the graphs.

inhibitory synapse formation occurs rapidly upon BDNF stimulation. However, because dendrite formation exceeded synaptogenesis, BDNF did not increase synapse density. Using morphologically constrained mathematical models, I obtained evidence that the spatial distribution of synapses resulting from BDNF addition is more likely to produce action potentials. However, these models also showed that the impact of the BDNF-altered synapse distribution is functionally antagonized by the expansion of the dendritic arbor. I propose that the coordinated addition of dendrites and both excitatory and inhibitory synapses in specific domains of the dendritic tree are important aspects of the mechanism that allows BDNF to modulate cortical circuitry.

3.4 Detailed Methods

Primary neuron culture, transfection and immunocytochemistry were performed with methods identical to those described in Chapter 2.

Live Cell Microscopy

Primary cortical cultures were plated onto glass bottom dishes (Mat-Tek). Neurons were cultured and transfected using the same procedures that were used for neurons grown on coverslips. At 12-14 DIV, dishes were placed into a pre-equilibrated, environmentally controlled stage (5% CO_2, 50% humidity, 36.5^{o}) that was attached to a Nikon spinning disk confocal microscope with a 512x512 EM-CCD camera and fitted with a 0.95 N.A. 40x objective. GFP was excited with a 473 nm laser excitation source. 5-10 GFP positive neurons were identified per dish and their locations were programmed into the automated stage controller that was run by MetaMorph software. After neurons were identified, images

were acquired every 2 hours as a Z-stack with Z spacing of 1 μm and 50-150 ms exposures per frame. The first image was acquired as the neurons were identified and drug application was performed immediately after the final neuron was identified, with a typical delay of 10-20 minutes between the identification of the first neuron and the application of drug.

Multi-Electrode Array Analysis

Sister cultures from 3 individual cultures prepared on 3 different days were plated on multi-electrode arrays (MEA; Axion Biosystems; M64-GL1-30Pt200) containing 64 evenly spaced platinum electrodes (electrode diameter = 30 μm; center to center spacing = 200 μm) in an 8 by 8 grid. They were allowed to develop until 12-14 days in vitro before recording commenced. Dishes were transferred to the incubator containing the MEA recording unit (Axion Biosystems Muse) at least 24 hours prior to the first recording in order to avoid artifacts due to culture movement while transporting the cultures into the room containing the MEA recording unit.

Each experiment consisted of two sister cultures, where one culture was stimulated with vehicle and the other culture was stimulated with BDNF. The recording procedure was as follows. Activity was recorded for a 2 hour pre-drug baseline (-2 to 0 hours). After the baseline, cultures were removed and stimulated with vehicle or BDNF and activity was recorded for another 2 hours (0 to 2 hours) and again at 12 hours (12 to 14 hours). Extreme care was taken when removing dishes from the recording unit and when placing cultures into the recording unit according to the advice of Wagenaar et al (2006). Activity at each electrode was monitored with a sampling frequency of 12.5 kHz and spikes were detected in real time using the AdaBand spike detections system set to a threshold of 5 standard deviations. Spikes were summed into 1 second bins and split into individual chunks of 5 minutes. The post-drug spike rates for an individual culture were normalized to its own pre-drug spike rate, to minimize the impact of variable firing patterns when comparing vehicle to BDNF stimulated cultures.

Chapter 4. BDNF-Induced Gene Expression and Synapse Formation

4.1 Introduction

In the previous chapter I presented evidence that BDNF influences action potential generation by creating a favorable distribution of excitatory and inhibitory synaptic inputs within the dendritic arbor. However, the intracellular mechanisms that translate the BDNF signal into an altered distribution of excitatory and inhibitory synapse inputs are not clear. Similar to other growth factors, one of the primary consequences of BDNF signaling is altered gene expression. However, because hundreds to thousands of individual genes are regulated by BDNF, identifying how individual target genes function downstream is challenging. In this chapter I discuss the process of synapse formation and stabilization, before presenting an introduction to two specific proteins that function at the synapse: Arc and LRRTM1. I will then present evidence that Arc is required for BDNF-induced excitatory synapse formation and LRRTM1 is a novel BDNF target genes displays an additive interaction with BDNF during the process of excitatory synapse formation.

4.2 Synapse Formation and Plasticity

Synapse formation proceeds via coordinated events between axons and dendrites (McAllister, 2007). As discussed in Chapter 1, the synapse consists of two hemi-structures separated by a physical space, or cleft. The pre-synapse is composed of neurotransmitter vesicles that fuse with the plasma membrane at the active zone. The post-synapse is composed of neurotransmitter receptors that are embedded within a matrix of scaffolding molecules. In addition, synapses contain pre and post-synaptic adhesion molecules, which play an important role in initiating and maintaining contact between the pre and post-synaptic membranes. Synaptic adhesion molecules are single pass transmembrane proteins that contain extracellular domains which facilitate physical interactions between axons and dendrites. Typically, synaptic adhesion molecules contain extracellular protein domains, such as immunoglobulin-like domains, leucine-rich repeats and cysteine-rich domains, which participate in a wide range of

homophillic and heterophillic interactions (Poulopoulos et al., 2009). The intracellular portions of synaptic adhesion molecules typically contain PDZ domains to promote the anchoring of post-synaptic adhesion molecules within the post-synaptic density. During the process of trans-synaptic adhesion, unique pairs of presynaptic adhesion molecules physically interact with post-synaptic adhesion partners to create a physical link between axons and dendrites (Figure 4.1) (Südhof, 2008).

The synaptogenic capability of synaptic adhesion molecules was discovered using heterologous systems in which non-neuronal cells are transfected with synaptic adhesion molecules and are co-cultured with primary dissociated neurons. Using this system, it was found that the post-synaptic adhesion molecule neuroligin was sufficient to induce the formation of functional pre-synapses onto the non-neuronal cells (Scheiffele et al., 2000). Conversely, overexpressing the presynaptic adhesion molecule neurexin was sufficient to induce the formation of functional post-synapses onto the non-neuronal cells (Graf et al., 2004). These initial studies provided the first evidence that synaptic adhesion molecules can instruct pre and post-synaptic differentiation. The neurexin and neuroligin families contain multiple family members (Südhof, 2008). Furthermore, other synaptogenic adhesion molecules have been discovered, including SynCAM, LRRTMs and SALMs (Biederer et al., 2002; Linhoff et al., 2009; Mah et al., 2010). In addition to an expanding array of individual families, there also appears to be extensive alternative splicing within some families that provides even greater diversity in trans-synaptic interactions (Koehnke et al., 2010). It is currently believed that the diverse binding capabilities of adhesion molecules reflect the diversity of synaptic connections within the central nervous system. This view has gained credibility as complex psychiatric disorders, including autism spectrum disorders, have been linked to polymorphisms in the genes that encode synaptic adhesion molecules, such as neuroligins (Reichelt et al., 2012; Tabuchi et al., 2007).

Synaptic adhesion molecules facilitate synaptogenesis by promoting the clustering of pre and post-synaptic components. Neurexin binds to the presynaptic proteins CASK and synaptotagmin, which

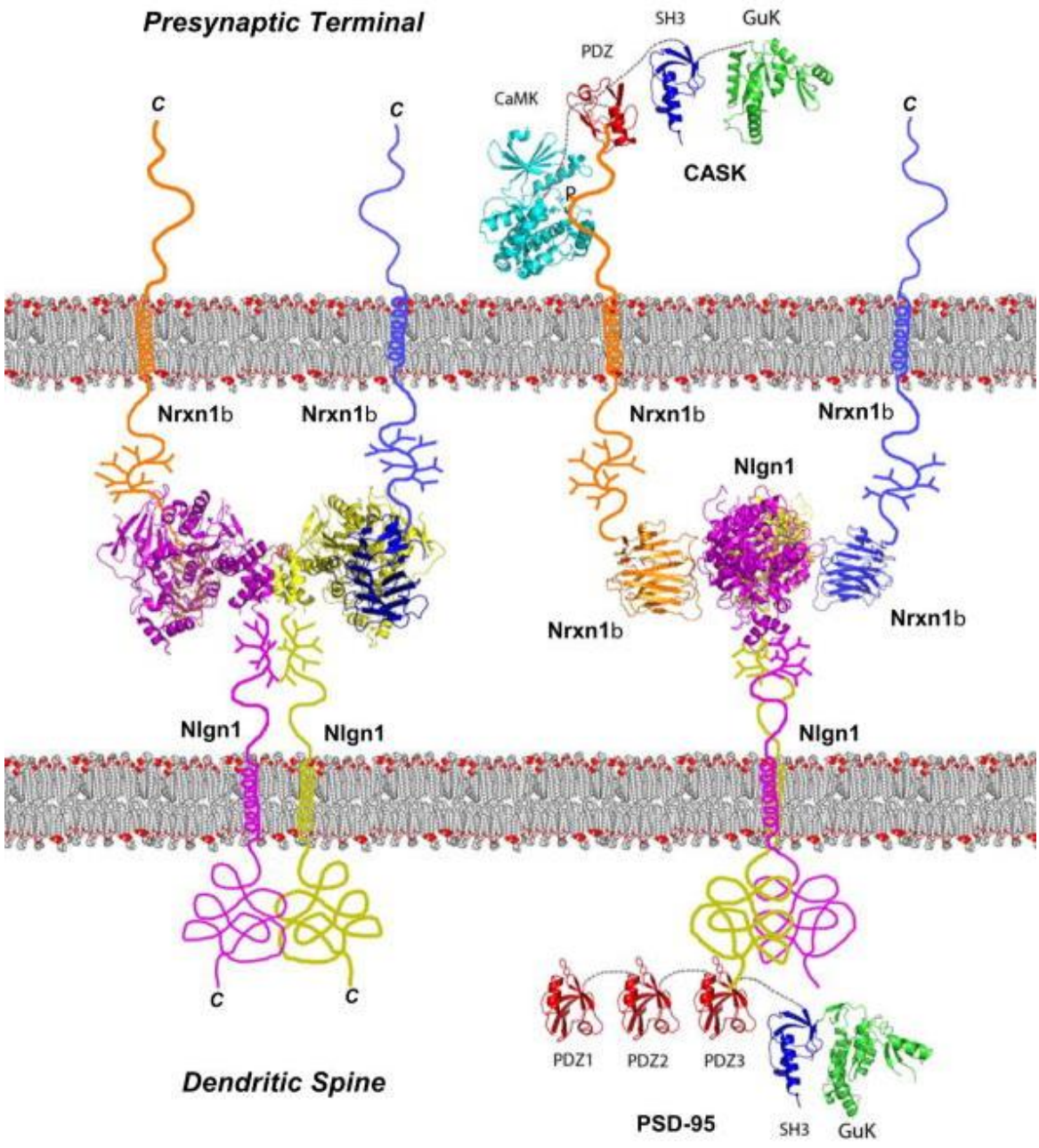

Figure 4.1. A schematic representation of synaptic adhesion at an excitatory synapse. (Top) Neurexin molecules are embedded within the presynaptic membrane where they associate with various presynaptic scaffolding molecules such as CASK. (Bottom) Neuroligin molecules are embedded within the postsynaptic membrane where they associate with various postsynaptic scaffolding molecules such as PSD-95. (Middle) Neuroligin directly binds to neurexin within the synaptic cleft. The neuroligin/neurexin adhesion complex is a tetrameric assembly. Reproduced from Sudhof, 2008 without permission.

have binding partners within the active zone including α-liprins (Dean et al., 2003; Hata et al., 1996). In addition, neurexin colocalizes with CASK in axonal transport vesicles, which are packets of presynaptic proteins that are thought to provide the functional building blocks for neurotransmitter release at nascent presynaptic sites (Fairless et al., 2008). Neurexin clustering, either artificially or via the overexpression of neuroligins, is sufficient to induce the accumulation of presynaptic vesicles containing VGlut1 or VGAT (Craig and Kang, 2007). Neuroligins bind to the post-synaptic scaffolding molecules PSD95 and gephyrin, which stabilize glutamate receptors and GABA receptors within the post-synaptic membrane (Irie et al., 1997; Poulopoulos et al., 2009). Neuroligin-1 associates with NMDA receptor subunits within post-synaptic transport packets, which, similar to presynaptic packets, are thought to contain protein components necessary for rapid post-synaptic assembly (Barrow et al., 2009). Finally, neuroligin clustering, via artificial bead-based methods or neurexin overexpression, increases the accumulation of AMPA receptors, NMDA receptors and associated post-synaptic scaffolding molecules such as PSD95 and SAP102 (Krueger et al., 2012). Although I have presented trans-synaptic adhesion in general terms, it should be noted that individual synaptic adhesion molecules appear to preferentially cluster excitatory or inhibitory synaptic components. The best characterized example of this preference is with neuroligin-1 and neuroligin-2. Whereas clustering of neuroligin-1 results in the accumulation of excitatory post-synaptic components, clustering of neuroligin-2 causes the accumulation of inhibitory post-synaptic components (Giannone et al., 2013; Woo et al., 2013).

Gain of function studies clearly indicate that neurexin and neuroligin promote the formation of pre and post-synaptic specializations, respectively. However, loss-of-function experiments have been less conclusive and, generally, indicate that synaptic adhesion is highly redundant. In rodents, there are three neurexin genes, each with two promoters (α and β), which allows for the production of six presynaptic neurexins (Reissner et al., 2013). Sudhof and colleagues undertook the heroic task of deleting the α promoter from each of the three neurexin genes. From single knockouts to triple

knockouts they observed synaptic phenotypes of increasing severity, with triple knockouts displaying a ~75% reduction in the frequency of mEPSPs and mIPSPSs within neocortical slices (Missler et al., 2003). A similar analysis was carried out on neuroligin triple knockout mice and similar results were observed, with the exception that single knockout mice did not display a synaptic phenotype. However, it should be noted that in neuroligin-1 knockdown is sufficient to reduce dendritic spine density in a cell-autonomous fashion when the majority of neighboring neurons have normal levels of neuroligin-1 protein (Kwon et al., 2012). In addition, while mEPSPs and mIPSPs were reduced in the triple knockouts, morphological analysis did not identify any significant reduction in synapse numbers or morphology (Varoqueaux et al., 2006). These results suggest that neuroligins are not required for the formation of synapses, but they are required for normal synapse function. In addition, because the neurexin and neuroligin gene families are required for normal synaptic transmission but individual members of the family are not, these results argue that synaptic adhesion is an extremely redundant biological process.

Synaptogenesis is also characterized by stereotyped cellular events. Axons and dendrites are decorated with filopodia, and evidence suggests that filopodia initiate contact between axons and dendrites that leads to synapse formation (Koleske, 2013). Developing axons display two classes of filopodia. Their growth cones harbor filopodia, which participate in axon pathfinding, and their axonal shaft exhibits transient filopodia that participate in synapse formation. Evidence that axonal filopodia can form presynaptic contacts comes from the localization of dynamic synaptotagmin and VAMP positive vesicles within axonal filopodia that stabilize upon contact with dendrites (Chang and De Camilli, 2001; Dean et al., 2003). It is not clear whether axonal filopodia retract upon synapse formation and become en passant synapses. Also it is not clear whether filopodia from excitatory axons and inhibitory axons behave differently during the process of synapse formation. In contrast to axonal filopodia, the role of dendritic filopodia in excitatory synapse formation is well understood. During the process of synapse formation, dendritic filopodia explore their surroundings and make contact with

axonal projections at sites that uptake the synaptic dye, FM1-43 (Hoopmann et al., 2012; Ziv and Smith, 1996). Subsequent to initial contact and synaptic differentiation, dendritic filopodia recruit AMPA and NMDA receptors and associated scaffolding molecules and display AMPA and NMDA synaptic currents (Friedman et al., 2000; Zito et al., 2009). Typically the process of excitatory synapse formation is associated with an enlargement of the filopodia head and a shortening of the filopodia neck leading to a mature dendritic spine synapse (Yuste and Bonhoeffer, 2004). It is not clear whether inhibitory synaptogenesis within the dendritic arbor proceeds via the extension of dendritic filopodia as well.

A remarkable aspect of synapse development is that synapses are plastic and undergo structural and functional changes throughout development. Generally, synapses can be strengthened (long-term potentiation; LTP) or weakened (long-term depression; LTD), which enhances or reduces the post-synaptic response, respectively (Castillo, 2012). Both presynaptic and post-synaptic mechanisms contribute to long-term synapse modification. The induction of presynaptic plasticity is likely to rely upon PKA-mediated phosphorylation of presynaptic terminal proteins, such as RIM1a, MUNC13, Rab3 and voltage-gated calcium channels, which can modulate the efficacy of synaptic vesicle fusion (Yang and Calakos, 2013). VGlut1 and VGAT expression have been correlated with synapse strength, and it is possible that changes in the levels of these transporters contribute to presynaptic plasticity as well (Tabuchi et al., 2007; Wilson et al., 2005). The mechanisms that underlie post-synaptic plasticity are well understood and generally revolve around the insertion and removal of ionotropic neurotransmitter receptors from the post-synaptic density. The potentiation of excitatory synapses is associated with strong NMDA receptor activation which leads to the insertion of AMPA and NMDA receptor subunits from a rapidly recycling pool and a general expansion of the post-synaptic density (Anggono and Huganir, 2012; Grosshans et al., 2002; Petrini et al., 2009). Similarly, the potentiation of inhibitory synapses is associated with increased surface expression of $GABA_A$ receptors (Marsden et al., 2007). In both cases, phosphorylation of the cytoplasmic tails of these receptors, which can be modulated via

ligand-dependent and calcium-dependent kinases, appears to be a critical modulator of their surface stability and, thus, synapse strength (Anggono and Huganir, 2012; Saliba et al., 2012).

4.3 BDNF Regulates the Expression of Genes that Influence Synapse Function

BDNF regulates the expression of numerous genes that encode for proteins that have known roles in modulating the function of excitatory synapses (for reviews, see (Bramham and Panja, 2013; Carvalho et al., 2008; Greer and Greenberg, 2008); for a sampling of large scale analyses, see (Alder et al., 2002, 2003; Schratt et al., 2004; Strand et al., 2007; Wibrand et al., 2006)). However, due to the sheer number of BDNF target genes, many of which have similar functions and are regulated with similar kinetics, it has been difficult to identify the specific target genes that mediate BDNF-induced plasticity. Nonetheless, some progress has been made towards creating molecular pathways that link BDNF signaling to excitatory synapse formation. In cultured cortical neurons, BDNF regulates the expression of members of the Wnt family of proteins, and inhibition of Wnt signaling is sufficient to block BDNF-induced increases in dendritic spine formation (Hiester, 2012). In cultured hippocampal neurons, BDNF activates a nonselective cationic current that is mediated by TRPC 3 channels, and TRPC 3 knockdown with siRNA blocks BDNF-induced dendritic spine formation (Amaral and Pozzo-Miller, 2007). BDNF increases the expression of Rab3a and BDNF-induced synaptic potentiation is impaired in cultured hippocampal cells from Rab3a knockout mice (Alder et al., 2003). Similarly, BDNF enhances the expression of ryanodine receptors in hippocampal pyramidal neurons, and pharmacological inhibition of ryanodine receptor function prevents BDNF-induced dendritic spine addition (Adasme et al., 2011). Finally, BDNF increases the dendritic localization of the recycling endosome component Rab11, while a Rab11 dominant negative construct is sufficient to prevent BDNF-induced dendritic arborization (Lazo et al., 2013). Although each of these mechanisms contributes to BDNF-induced plasticity at synapses, BDNF has not been shown to specifically regulate the process of trans-synaptic adhesion.

In an attempt to uncover additional physiologically relevant BDNF target genes that directly participate in synapse formation, a previous study within the lab analyzed mRNA expression in the brains of BDNF knockout mice using microarray analysis (Strand et al., 2007). In total, the expression of over 20,000 individual mRNAs was analyzed in four different brain regions (anterior cortex, posterior cortex, striatum and cerebellum). Of these, ~2000 showed statistically significant differential expression, including the cytoplasmic protein Arc and the synaptic adhesion molecule LRRTM1

Arc is a cytoplasmic protein that localizes to synapses in response to strong synaptic stimulation (Bramham et al., 2008) (Figure 4.2; Top). The Arc promoter contains a synaptic response element (SARE) that consists of a cluster of CREB, SRF and MEF2 binding sites, which is both necessary and sufficient for rapid neuronal activity-induced transcription (Kawashima et al., 2009). Upon synthesis, Arc mRNA is rapidly transported to dendrites where it docks at the base of dendritic spines and is locally translated (Dynes and Steward, 2012). In addition, Arc transcription and local Arc mRNA translation are both stimulated by elevated BDNF (Ji et al., 2010; Wibrand et al., 2006; Yin et al., 2002). A unique feature of the Arc mRNA is that it contains two introns within its 3' UTR, which makes the Arc mRNA a target for rapid translation-dependent degradation via the process of nonsense mediated decay (NMD) (Giorgi et al., 2007). Arc protein interacts with dynamin and endophilin to facilitate the process of AMPA receptor endocytosis in response to synaptic stimulation, which is an essential component of the homeostatic scaling of excitatory synaptic inputs that was introduced in Chapter 3 (Chowdhury et al., 2006; Shepherd et al., 2006). Specifically, Arc depletion increases the level of surface AMPA receptors and Arc overexpression decreases the level of surface AMPA receptors and impairs TTX-induced homeostatic synaptic scaling, allowing Arc to mediate activity-dependent synapse maturation and stabilization. Arc overexpression has been shown to increase the percentage of filopodial dendritic spines that express surface AMPA receptors and Arc knockout mice have reduced spine density within the hippocampus (Peebles et al., 2010). Although the overexpression result is intuitive considering Arc's general role as a

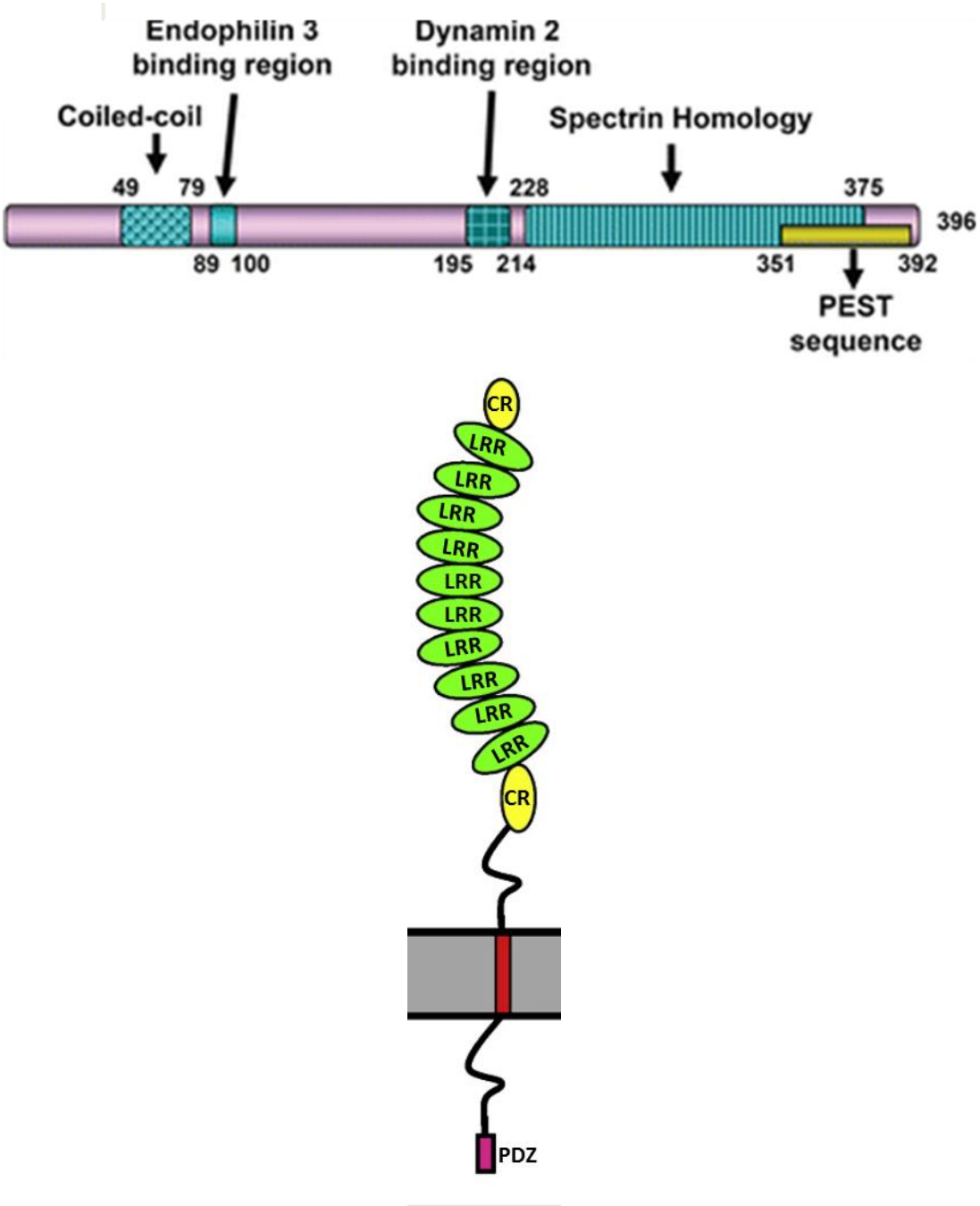

Figure 4.2. A schematic representing the functional domains of Arc and LRRTM1. (Top) Arc is a cytoplasmic protein with a single coiled-coil domain to mediate oligomerization, endophilin and dynamin ineracting domains to facilitate endocytosis, a spectrin homology domain with unknown function and a PEST domain to facilitate protein degradation. Reproduced from Bramham et al, 2010 without permission (Bottom) LRRTM1 is a single pass Type-1 transmembrane protein with an intracellular PDZ domain, two extracellular cysteine-rich domains and 10 extracellular leucine-rich repeats. Reproduced from Linhoff et al, 2009 without permission

negative regulator of synapse maturation, the decrease spine density in Arc knockout mice is confusing and may indicate that compensatory mechanisms in the Arc knockout animals drive spine loss. From a functional standpoint, Arc appears to be a critical mediator of LTP. Infusion of Arc antisense oligonucleotides impairs the maintenance phase of HFS-induced LTP within the dentate gyrus, while Arc knockout mice have enhanced early phase LTP but abolished late phase LTP (Guzowski et al., 2000; Plath et al., 2006). Interestingly, Arc antisense oligonucleotide infusion revealed that sustained Arc expression is specifically required for BDNF-induced LTP (Messaoudi et al., 2007).

The Mechanisms that Regulate LRRTM1 Expression are Unknown

LRRTM1 is a type-1 transmembrane protein that participates in synaptic adhesion at excitatory synapses (Figure 4.2; Bottom). LRRTM1 is part of a four gene family (LRRTM1-4) that is expressed with regional specificity within the central nervous system (Laurén et al., 2003). LRRTM1 is predominantly expressed within the cortex, hippocampus, thalamus and striatum. The LRRTM1 gene is located on the opposite strand of the α-catenin 2 gene, and a single nucleotide polymorphism in the putative bi-directional promoter of LRRTM1 is associated with schizophrenia and left-handedness (Francks et al., 2007; Kask et al., 2011). However, other than a general characterization of its promoter, little is known about the mechanisms that regulate LRRTM1 transcription. The LRRTM1 gene encodes for a 522 amino acid type-I transmembrane protein that is produced from a single exon. The N-terminus of LRRTM1 contains 10 leucine-rich repeats, which are evolutionarily conserved domains that mediate a wide range of protein-protein interactions. The extreme C-terminus of LRRTM1 contains a four amino acid E-C-E-V PDZ domain, which may anchor LRRTM1 within the post-synaptic density (Laurén et al., 2003). Similar to neuroligins, it appears that the extracellular domain of LRRTM1 interacts with the presynaptic neurexins (Siddiqui et al., 2010; de Wit et al., 2009). LRRTM1 overexpression within Cos cells that were co-cultured with primary hippocampal neurons caused synaptophysin and VGlut1 positive specializations to form on the surface of the Cos cells. LRRTM1 overexpression within neurons was sufficient to induce the

clustering of presynaptic VGlut1 and post-synaptic PSD-95 but not gephyrin. In addition, artificial clustering of LRRTM1 with beads is sufficient to induce the clustering of NMDAR subunits, suggesting that LRRTM1 is sufficient to mediate the formation of functional post-synaptic sites (Linhoff et al., 2009). Similar to what was observed for the neuroligins, LRRTM1 single knockout mice have a subtle synaptic phenotype that is characterized by a more diffuse collection of presynaptic vesicles and elongated dendritic spines, two characteristics which are reminiscent of immature excitatory synapses (Takashima et al., 2011). However, in cultured hippocampal cells, simultaneous depletion of LRRTM1, LRRTM2, neuroligin-1 and neuroligin-3 caused a ~40% decrease in excitatory synaptic puncta density that was dependent upon neuronal activity (Ko et al., 2011). From a functional standpoint, simultaneous knockdown of LRRTM1 and LRRTM2 impairs hippocampal LTP in CA1, while LRRTM1 knockout mice have an altered behavioral response when presented with novel objects and they display a peculiar aversion to small spaces (Soler-Llavina et al., 2013; Voikar et al., 2013).

Arc and LRRTM1 have the potential to mediate unique aspects of excitatory synapse development. Based on previous work within the lab, we identified Arc and LRRTM1 as putative BDNF targets in vivo. In the following section, I will present my research investigating the role of Arc and LRRTM1 during the process of BDNF-induced excitatory synapse and dendrite formation.

4.4 Results: The Role of Arc and LRRTM1 During BDNF-Induced Excitatory Synapse Formation

Microarray analysis revealed that conditional deletion of BDNF from the forebrain results in mRNA expression changes in the striatum that are similar to those changes observed in the brains of human Huntington's disease patients. Since microarray analysis is prone to producing false positive results, it is necessary to validate microarray expression changes with an independent method. To accomplish this, I used qRT-PCR to assess the expression of a handful of differentially expressed genes that could participate in the formation and/or stabilization of dendrites and synapses. We chose genes based on the strength of their P-values and their potential to mediate synapse development. The genes

were grouped into four classes. The first class consisted of endoplasmic reticulum calcium channels (ryanodine receptor 1, RYR1; ryanodine receptor 3, RyR3; inositol triphosphate receptor 1, ITPR1), which contribute to calcium-induced calcium release, a known regulator of post-synaptic plasticity. The second class consisted of activity-induced immediate-early genes (Arc; Homer1a; cFos), each of which had previously been linked to synaptic plasticity. The third class consisted of adhesion molecules (LRRTM1; cadherin 13, Cdh13), which can mediate interactions between axons and dendrites. The final gene was Caspase 2, which was upregulated in the absence of BDNF and has been implicated as a positive regulator of neurodegeneration. Linear regression revealed a strong correlation (r^2=0.960) between expression changes detected via microarray analysis and the expression changes determined with qRT-PCR, suggesting that the striatal microarray results reflect actual changes in mRNA expression for a number of individual genes (Figure 4.3A). In addition, our analysis specifically confirmed that both Arc and LRRTM1 are downregulated within the striatum of BDNF fsKO mice. We chose to continue our analysis by further characterizing Arc and LRRTM1 (Figure 4.3B), as the literature suggested that they represented the most direct link to excitatory synapse modulation.

The above results suggest that BDNF is required for Arc and LRRTM1 mRNA expression *in vivo*. However, as the analysis was performed at P35 on striatal RNA, these results provide little insight into the directness between BDNF levels and Arc and LRRTM1 expression within the cortex. Therefore, to determine whether BDNF acutely regulates Arc and LRRTM1 mRNA levels, I used qRT-PCR to analyze their expression within primary cortical cultures that were treated with 25 ng/ml BDNF. To assess early BDNF-induced responses, I analyzed Arc and LRRTM1 mRNA expression after 4 hours of BDNF treatment. Similar to what has been observed in other labs, a single dose of BDNF caused a dramatic ~25-fold increase in the abundance of Arc mRNA (Figure 4.3C; Left). However, acute BDNF administration did not alter the abundance of LRRTM1 mRNA, although a more prolonged BDNF treatment over the course of 48 hours did modestly increase LRRTM1 mRNA abundance (Figure 4.3C;

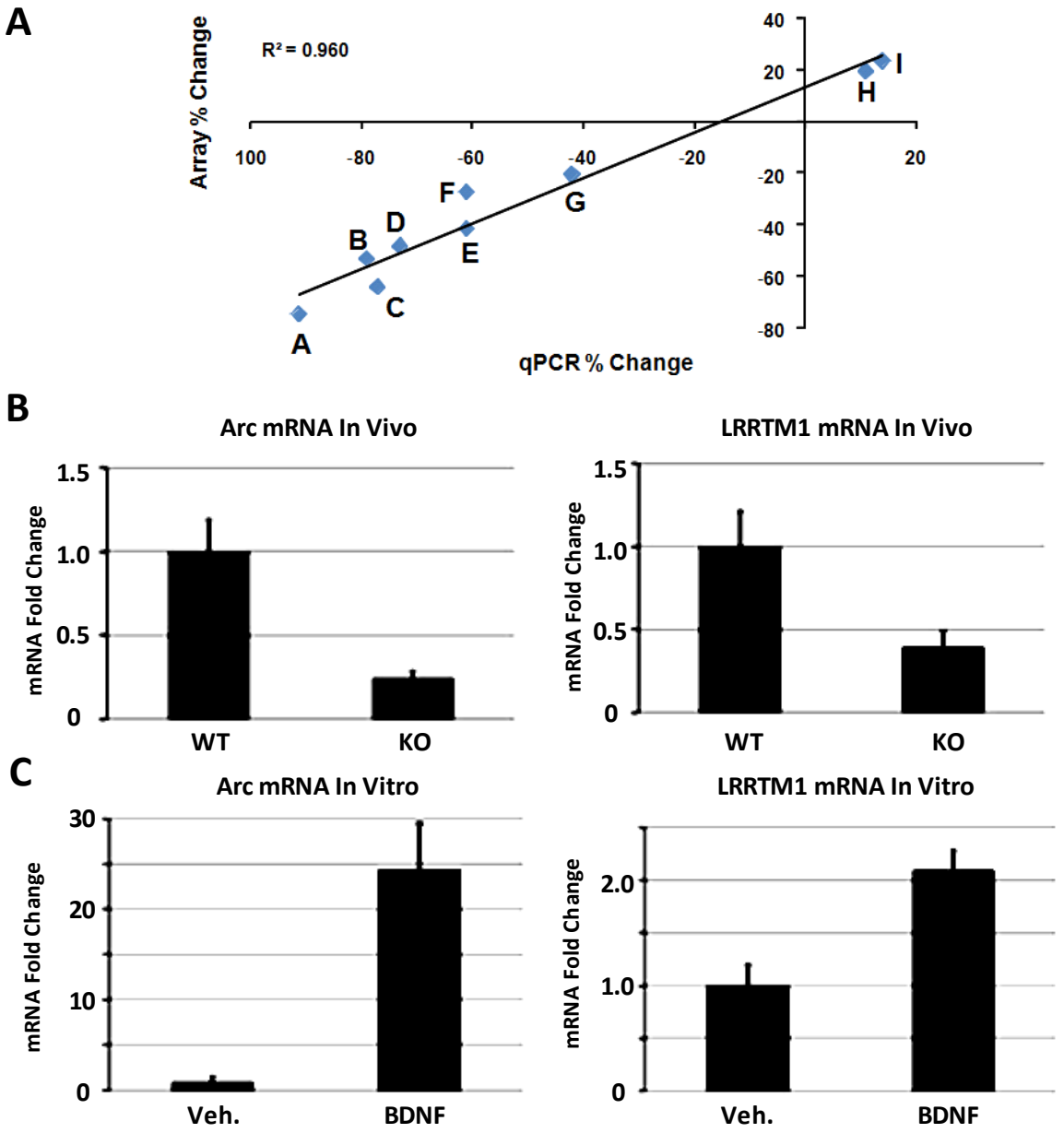

Figure 4.3. Striatal microarray validation and BDNF-induced Arc and LRRTM1 mRNA expression. A) Correlation plot comparing the microarray mRNA expression % change (Y-Axis) versus qRT-PCR mRNA expression % change (X-Axis) in P35 BDNF fsKO striatum. (A) RyR1, (B) cFos, (C) Arc, (D) Homer, (E) LRRTM1, (F) ITPR1, (G) RyR3, (H) Casp2, (I) Cdh13. Individual squares represent the average expression level. **B)** Arc and LRRTM1 mRNA expression in P35 BDNF fsKO striatum normalized to P35 WT striatum as detected with qRT-PCR. **C)** Arc and LRRTM1 mRNA expression in 12 DIV BDNF stimulated primary cultures normalized to vehicle stimulated cultures. For Arc, 25 ng/ml BDNF was applied as a single 4 hour dose. For LRRTM1, 25 ng/ml BDNF was applied as 4 consecutive 12 hour doses (48 hours total). B and C represent the average expression in 4 independent samples. Error bars represent SEM. * $p<0.05$; ** $p<0.01$.

Right). These results suggest that BDNF is sufficient to acutely increase the abundance of Arc mRNA, while chronic BDNF administration is sufficient to increase LRRTM1 mRNA abundance.

Acute BDNF stimulation causes a dramatic increase in the abundance of Arc mRNA, while chronic BDNF stimulation causes a much more modest increase in the abundance of LRRTM1 mRNA. To determine whether these changes reflect altered protein expression, I turned to the protein synthesis reporter system TimeStamp (TS). TimeStamp is a fusion protein cloned in frame with a gene of interest in which an epitope tag is situated downstream of a rapidly acting and self-cleaving Hepatitis C viral protease, which is potently inhibited by a cell permeable compound (BILN2061) (Figure 4.4A). Therefore, in the absence of BILN, the epitope tag is cleaved and the protein of interest is untagged, while in the presence of BILN, the epitope tag is retained and can be used to visualize the protein population that is translated after the addition of BILN (Lin et al., 2008). TimeStamp is useful because it allows one to estimate protein expression in the absence of a reliable antibody against the endogenous protein, and, further, because it allows one to localize the population of newly synthesized proteins.

Arc antibodies are available, while a reliable LRRTM1 antibody has not been described. Therefore, to determine whether TimeStamp provides an accurate representation of BDNF-induced protein synthesis in primary cortical cultures, I compared the expression of endogenous Arc to the expression of Arc-TS via western blot (Figure 4.4B). I chose a 12 hour BDNF stimulation to match the results in Chapter 3, which documented that a single 12 hour dose of BDNF is correlated with increased spontaneous network activity and synapse formation. As previously reported, unstimulated primary cortical cultures display minimal Arc protein expression. However, upon treatment with BDNF, Arc protein expression was induced as demonstrated by a single Arc immunoreactive band at approximately 50 kDa. To evaluate the expression of Arc-TS, cortical cultures were transfected with Arc-TS plasmid and 24 hours later BILN was added to the culture media along with either vehicle or BDNF and Arc-TS was detected via western blot with HA antibody. The Arc-TS expression profile was nearly identical to

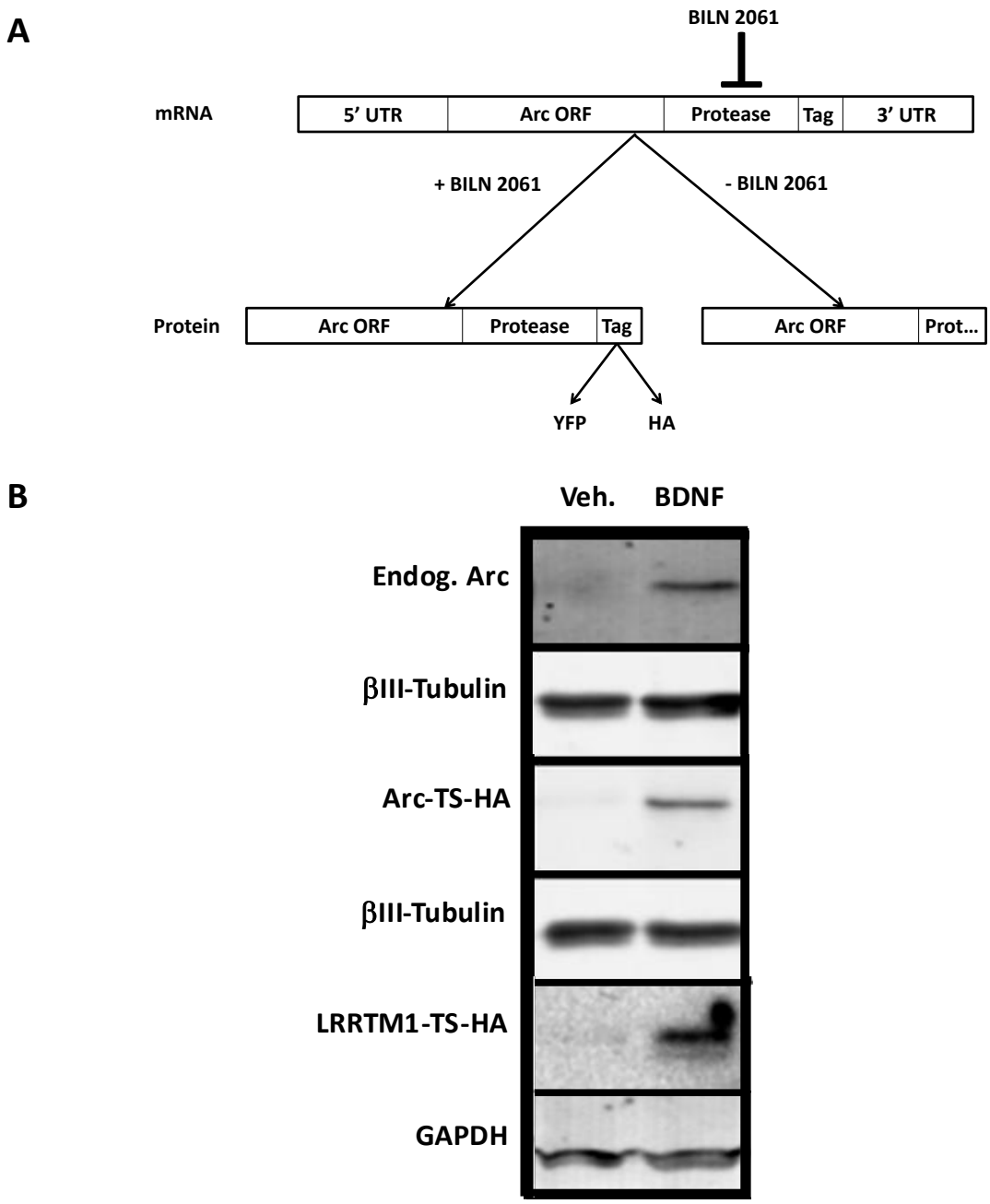

Figure 4.4. TimeStamp analysis of BDNF-induced Arc and LRRTM1 expression. A) A schematic representing the TimeStamp concept. The TimeStamp tag is a fusion protein consisting of a rapid, self-cleaving hepatitis C viral protease in frame with an epitope tag. In the absence of the protease inhibitor, BILN2061, the protease cleaves the epitope tag, rendering the fusion protein undetectable. In the presence of the protease inhibitor, the protease is inactive and all fusion proteins translated after the addition of BILN2061 will be detectable via their epitope tag. **B)** Western blot analysis of endogenous Arc, Arc-TS and LRRTM1-TS after 12 hours of BDNF stimulation in 12 DIV primary cortical cultures. 12 hours after transfection (mock transfection for endogenous Arc), 2 mm BILN was coapplied with vehicle or 25 ng/ml BDNF for an additional 12 hours. Lysates were harvested and analyzed via western blot with the indicated antibodies. TimeStamped proteins were detected with anti-HA.

endogenous Arc, suggesting that Arc-TS is a reasonable proxy for endogenous Arc protein synthesis. Next, I assessed the expression of LRRTM1-TS using the same transfection and stimulation paradigm. Similar to Arc-TS, LRRTM1-TS was barely detectable in unstimulated primary cortical cultures, and application of a single dose of BDNF increased LRRTM1-TS expression to detectable levels. These results suggest that TimeStamp reports aspects of endogenous protein expression regulation. Further, they suggest that acute BDNF stimulation is sufficient to increase the abundance of Arc and LRRTM1 TimeStamped proteins when their mRNA is artificially produced via transfection.

It has been demonstrated that both Arc and LRRTM1 localize to excitatory synapses. In the case of Arc, there is considerable evidence that newly-synthesized Arc protein targets to dendritic spines and excitatory synapses. However, the accumulation of newly synthesized LRRTM1 at excitatory synapses has not been analyzed. In order to assess the neuronal distribution of BDNF-induced Arc-TS and LRRTM1-TS, I co-transfected primary cortical cultures with mCherry and Arc-TS or LRRTM1-TS and performed immunofluorescence for HA to visualize BDNF-induced TimeStamped proteins. Similar to the results obtained via western blot, mCherry positive neurons in unstimulated cultures displayed miniscule HA immunoreactivity. However, upon BDNF stimulation, Arc-TS and LRRTM1-TS became readily detectable (Figure 4.5). In terms of their cellular distribution, both Arc-TS and LRRTM1-TS were localized throughout the somatodendritic compartment. However, whereas the TimeStamped proteins displayed homogeneous accumulation in the soma itself, both Arc-TS and LRRTM1-TS accumulated at discrete puncta throughout the proximal dendritic arbor. To determine if the Arc-TS and LRRMT1-TS punctae represented excitatory synapses, I co-transfected cultures with mCherry and Arc-TS or LRRTM1-TS and performed immunofluorescence for HA and the presynaptic excitatory synapse marker, VGlut1. Although some dendritic branches displayed a diffuse accumulation of Arc-TS and LRRTM1-TS, a fraction

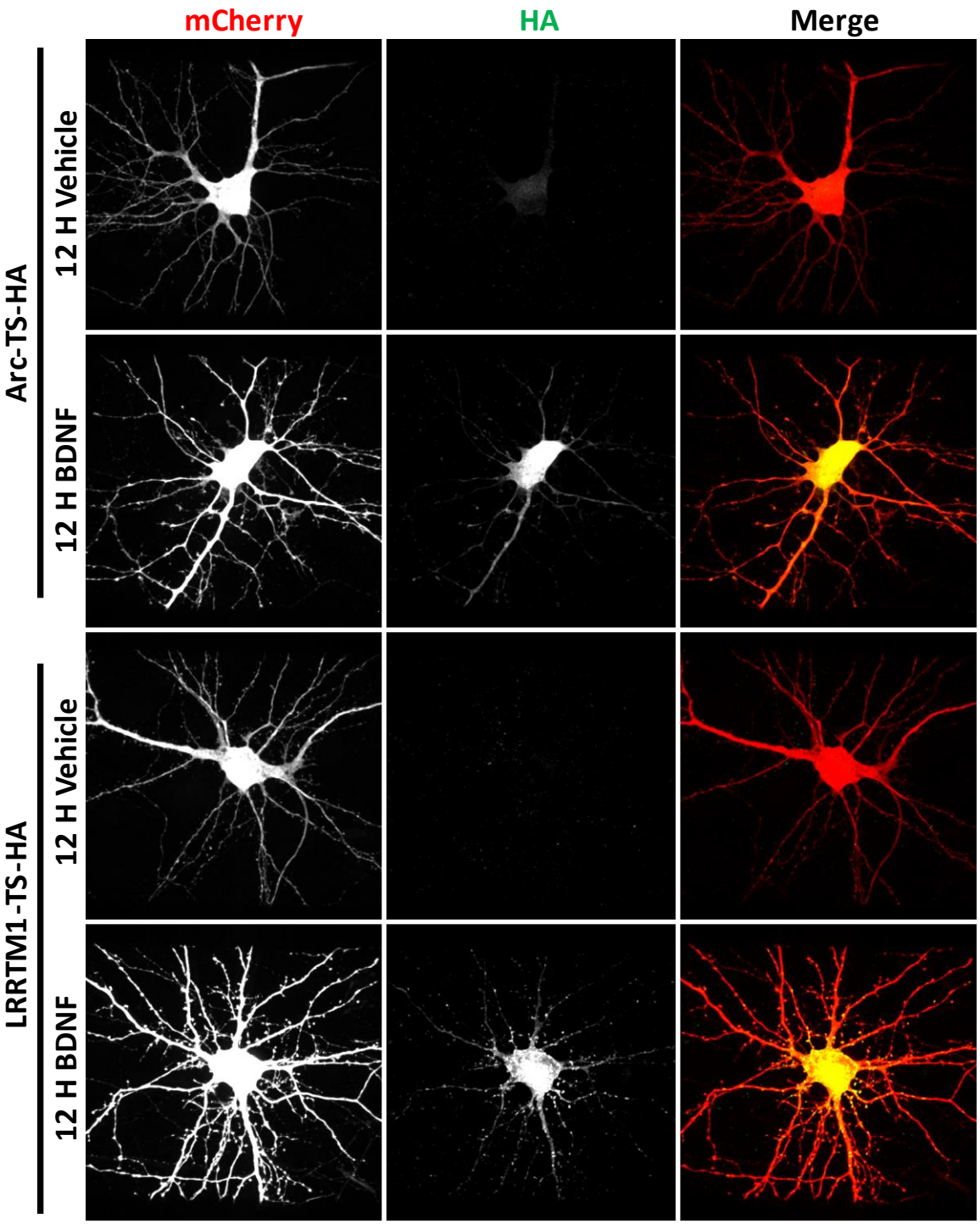

Figure 4.5. Analyzing the gross localization of BDNF-induced Arc and LRRTM1 within primary cortical neurons. Primary cortical cultures were transfected and treated with BILN and BDNF as in Figure 4.4 except that cultures were co-transfected with mCherry to visualize neuronal morphology. TimeStamped proteins (Arc, Top; LRRTM1, Bottom) were visualized using immunocytochemistry with anti-HA antibodies. Upon stimulation with BDNF Arc and LRRTM1 accumulate within the cell soma and the proximal dendritic arbor. Somatic accumulation is uniform and intense. Accumulation within dendrites is more punctate.

of the more punctate Arc-TS and LRRTM1-TS signal was localized to dendritic protrusions, presumably dendritic spines, that colocalized with VGlut1 (Figure 4.6). Collectively, these results suggest that BDNF-induced Arc-TS and LRRTM1-TS rapidly accumulate at excitatory synapses.

A fraction of BDNF-induced Arc and LRRTM1 localizes to excitatory synapses, which may indicate that Arc and/or LRRTM1 proteins may be directly participating in the process of BDNF-induced excitatory synapse formation and/or modification. If this is the case, over-expression of Arc and/or LRRTM1 should modulate the number of excitatory synapses. To address this possibility, I co-transfected primary cortical neurons with GFP and Arc or LRRTM1 V5 epitope-tagged fusion proteins and quantified the number of VGlut1 punctae and the dendrite length of vehicle- stimulated and BDNF-stimulated neurons. The analysis of dendrite length and VGlut1 punctae was performed in an identical fashion and are reported as the total length within the proximal arbor as well as in size binned increments. Arc-V5 overexpression did not have any effect on the number of excitatory synapses or dendrite length. However, LRRTM1-V5 overexpression significantly increased the total number of VGlut1 punctae without altering total dendrite length (Figure 4.7; Top and Figure 4.8; Top). A Sholl-type distance analysis revealed that LRRTM1-V5 overexpression increased the number of VGlut1 punctae throughout the majority of the proximal arbor. To determine if LRRTM1-V5 overexpression saturated the system and rendered neurons incapable of undergoing BDNF-induced excitatory synapse formation, I analyzed the response of LRRTM1-V5 overexpressing neurons that were stimulated with recombinant BDNF. This analysis revealed that BDNF stimulation and LRRTM1 overexpression combine to produce an additive increase in the number of VGlut1 punctae, with the most striking additive effect occurring in the more proximal regions of the neuron (Figure 4.8; Bottom).

The overexpression analysis indicated that BDNF and LRRTM1 display an additive effect on excitatory synapse numbers, while Arc overexpression did not influence excitatory synapse number. However an additive interaction does not imply that LRRTM1 is required for BDNF-induced excitatory

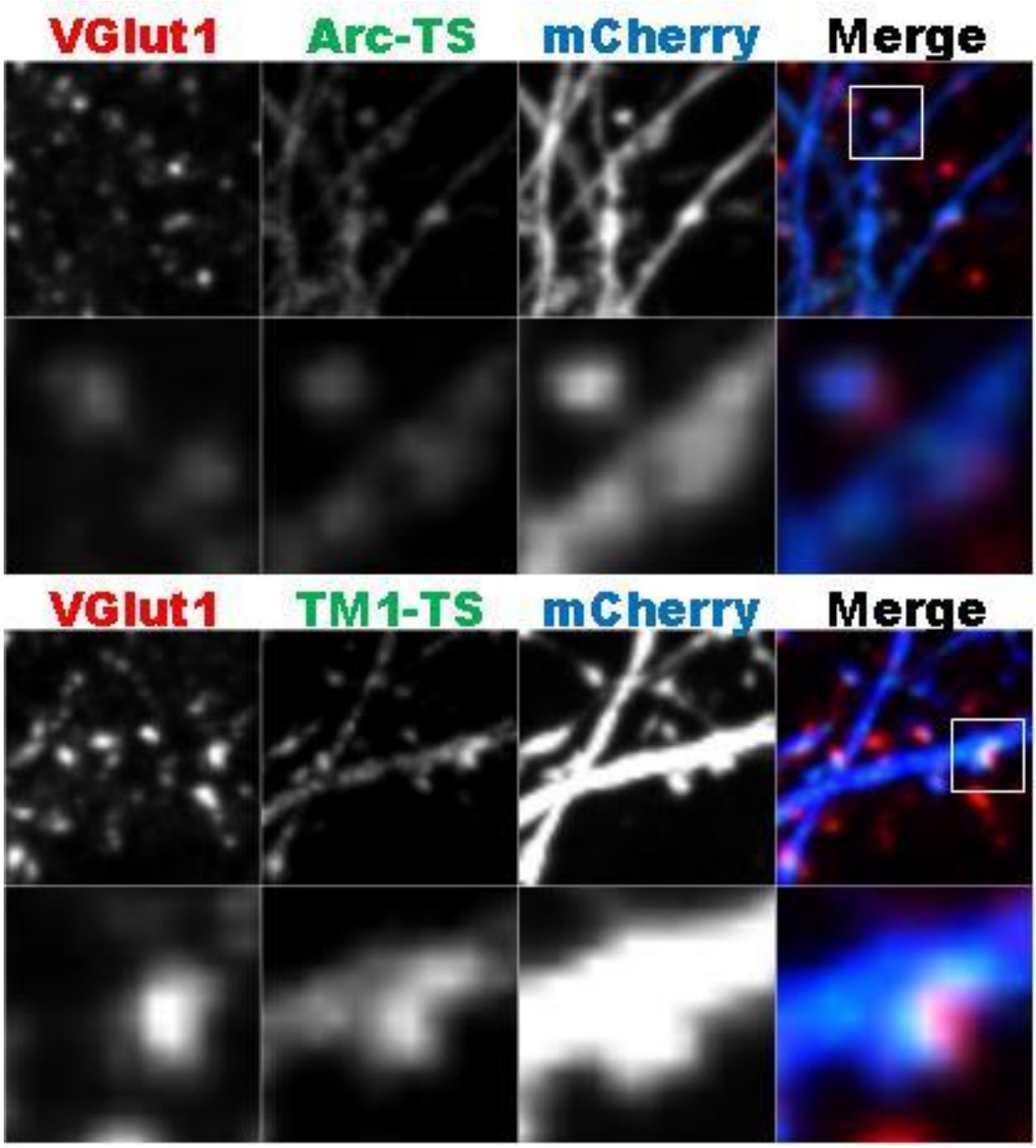

Figure 4.6. Analyzing the synaptic localization of BDNF-induced Arc and LRRTM1 within primary cortical neurons. Primary cortical cultures were transfected and treated with BILN and BDNF as in Figure 4.5. TimeStamped proteins (Arc, Top; LRRTM1, Bottom) were visualized using immunocytochemistry with anti-HA antibodies and excitatory synapses were visualized with the presynaptic excitatory synapse marker VGlut1. Upon stimulation with BDNF Arc and LRRTM1 accumulate within a subset of mCherry positive dendritic protrusions that are also positive for VGlut1, suggesting dendritic spine synapses.

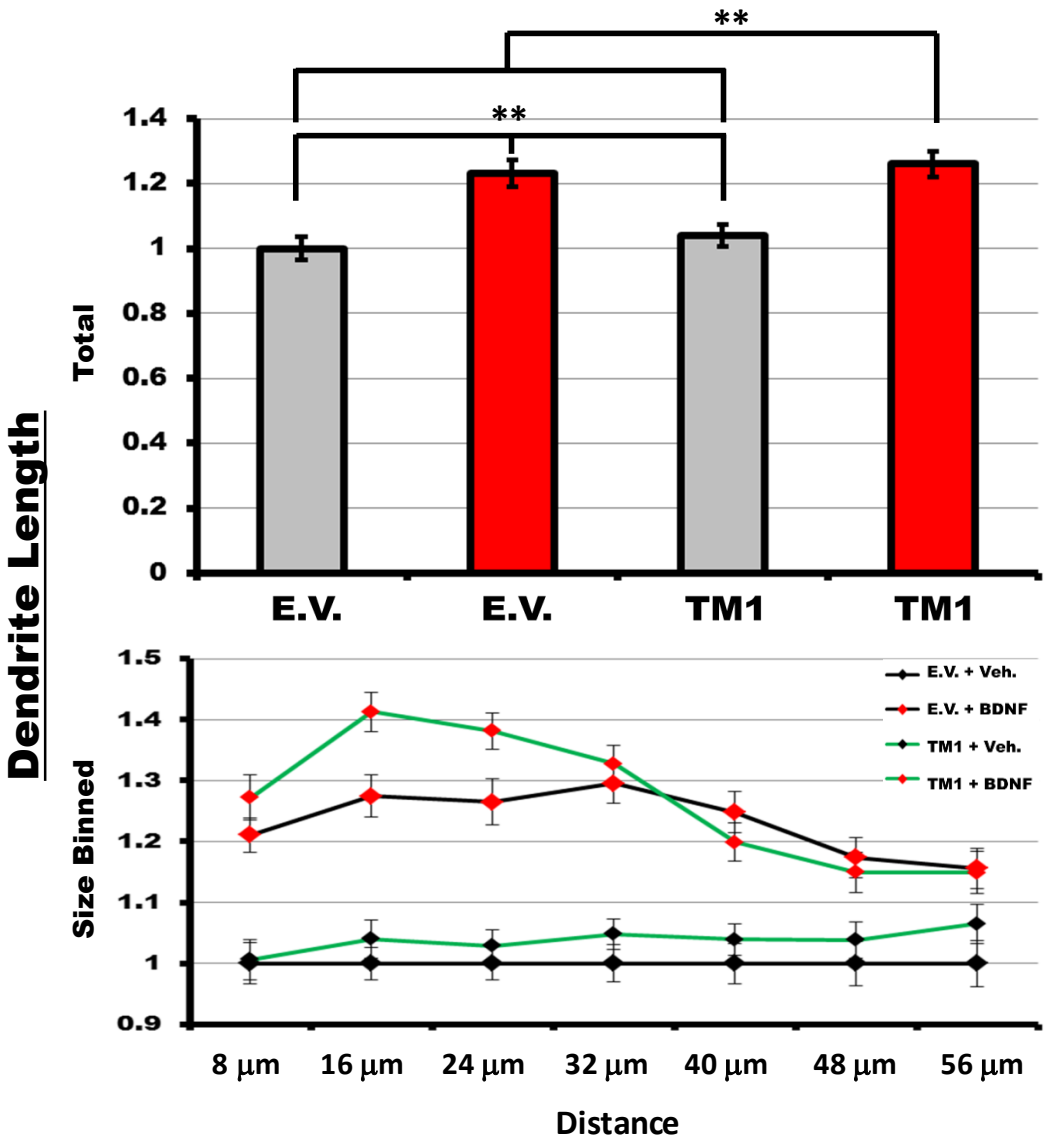

Figure 4.7. Evaluating the effect of BDNF and LRRTM1 on total dendrite length within the proximal dendritic arbor. 13 DIV primary cortical cultures were co-transfected with GFP and pcDNA3.1 (E.V.) or LRRTM1-V5. Cultures were treated at 13.5 DIV with vehicle or 5 ng/ml BDNF for an additional 12 hours. Total dendrite length was measured using the algorithm developed in Chapter 2. (Top) Bar graphs representing the average total dendrite length normalized to the E.V./vehicle condition. Red bars represent BDNF treated cultures. Grey bars represent vehicle treated cultures. n=45 neurons. ** $p<0.01$ assessed with ANOVA and Tukey post-test. (Bottom) Line graphs representing the average total dendrite length at a specific distance from the neuron soma normalized to the E.V./vehicle condition. Black lines represent E.V. transfected cultures. Green lines represent LRRTM1-V5 transfected cultures. Black squares indicate vehicle treatment. Red squares represent BDNF treatment.

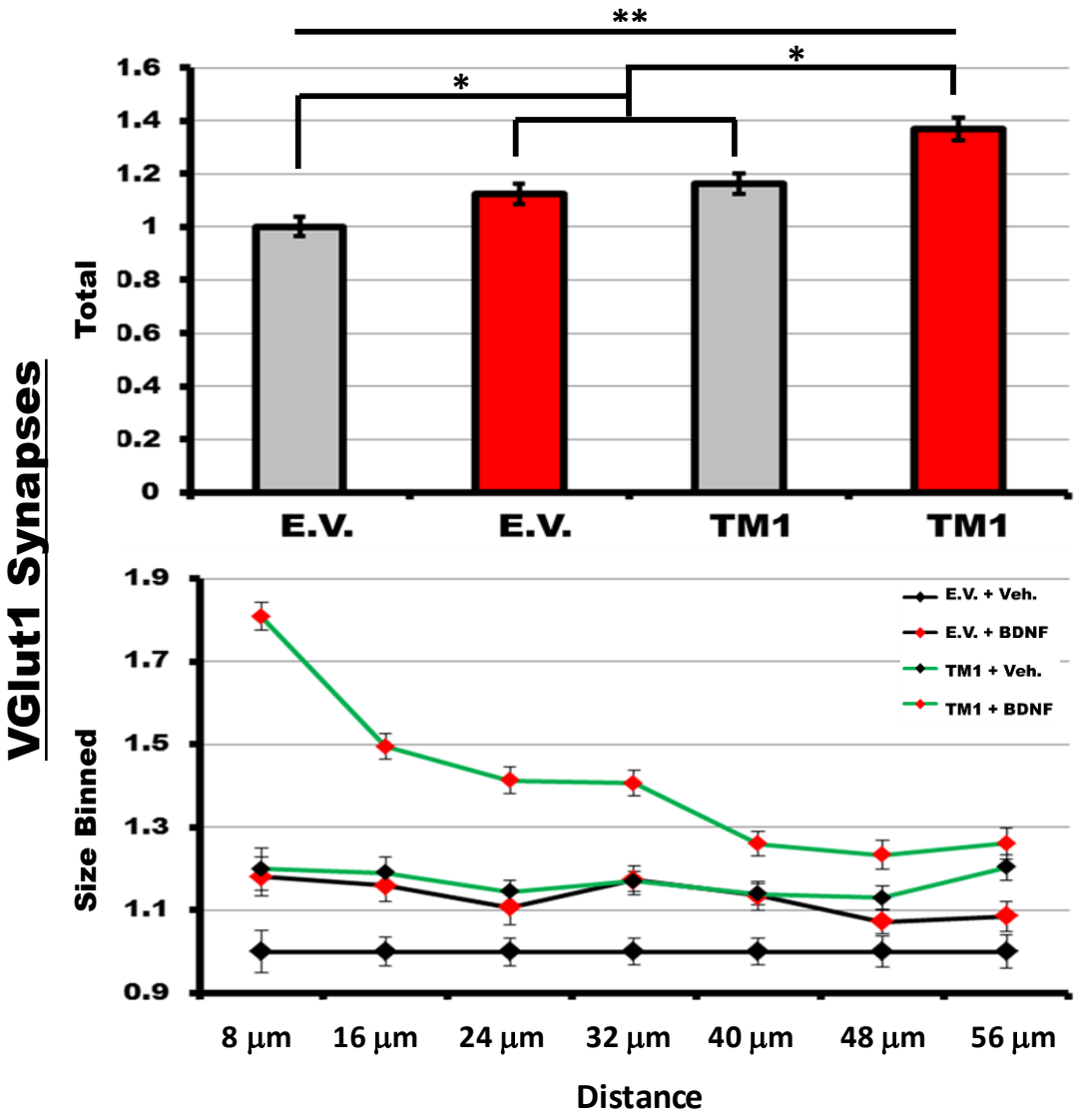

Figure 4.8. Evaluating the effect of BDNF and LRRTM1 on the total number of VGlut1 synapses within the proximal dendritic arbor. 13 DIV primary cortical cultures were co-transfected with GFP and pcDNA3.1 (E.V.) or LRRTM1-V5. Cultures were treated at 13.5 DIV with vehicle or 5 ng/ml BDNF for an additional 12 hours. Total dendrite length was measured using the algorithm developed in Chapter 2. (Top) Bar graphs representing the average total number of VGlut1 synapses normalized to the E.V./ vehicle condition. Red bars represent BDNF treated cultures. Grey bars represent vehicle treated cultures. n=45 neurons. ** $p<0.01$ assessed with ANOVA and Tukey post-test. (Bottom) Line graphs representing the average total number of VGlut1 synapses at a specific distance from the neuron soma normalized to the E.V./vehicle condition. Black lines represent E.V. transfected cultures. Green lines represent LRRTM1-V5 transfected cultures. Black squares indicate vehicle treatment. Red squares represent BDNF treatment.

synapse formation. Similarly, Arc's inability to influence excitatory synapses does not preclude it from having during the specific process of BDNF-induced excitatory synapse formation. To determine if Arc or LRRTM1 are required for BDNF-induced synapse or dendrite formation, I reduced their expression with shRNA and assessed BDNF's ability to increase the number of excitatory synapses and dendrite length. First, I evaluated the efficacy of Arc and LRRTM1 shRNA and determined that Arc shRNA completely blocked BDNF-induced Arc-TS expression, while LRRTM1 shRNA was only ~70% efficient (Figure 4.9). Next, I determined whether Arc or LRRTM1 expression were required for BDNF-induced excitatory synapse formation by blocking their expression with the shRNAs validated above. In contrast to the overexpression analysis, LRRTM1 shRNA did not affect the baseline number of VGlut1 punctae, nor did it block a BDNF-induced increase in the number of VGlut1 punctae (Figure 4.10 and Figure 4.11). Similarly, Arc shRNA did not alter the baseline density of VGlut1 punctae. However, Arc shRNA completely blocked a BDNF-induced increase in VGlut1 punctae (Figure 4.12). In addition, Arc shRNA blocked BDNF-induced dendrite elongation by ~ 60% (Figure 4.13). Collectively, these results suggest that BDNF-induced Arc synthesis is required for the formation of BDNF-induced excitatory synapses and dendrites.

Arc is required for the formation and/or elongation of BDNF-induced dendrites. However, Arc's role in this process is not clear. Since Arc is thought to play a role in the synapse maturation and the maturation of synapses on new dendrites is believed to contribute to dendrite stabilization, I hypothesized that BDNF-induced Arc may localize to nascent dendrites allowing it to directly participate in synapse maturation. To test this hypothesis, I co-transfected cortical neurons with mCherry and Arc-TS-YFP, which acquires YFP fluorescence in the presence of BILN, and I tracked the localization of BDNF induced Arc within BDNF-induced dendrites. Similar to the results in Chapter 3, BDNF induced the formation of dendrites with filopodia, and in a fraction of these dendrites I observed the accumulation of Arc-TS-YFP puncta, suggesting that BDNF-induced Arc protein may directly participate in the stabilization of nascent dendrites (Figure 4.14).

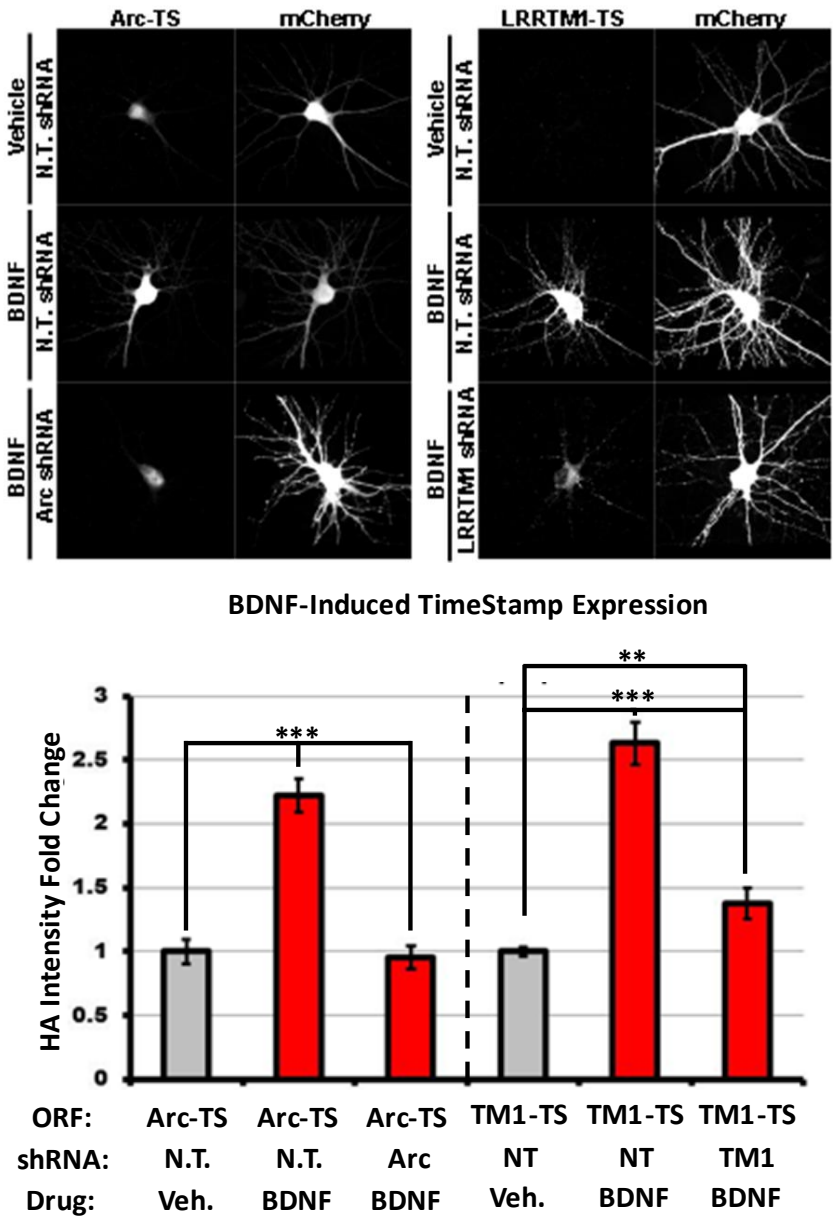

Figure 4.9. Assessing the efficacy of Arc and LRRTM1 shRNA to block BDNF-induced protein accumulation using the TimeStamp system. 12 DIV primary cortical cultures were triple transfected with TimeStamp constructs (Arc-TS or LRRTM1-TS), shRNA constructs (N.T. = non targeting; Arc = Arc shRNA; LRRTM1= LRRTM1 shRNA) and mCherry. 12 hours after transfection, cultures were stimulated with 2 mm BILN along with vehicle or 5 ng/ml BDNF. TimeStamp accumulation was assessed with anti-HA and anti-mCherry immunocytochemistry. Quantification was performed by normalizing the HA intensity to mCherry intensity on a per neuron basis. The average mCherry-normalized HA intensity for each condition was then normalized to the N.T./vehicle condition. The BDNF-induced increase is represented by the increase in HA intensity between the N.T./vehicle condition compared to the N.T./BDNF condition. The shRNA efficacy is represented by the decrease in HA intensity between the N.T./BDNF condition and the Arc/BDNF or LRRTM1/BDNF condition. **A)** Representative images. **B)** Summary quantification. Error bars represent SEM with n=30 neurons. ** p<0.01; *** p<0.001 assessed with ANOVA and Tukey post-test.

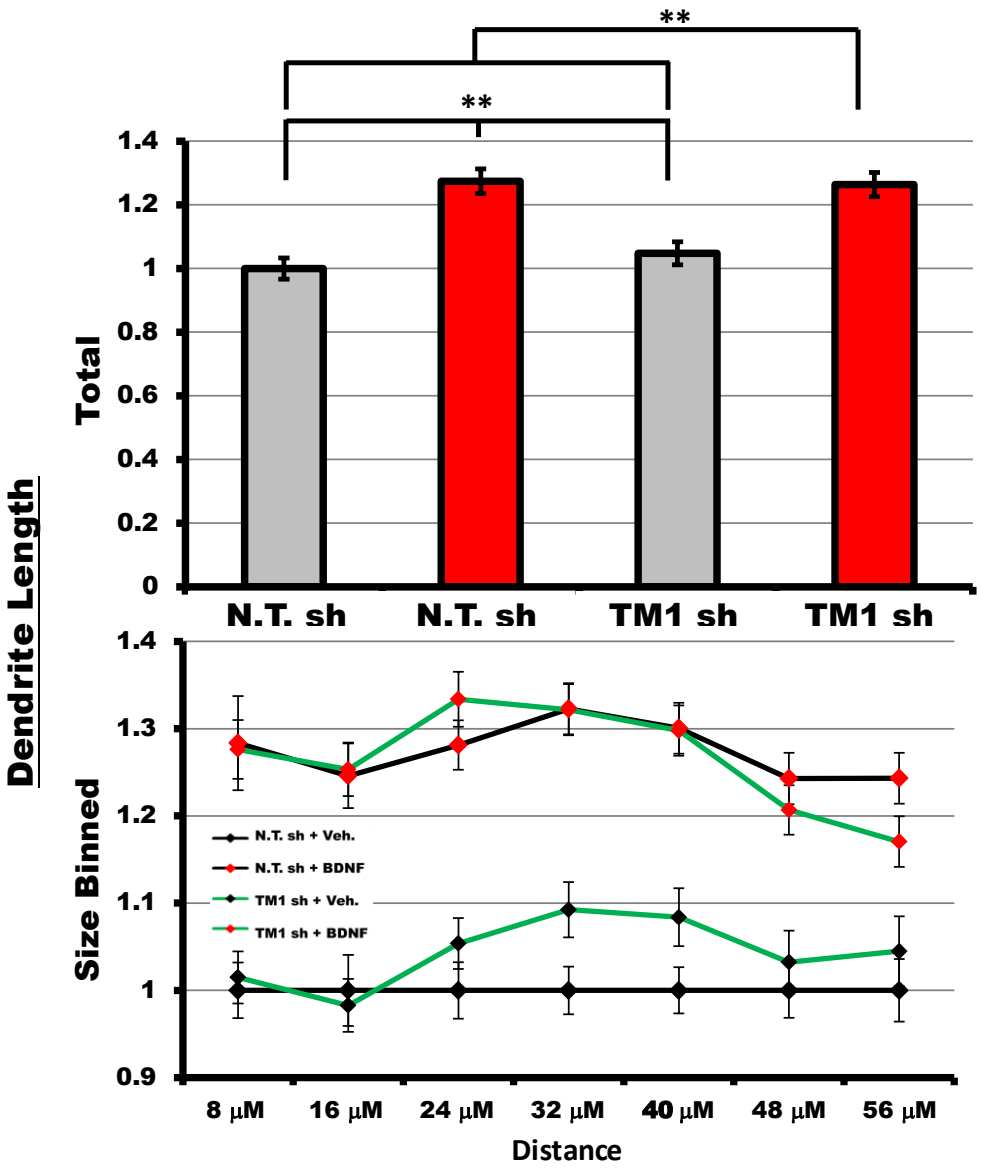

Figure 4.10. Evaluating the effect of LRRTM1 shRNA on total dendrite length within the proximal dendritic arbor. 13 DIV primary cortical cultures were co-transfected with GFP and non-targeting shRNA (N.T. sh) or LRRTM1 shRNA (TM1 sh). Cultures were treated at 13.5 DIV with vehicle or 5 ng/ml BDNF for an additional 12 hours. Total dendrite length was measured using the algorithm developed in Chapter 2. (Top) Bar graphs representing the average total dendrite length normalized to the N.T. sh/ vehicle condition. Red bars represent BDNF treated cultures. Grey bars represent vehicle treated cultures. n=45 neurons. *p<0.05;** p<0.01 assessed with ANOVA and Tukey post-test. (Bottom) Line graphs representing the average total dendrite length at a specific distance from the neuron soma normalized to the E.V./vehicle condition. Black lines represent N.T. shRNA transfected cultures. Green lines represent LRRTM1 shRNA transfected cultures. Black squares indicate vehicle treatment. Red squares represent BDNF treatment.

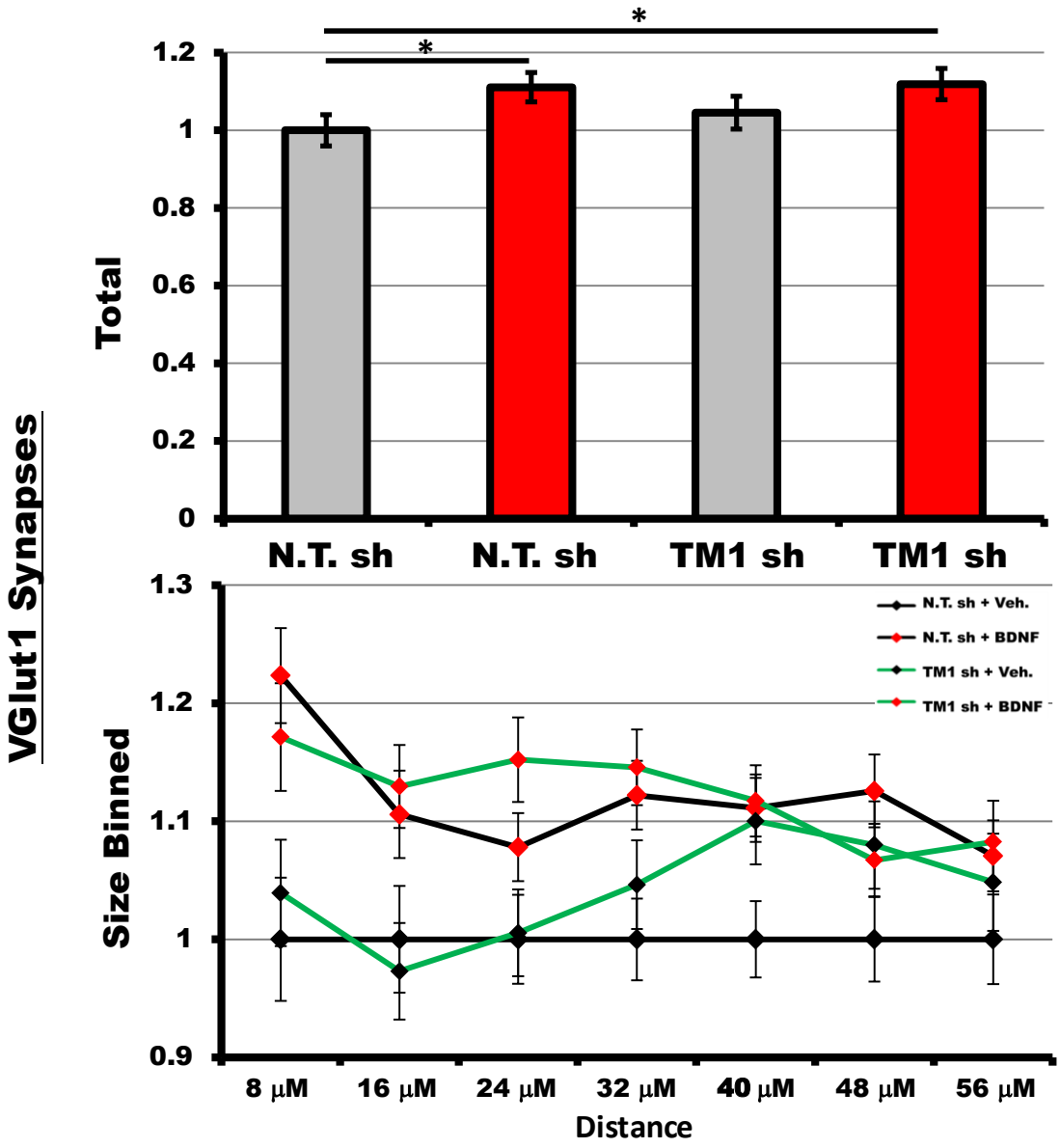

Figure 4.11. Evaluating the effect of LRRTM1 shRNA on BDNF-induced increases in VGlut1 synapses in the proximal arbor. 13 DIV primary cortical cultures were co-transfected with GFP and non-targeting shRNA (N.T. sh) or LRRTM1 shRNA (TM1 sh). Cultures were treated at 13.5 DIV with vehicle or 5 ng/ml BDNF for an additional 12 hours. Total dendrite length was measured using the algorithm developed in Chapter 2. (Top) Bar graphs representing the average total number of VGlut1 synapses normalized to the N.T. sh/vehicle condition. Red bars represent BDNF treated cultures. Grey bars represent vehicle treated cultures. n=45 neurons. *p<0.05;** p<0.01 assessed with ANOVA and Tukey post-test. (Bottom) Line graphs representing the average total number of VGlut1 synapses at a specific distance from the neuron soma normalized to the E.V./vehicle condition. Black lines represent N.T. shRNA transfected cultures. Green lines represent LRRTM1 shRNA transfected cultures. Black squares indicate vehicle treatment. Red squares represent BDNF treatment.

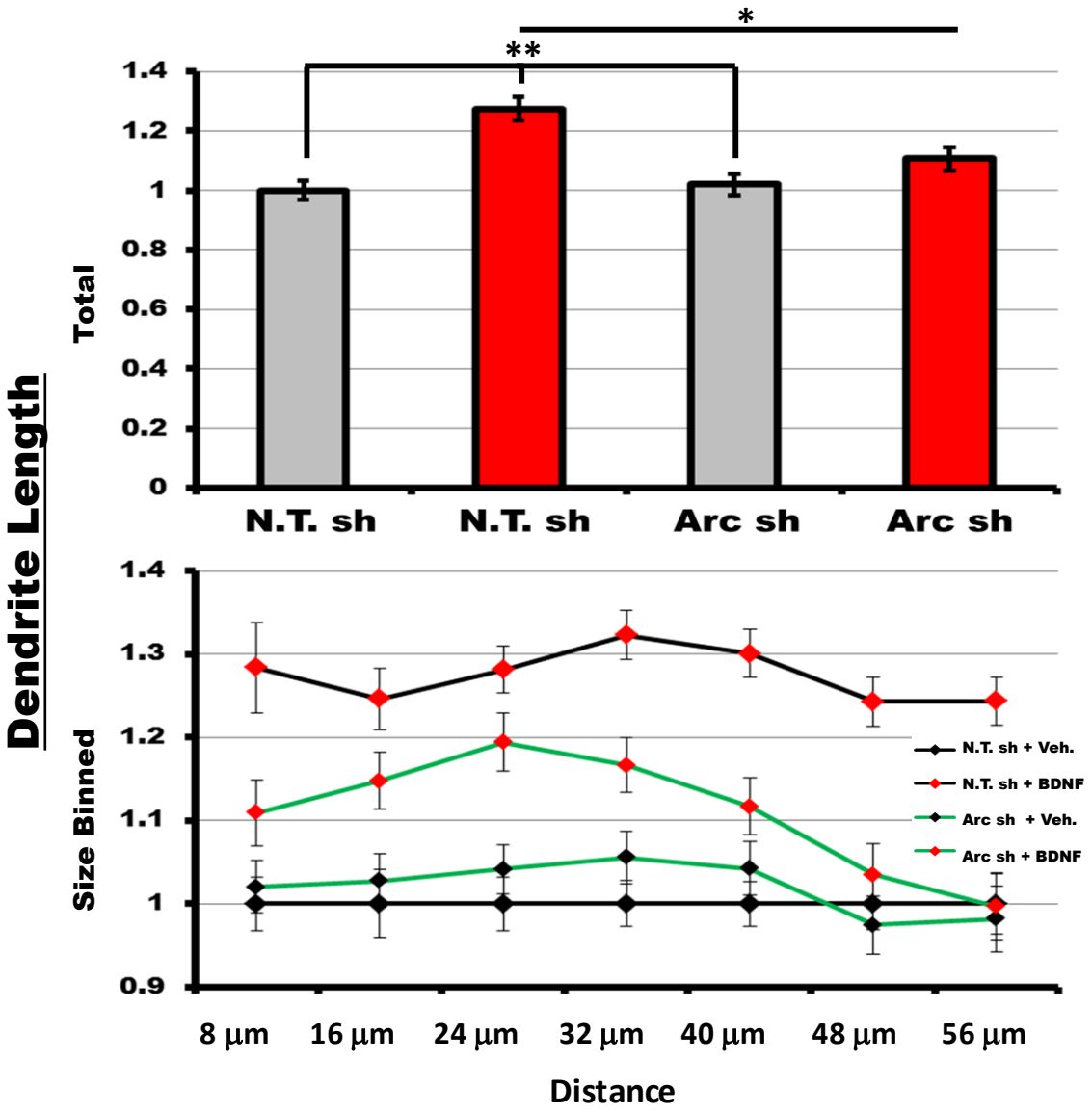

Figure 4.12. Evaluating the effect of Arc shRNA on total dendrite length within the proximal dendritic arbor. 13 DIV primary cortical cultures were co-transfected with GFP and non-targeting shRNA (N.T. sh) or Arc shRNA (Arc sh). Cultures were treated at 13.5 DIV with vehicle or 5 ng/ml BDNF for an additional 12 hours. Total dendrite length was measured using the algorithm developed in Chapter 2. (Top) Bar graphs representing the average total dendrite length normalized to the N.T. sh/vehicle condition. Red bars represent BDNF treated cultures. Grey bars represent vehicle treated cultures. n=45 neurons. *p<0.05;** p<0.01 assessed with ANOVA and Tukey post-test. (Bottom) Line graphs representing the average total dendrite length at a specific distance from the neuron soma normalized to the E.V./ vehicle condition. Black lines represent N.T. shRNA transfected cultures. Green lines represent Arc shRNA transfected cultures. Black squares indicate vehicle treatment. Red squares represent BDNF treatment.

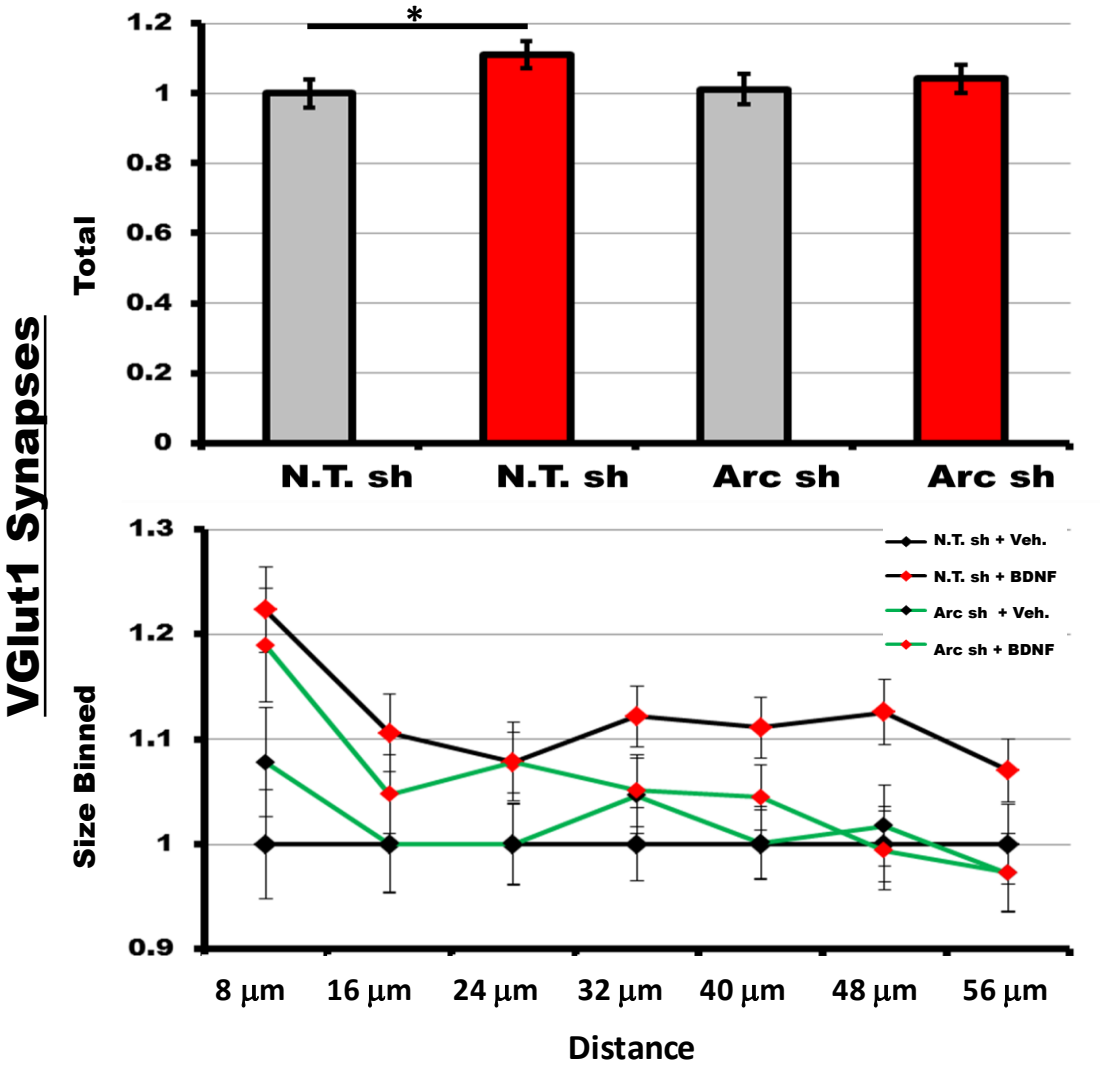

Figure 4.13. Evaluating the effect of Arc shRNA on BDNF-induced increases in VGlut1 synapses in the proximal arbor. 13 DIV primary cortical cultures were co-transfected with GFP and non-targeting shRNA (N.T. sh) or Arc shRNA (Arc sh). Cultures were treated at 13.5 DIV with vehicle or 5 ng/ml BDNF for an additional 12 hours. Total dendrite length was measured using the algorithm developed in Chapter 2. (Top) Bar graphs representing the average total number of VGlut1 synapses normalized to the N.T. sh/vehicle condition. Red bars represent BDNF treated cultures. Grey bars represent vehicle treated cultures. n=45 neurons. *p<0.05;** p<0.01 assessed with ANOVA and Tukey post-test. (Bottom) Line graphs representing the average total number of VGlut1 synapses at a specific distance from the neuron soma normalized to the E.V./vehicle condition. Black lines represent N.T. shRNA transfected cultures. Green lines represent Arc shRNA transfected cultures. Black squares indicate vehicle treatment. Red squares represent BDNF treatment.

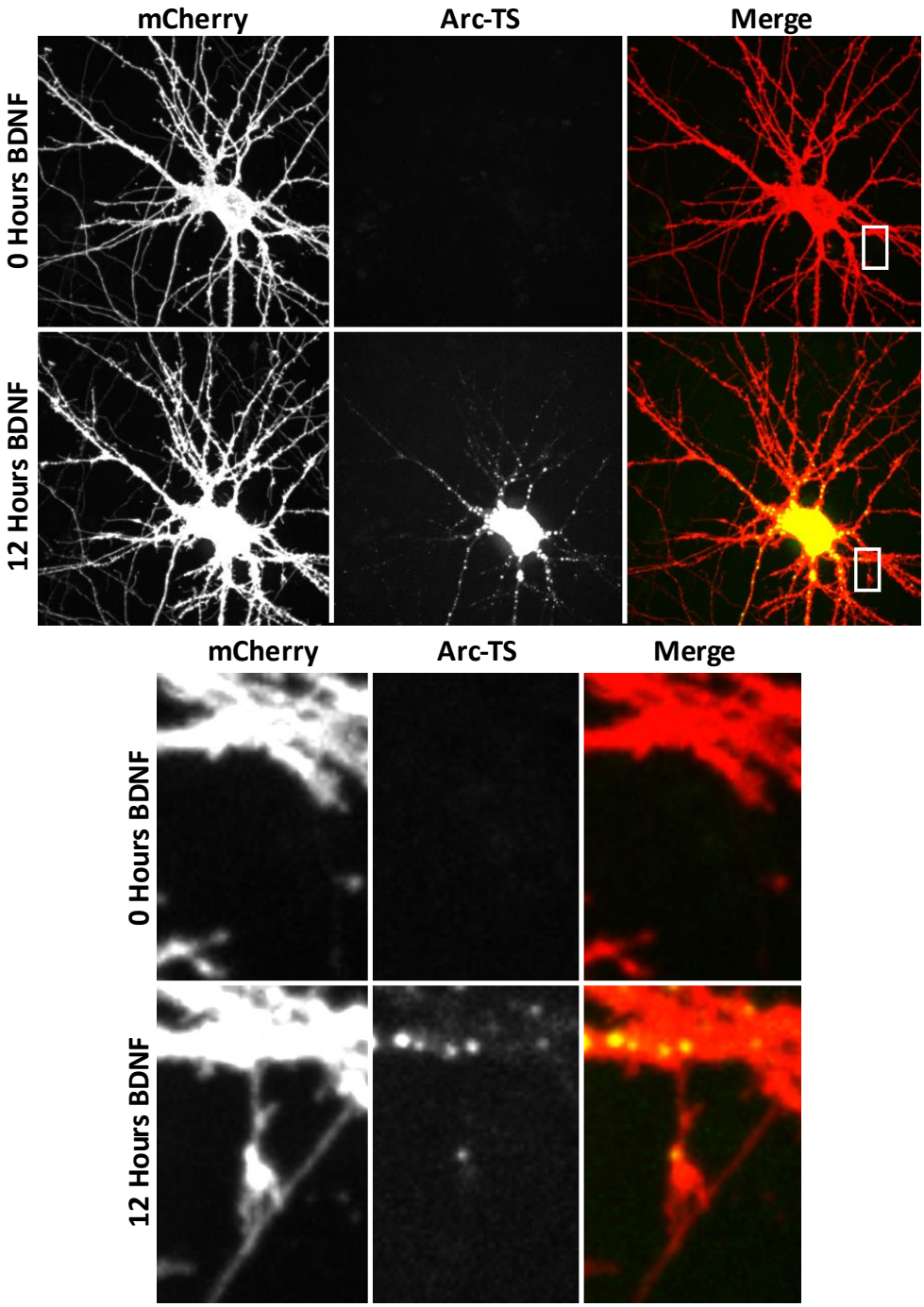

Figure 4.14. BDNF-induced Arc protein localizes to BDNF-induced dendrites. 13 DIV primary cortical cultures were co-transfected with GFP and Arc-TS-YFP. Cultures were treated at 13.5 DIV with 5 ng/ml BDNF and 2 μm BILN for an additional 12 hours and imaged with time lapse microscopy. In the top panels are the 0 hour time point and the 12 hour time point at the original magnification. Notice the expansion of the mCherry-labeled dendritc arbor by 12 hours and the accumulation of Arc-TS-YFP punctae. The white box represents the digitially zoomed panel in the bottom panels. Notice the appearance of the BDNF-induced branch that is decorated with filopodia and a single BDNF-induced Arc-YFP puncta.

4.5 Conclusions

I have confirmed that Arc is a BDNF target gene and I have identified LRRTM1 as putative BDNF target gene *in vivo* and *in vitro*. Originally identified in a microarray analysis, I validated that Arc and LRRTM1 mRNA levels are reduced within the striatum of adult forebrain-restricted BDNF knockout animals. In addition, I determined that acute BDNF administration to primary cortical cultures rapidly increases the level of Arc but not LRRTM1 mRNA, though prolonged BDNF administration is sufficient to increase LRRTM1 mRNA. Using the protein synthesis reporter TimeStamp, I documented that BDNF-induced Arc and LRRTM1 both localize to excitatory synapses and that a fraction of BDNF-induced Arc localizes to BDNF-induced dendritic branches. Overexpression analysis revealed that LRRTM1 and BDNF display an additive effect on the number of VGlut1 positive excitatory synapses within the proximal dendritic arbor. Loss-of-function analysis revealed that Arc is required for BDNF-induced excitatory synapse and dendrite formation.

4.6 Detailed Methods

Primary neuron culture, transfection, live cell microscopy and immunocytochemistry were performed with methods identical to those described in Chapters 2 and 3.

qRT-PCR Analysis

RNA was isolated according to the procedure in (Strand et al., 2007). As some of the primer combinations did not span exon/exon junctions, prior to qRT-PCR analysis RNA was treated with DNAase (Sigma) in order to degrade contaminating genomic DNA. Total RNA was then converted to cDNA using the iScript cDNA synthesis kit (BioRad). cDNA and forward and reverse primers were added to 5X Sybr-Green qRT-PCR master mix and brought to a final volume of 25 μl per reaction. Reactions were performed in 96 well plates (ISC Bioexpress) and analyzed using an Applied Biosystems 7500 Fast qRT-PCR machine. For gene expression analysis, standard curves were prepared by creating a mixture of cDNA from each experimental condition and diluting across a 4 log range (0.1 ng to 100 ng). Each primer

pair displayed linear amplification across at least 3 logs of the dilution series and standard curves were run on the same plate as the variable and control reactions. Gene expression was normalized to the expression of GAPDH or 18s rRNA.

Primers:

Caspase 2 F: ATGGCTTGCCAGAAGATACC

Caspase 2 R: AAAGGGACTGGATGAACCAC

RyR1 F: TTTGTACCCTGTCCTGTGGA

RyR1 R: GAGTCAGTGCCCAGAGTTCA

RyR3 F: ACTCCTATGGCTTTGATGGG

RyR3 R: ATGCTGGGTACTCCAAGGTC

ITPR1 F: AAGCAGCATGTGTTCCTGAG

ITPR1 R: ATTCCAGTACCCAGCTCCAC

Arc F: AGCCTACAGAGCCAGGAGAA

Arc R: AGGCAGCTTCAGGAGAAGAG

Homer1 F: TTGACCCGAACACAAAGAAG

Homer1 R: ATGTTTGGTGTGATGGTGCT

Fos1 F: GAGAAACGGAGAATCCGAAG

Fos1 R: CTGTCTCCGCTTGGAGTGTA

Cdh13 F: TGTTACACATCCACCAGCCT

Cdh13 R: GTAGTGCAGCTTCTCGTTG

LRRTM1 F: GGCTTGTTCAAGCTCACAGA

LRRTM1 R: CGAGAGAGCTGACCACAA

GAPDH F: TGTGTCCGTCGTGGATCTGA

GAPDH R: CCTGCTTCACCACCTTCTTGA

18s F: TAAAGGAATTGACGGAAGGG

18s R: CTGTCAATCCTGTCCGTGTC

Cell Lysate Preparation and Western Blotting

Cell lysates were prepared by lysing cells in the cell culture dish with 1X RIPA buffer containing a protease inhibitor cocktail (Sigma, P8430). For confluent HEK cells and high-density cortical cultures, 150 μl of RIPA buffer was added per well of a 12 well culture vessel and scaled linearly for larger and smaller wells. Lysates were cleared by centrifugation at 18,000 x g for 10 minutes at 4^{o} C and the supernatant was transferred to a fresh tube and protein quantification was performed with a BCA assay kit (Pierce). 5X Laemmli buffer containing 100 mM DTT was then added to the cleared lysates to make them 1X and lysates were stored at -80^{o} C. 15 mg of total protein were size separated on 10% SDS-PAGE gels which were transferred to PVDF membrane. PVDF blots were blocked for 1 hour (0.2% Tween-20, 5% powdered milk, 1X TBS) and sequentially incubated in primary antibody (mouse anti-HA, Santa Cruz F-7; mouse anti-Arc, Santa Cruz c-7; rabbit anti-GAPDH, Abcam; mouse anti-Tubulin, Promega) and secondary antibody in blocking buffer (goat anti-rabbit and anti-mouse HRP, Millipore; goat anti-rabbit and goat anti-mouse Alexa700 and Alexa800). Blots were developed using high sensitivity ECL substrate (GE, Amersham) or using a Li-Cor Odyssey infra-red imaging system.

TimeStamp Cloning

The Arc-TS construct and PSD95-TS construct were generous gifts from Dr. Michael Lin and are described in (Lin et al., 2008). LRRTM1-TS was generated by PCR amplifying 3 separate fragments from mouse genomic DNA and a single PCR fragment from the PSD95-TS construct, which were then sequentially cloned into pcDNA3.1. The first fragment was generated by amplifying the 5' UTR from the transcriptional start site to the nucleotide preceding the ATG start codon and inserting a 5' HindIII site and a 3' BamHI site (F Primer: AAGCGAAGCTTGGCGTTCT CCAACCTGGACTC; R Primer: AAGCGGGATCCTAGCGAGAATCTTTCCAGAGAGAC TGGAG). The second fragment was generated by

amplifying the coding region from the ATG start codon to the nucleotide preceding the TAG stop codon and inserting a 5' BamHI site and a 3' XhoI site (F Primer: GCGGGATCCGCCACCATGGATTTCCTGCTACTC GGCCTCTG; R Primer: CGCCTCGAGCACCTCGCATTCCCTCGCAGGCTG). The third fragment was generated by amplifying the 3' UTR from the nucleotide following the TAG stop codon to the end of the putative polyadenylation signal and inserting a 5' XbaI site and a 3' ApaI site (F Primer: AATCTAGATTGTCCCAGAGGCTCCCAACC; R Primer: AAGGGCCCTCTGTAGAAACTGTAAATGCTA). The fourth fragment was generated by amplifying the TimeStamp cassette from the PSD95-TS construct and inserting a 5' XhoI site and a 3' XbaI site (F Primer: AAAACTCGAGCCCATGGCCAGCATGAC; R Primer: AAAATCTAGATCAAGGCGCGCCAGCGTAATC). BILN2061 (Boehringer) was dissolved in DMSO at a stock concentration of 10 mM and stored at -80^{o}. Individual aliquots were diluted to 1 mM in DMSO and used as working stocks.

shRNA and Expression Plasmids

Three Arc shRNA plasmids and four LRRTM1 shRNA plasmids were acquired from the Sigma shRNA library (Sigma Aldrich, St. Louis, Missouri). The three Arc shRNA plasmids were clones TRCN0000108905 (target sequence: CAGTGATTCATACCAGTGAA), TRCN0000108906 (target sequence: GAGGAGATCATTCAGTAT), and TRCN0000108908 (target sequence: CCCAATGTGATCCTGCAGATT). The four LRRTM1 shRNA plasmids were clones TRCN0000106505 (target sequence: CGCTCTGATTTGTTGACTGAA), TRCN0000106506 (target sequence: CCTGGTTATCATCAACGAGTA), TRCN0000106508 (target sequence: CAGCCTCAAGTTTCTCGACAT), and TRCN0000106509 (target sequence: TGGCTGTATTTGGATCACAAT). The non-targeting shRNA control plasmid was the Sigma Non-Mammalian control shRNA (SHC002). The human Arc-V5 (ccsbBroad304_07860) and human LRRTM1-V5 plasmids (ccsbBroad304_10055) were acquired from the CCSB Broad Lentiviral Expression library and were retained in their pLX304 plasmid backbone.

Chapter 5. Discussion

In this thesis, I developed a novel method for constraining mathematical models of action potential generation with morphological data describing excitatory and inhibitory synapse location. I then used this methodology to test the functional consequences of BDNF-induced synapse and dendrite addition within the proximal dendritic arbor of cortical neurons in culture. Finally, I identified Arc and LRRTM1 as potential molecular intermediates between elevated BDNF signaling and excitatory synapse formation. In the following sections, I will attempt to integrate my findings into scientific literature at-large.

5.1 A Novel Method to Constrain Compartmental Models that Generate Action Potentials

Computational models have a rich history in the field of neuroscience. Whereas computational models were previously accessible only to those who were extremely proficient in both mathematics and software programming, the advent of user friendly simulation packages has broadened the modeling audience. This has been specifically helpful when testing hypothesis that currently cannot be experimentally addressed, such as determining the input-output relationship between collections of thousands of excitatory and inhibitory synaptic inputs. In Chapter 2, I developed an algorithmic approach for converting confocal images of excitatory and inhibitory presynaptic inputs into computational models. The potential benefits as well as the limitations of my approach will be discussed below.

Automated Image Analysis to Quantify Synaptic Puncta

A number of methods have been developed to automatically and reproducibly quantify pre and post-synaptic punctae. In fact, the sheer number of individual methods precludes a thorough discussion of each one in detail, so instead I will focus on three papers that represent three different themes in automated puncta analysis.

Paradis and colleagues screened for candidate molecules that were required for excitatory and inhibitory synaptogenesis, by examining excitatory (PSD95) and inhibitory post-synaptic structures ($GABA_A$ receptor) on cultured hippocampal cultures (Paradis et al., 2007). To automate quantification, they used a global thresholding approach where all pixels that were above the global mean of the image plus two standard deviations were considered to be synaptic structures. Though easy to implement and amenable to high-throughput automated image analysis, this approach is limited in that, by definition, it will tend to detect the same number of pixels for all images regardless of the actual amount of signal. In addition, because this approach requires the end user to manually identify individual dendritic branches for quantification, and users are likely to differentially identify "representative" branches, this approach makes it difficult to achieve reproducibility.

McAllister and colleagues developed a semi-automated protocol to identify synaptic punctae that is based on the user manually discriminating punctate signal from background signal (Glynn and McAllister, 2006). With this protocol, the user creates a circular region of interest (ROI) and uses the ROI to measure the intensity within non-punctate regions of the image. The average of the non-punctate regions within the neurite is then calculated and this value is subtracted from the entire image, which effectively sets the background of the image close to 0. With the contrast artificially enhanced, the user manually annotates synaptic punctae or utilizes a size threshold to automatically identify all structures that are greater than a given number of voxels. While this approach provides more flexibility than the standard deviation approach, its main limitations are throughput and reproducibility. Manual annotation is time consuming and different users are likely to vary in their subjective discrimination between punctate signals versus background. In addition, similar to the standard deviation approach, this method requires that the user identify individual dendritic branches for quantification, which further limits reproducibility.

A more recent method that utilizes more sophisticated image analysis procedures was developed by Schmitz and colleagues and published as a MatLab package called SynD (Schmitz et al., 2011). This method is convenient in that it is highly automated and has a built in means for data analysis. In addition, this method represents a significant advancement because it simultaneously quantifies dendrite morphology and it catalogs synaptic structures as a function of their distance from the cell soma, using a Sholl analysis-like procedure. Another noteworthy difference between SynD and other methods is that SynD allows one to sum the total number of synapses across the entire dendritic arbor, so the user does not have make a subjective decision when determining which dendritic branch to quantify. However, it is limited to working with single plane images or maximum intensity projections of confocal images and its synapse detection algorithm uses a rigid mean plus standard deviation approach similar to (Paradis et al., 2007). The inability to work with multi-plane images could be a significant limitation, particularly when analyzing punctae that are localized to thick dendrites where maximum intensity projection could merge spots that are in the same XY space but different Z space.

The approach that I have developed circumvents some of the major limitations in the above methods. By using the L.O.G. convolution approach to identify all features that are present within the image regardless of their intensity or their local noise, the potential inaccuracies inherent to the standard deviation approach are avoided. In addition, while the approach presented in this thesis is similar to SynD in that it simultaneously quantifies dendritic and synaptic morphology as well as the distance of these features from the soma, my approach has the advantage of being able to perform in 3 dimensions and for utilizing L.O.G. edge detection rather than a rigid standard deviation scheme. However, whereas my approach measures the Euclidean distance of each feature from the center of the soma, SynD has the capability of measuring the path length to the center of the soma which is a more accurate representation of distance.

Converting Morphological Data into Compartmental Models

Multiple approaches have been used to automate the process of synaptic puncta analysis, but, to date, none of the described methods provides a way to convert morphological data into compartmental models. Similarly, there are a number of approaches to create morphologically constrained compartmental models, but the vast majority of these approaches are focused exclusively on detailed reconstruction of dendritic morphology while ignoring the location of synapses within the dendritic arbor. Therefore, a single method does not exist to both quantify excitatory synapses, inhibitory synapses and dendritic morphology and to use these features to constrain compartmental models. The approach developed in this thesis represents one of the first attempts to automate the construction of realistic compartmental models that are partially constrained in terms of dendrite morphology, excitatory synapses and inhibitory synapses. However, to balance the ease of automation with the difficulty of incorporating detailed morphological characteristics, I was required to make a number of simplifications and these will be discussed below.

The fine details of the dendritic arbor can influence the neuronal input-output relationship. These details include the branching pattern, the presence of dendritic spines, the structure of individual dendritic branch points, the dendrite diameter and the absolute dendrite path length. The modeling process presented within this thesis made simplifications for each of these fine details. Sholl analysis provides a single method to describe the complexity of a highly branched dendritic arbor. However, it does not provide any information regarding branch symmetry within the arbor or the fine structure of individual branch points. Therefore, using a deterministic approach to directly convert individual Sholl into dendritic branches imparts artificial branch symmetry and it obscures fine branch point morphology, both of which can influence the integration of synaptic inputs (Ferrante et al., 2013; Komendantov and Ascoli, 2009). The majority of excitatory synapses form on the head of dendritic spines which are separated from the dendritic shaft by a thin dendritic spine neck (40-200 nm). The thin spine neck can generate up to 500 MΩ of resistance which can amplify spine head depolarization by up

to 45 fold (Harnett et al., 2012). The approach I used takes into account spine volume when calculating the diameter of individual compartments, but it does not take into account the localized increase in resistance due to the spine neck. Finally, the attenuation of synaptic voltage is influenced by the path length of the synaptic input to the site of action potential generation rather than the Euclidean distance. Therefore, by calculating the Euclidean distance of objects, my models minimize the impact of dendrite tortuosity on dendritic path length.

5.2 Synapse Distribution: A New way to Account for BDNF-induced Increases in Neural Activity

Typically synapse formation is studied by calculating the density of synaptic structures along individual dendritic branches. I developed a novel method that sums synaptic structures across individual dendritic arbors and incorporates the synaptic features into computational models, which allows one to predict the input-output properties of a given distribution of synaptic inputs. In Chapter 3, I used this approach to determine that BDNF increases the total number of excitatory and inhibitory synapses without increasing their density and that this effect is correlated with enhanced network activity. Further, I determined that the resulting distribution of synaptic inputs is tuned to produce a greater number of action potentials. In the sections below I will discuss the potential implications of these findings as well as some discrepancies between my findings and the pre-existing BDNF literature.

BDNF Induces the Formation of New Synapses on New Dendritic Branches

My results suggest that excitatory synapse formation and dendrite formation are tightly coupled during BDNF-induced structural plasticity. This is consistent with the synaptotrophic hypothesis, which posits that synaptic inputs are required to rapidly stabilize nascent dendritic branches(Cline and Haas, 2008; Vaughn, 1989). The precise role of BDNF in excitatory synapse formation and nascent branch formation remain unclear. I envision three distinct possibilities. First, BDNF could induce the formation of dendritic branches, but synapse formation on nascent dendritic branches could proceed independently of BDNF signaling. Alternatively, elevated BDNF signaling could initiate dendrite

formation and also be required for synapse formation on the nascent dendrites. Finally, BDNF could simultaneously initiate dendrite formation while also stimulating the production of factors required to stabilize synapses. In this scenario, BDNF-induced expression of synaptic proteins could be stimulated early during the structural response and then activity-dependent mechanisms could drive their incorporation into synapses. The role of BDNF in enhancing the translation of proteins incorporated into synapses supports the latter two models.

The relationship between BDNF-induced excitatory synapse formation and dendrite formation has been evaluated in other systems using time lapse microscopy but has led to some different conclusions. In *Xenopus*, BDNF infusion increased the density of synapses between retinal ganglion cells (RGCs) and tectal neurons. In contrast to our study, this analysis revealed that increased synapse density was correlated with enhanced RGC axonal arborization and not enhanced tectal neuron dendrite arborization (Cohen-Cory et al., 2010; Sanchez et al., 2006). This may reflect differential BDNF effects on axons and dendrites in different sub-populations of neurons. In ferret slice cultures of visual cortex, BDNF over-expression dramatically increased the number of dendrites, but it reduced dendritic spine density (Horch and Katz, 2002; Wilson Horch et al., 1999). However, in the latter studies dendritic spine analysis was restricted to "old" dendrites, and, consequently, the emergence of "new" spines on "new" dendrites was not documented. Therefore, my study represents previously undocumented evidence that BDNF induces the formation of dendritic spine synapses on nascent dendritic branches.

BDNF's Regulation of Inhibitory Synaptic Puncta Density

Others have estimated BNDF's influence on inhibition by quantifying proteins found at inhibitory synapses. In 10 DIV hippocampal neurons, 24 hours of BDNF application (50 ng/ml) decreased the density of $GABA_A$ (inhibitory) receptor clusters per μm of dendrite (Elmariah et al., 2004). In 8 DIV BDNF null mutant hippocampal neurons, either 24 hours of bath BDNF application or BDNF over-expression decreased the density of VGAT punctae per dendritic region of interest (Singh et al., 2006), which was

suggested to reflect BDNF-induced down-regulation of inhibitory synaptic input. However, BDNF increases the number of hippocampal dendrites in culture (Dijkhuizen and Ghosh, 2005; Singh et al., 2006). Therefore, net synapse formation cannot be easily determined using puncta per dendrite length measurements because of the increase in total dendrite length. In my study, by summing the number of synapses across entire neurons, I found that BDNF application increased the formation of inhibitory synapses. However, in my studies the increase in synapse formation is accompanied by a decrease in puncta density because dendrite elongation was more rapid than synapse formation. Therefore, I propose that, rather than BDNF promoting the specific disassembly of inhibitory synapses, BDNF-induced inhibitory synapse formation is robust but it lags behind dendrite formation. In support of this view, when BDNF's effect on inhibitory synaptic punctae were quantified using a field of view approach, in which punctae were not normalized to dendrite length (Huang et al., 1999; Marty et al., 2000), BDNF caused a robust increase in the density of GAD65 punctae per area. In addition, my results are in accordance with electrophysiological studies documenting that BDNF enhances the frequency of miniature inhibitory post-synaptic potentials (mIPSPs) in cultured neurons (Bolton et al., 2000; Vicario-Abejón et al., 1998) and in vivo (Hong et al., 2008), which is at odds with the notion that BDNF initiates the disassembly of inhibitory synapses.

Inhibitory synapses limit the flux of calcium (Ca^{2+}) from dendritic spines into the dendritic shaft in a spatially-restricted manner (Chiu et al., 2013; Miles et al., 1996). Ca^{2+} release from intracellular stores, which can be initiated by dendritic spine Ca^{2+} transients (Plotkin et al., 2013), participates in the process of activity-dependent dendrite stabilization (Lohmann et al., 2002). My results suggest that during the process of BDNF-induced dendrite formation, there is a global reduction in the density of inhibitory synapses per dendrite length. I speculate that reduced inhibitory synapse density may facilitate the activity-dependent stabilization of new dendrites by enhancing Ca^{2+} entry induced by excitatory synaptic transmission.

My results suggest that excitatory synapse formation is more tightly coupled to dendrite formation than inhibitory synapse formation, at least during the first 12 hours after BDNF addition that we studied. This discrepancy could reflect the gene expression programs that are initiated by BDNF stimulation. BDNF positively regulates the expression of the VGlut family of excitatory amino acid transporter (Melo et al., 2013), but it negatively regulates the expression of the inhibitory amino acid transporter VGAT (Henneberger et al., 2005) . Similarly, while BDNF positively regulates the expression of the post-synaptic excitatory scaffold molecule PSD-95 (Yoshii and Constantine-Paton, 2007), BDNF does not appear to regulate the expression of the post-synatpic inhibitory scaffold molecule gephyrin (Wuchter et al., 2012). Therefore, BDNF stimulation may initially favor the productive assembly of excitatory synapses over inhibitory synapses.

There is a long history of BDNF-dependent effects on excitatory synapse density, which conflicts with my finding that bath BDNF application increases the total number of excitatory synapses without affecting density. In acute slices from the CA1 region of the hippocampus, 24 hours of recombinant BDNF exposure increased the density of spines on secondary and tertiary dendrites emanating from the apical dendrite (Amaral et al., 2007). Similarly, in dissociated cortical cultures, 48 hours of BDNF over-expression increased the density of spines on a mixture of apical and basal dendrites (Hiester et al., 2013). However, in dissociated hippocampal cultures, 50 ng/ml recombinant BDNF increased the density of NMDA receptor clusters after 48 hours but not 24 hours, suggesting that BDNF's ability to modulate excitatory synapse density is sensitive to the length of stimulation (Elmariah et al., 2004). In an attempt to capture the earliest observable stage of BDNF-induced structural plasticity, I limited BDNF application to 12 hours. Therefore, the most parsimonious explanation to reconcile my observation that BDNF did not enhance VGlut1 density with previous reports is that longer BDNF doses increase excitatory synapse density while shorter BDNF doses do not.

My density measurements were calculated by dividing the total number of synapses within a Sholl radius by the total dendrite length within that Sholl radius, and I did not calculate the specific synapse density of individual branches. Rather my measurements reflect a global average density at a given distance from the soma. BDNF stimulation rapidly increased dendrite length, and, therefore, it is possible that "new" and "old" dendrites have different densities, which is not reflected in the global average. Although this possibility cannot be ruled out, my live cell observations document the occurrence of dendritic spines on new dendrites, which suggests that new dendrites are not completely devoid of excitatory synapses.

Modeling the Consequences of the BDNF-Induced Distribution of Synapses and Dendrites

It has been widely documented that BDNF application enhances the rate of action potential generation in cultured neurons as measured both intracellularly and exctracellularly (Bolton et al., 2000; Gambazzi et al., 2010; Kang and Schuman, 1995; Vicario-Abejón et al., 1998). It has been suggested that BDNF positively regulates action potential generation by specifically strengthening excitatory synapses. This notion is supported by an ample body of evidence documenting that BDNF positively regulates mEPSP frequency and amplitude (Bolton et al., 2000; Sherwood and Lo, 1999), BDNF increases the number of docked presynaptic vesicles at dendritic spine synapses as well as the number of dendritic spine synapses (Tyler and Pozzo-Miller, 2001) and BDNF increases the expression and synaptic localization of numerous post-synaptic proteins that positively regulate excitatory synapse strength (for review see (Carvalho et al., 2008; Gottmann et al., 2009). However, this simple view is confounded by studies documenting that BDNF also positively regulates the function of inhibitory synapses (Jovanovic et al., 2004; Rutherford et al., 1997; Yamada et al., 2002).

In this study, I have taken a modeling approach to reconcile aspects of this apparent conflict, which has led to two major conclusions. First, in a stochastic simulation of uncorrelated barrages of synaptic activity, BDNF stimulated neurons are more efficient at converting synaptic activity into action

potentials. Second, BDNF-induced expansion of the dendritic arbor has a normalizing effect on BDNF-induced increases in synapse density. My finding that the BDNF-induced collection of synapses and dendrites is more efficient at converting barrages of mixed synaptic activity into action potentials is likely an important mechanism by which BDNF participates in the plasticity of cortical circuitry.

5.3 Arc and LRRTM1 Mediate Unique Aspects of BDNF-induced Plasticity at Excitatory Synapses

In an attempt to understand the cellular mechanisms that facilitate the BDNF-induced increase of excitatory synapse numbers, I analyzed BDNF's ability to regulate two potential mediators of BDNF-induced excitatory synapse formation: Arc and LRRTM1. I confirmed that Arc is a BDNF-target gene and I discovered that BDNF-induced Arc localizes to "new" as well as "old" dendrites and that Arc may be required for BDNF-induced dendrite formation. I established LRRTM1 as a novel BDNF-target gene and I discovered that BDNF-induced LRRTM1 localizes to excitatory synapses where it may potentiate BDNF's effects on excitatory synapse formation. In this final section, I will discuss the potential implications of these findings.

Arc as a BDNF Target Gene

Arc is a well-established BDNF target gene, and, therefore, our findings that Arc expression is regulated by BDNF are largely confirmatory. However, the vast majority of studies have examined the relationship between BDNF levels and Arc mRNA within pyramidal neurons of the neocortex, and less is known about BDNF's regulation of Arc in other neuronal populations. In cultured striatal neurons bath BDNF application is sufficient to acutely upregulate Arc mRNA in a calcium and TrkB dependent manner (Gokce et al., 2009). By documenting that Arc mRNA is decreased in the striatum of BDNF knockout mice, our results suggest that, not only is BDNF sufficient to regulate Arc within the inhibitory neurons of the striatum, but sustained BDNF expression is also necessary for normal Arc mRNA levels. Interestingly, in a pharmacological model of Huntington's disease, corticostriatal synapses failed to depotentiate after LTP induction, which could be indicative of an inability to remove surface AMPA

receptors from the post-synaptic membrane (Picconi et al., 2006). BDNF-induced Arc facilitates surface AMPA receptor removal and reduced BDNF is thought to be a major contributor to striatal dysfunction in Huntington's disease. Therefore, the depotentiation defect could be the result of impaired BDNF-induced Arc accumulation at potentiated corticostriatal synapses.

BDNF regulates the abundance of Arc protein within the dendrites of cortical pyramidal neurons. However, BDNF-induced Arc accumulation has never been documented specifically within BDNF-induced cortical neuron dendrites (i.e. "new" dendrites). We used the TimeStamp protein synthesis reporter to visualize BDNF-induced Arc localization and we detected BDNF-induced Arc in both "old" and "new" dendrites. Given that Arc is considered to be a negative regulator of synapse strength, the appearance of Arc in new dendrites is peculiar because new dendrites are presumably strengthening their synapses in accordance with the synaptotrophic hypothesis. I envision 3 possibilities regarding Arc's role in "new" dendrites. First, Arc has the ability to regulate the expansion of the actin cytoskeleton (Messaoudi et al., 2007), so Arc in "new" dendrites could be promoting filamentous actin accumulation which is associated with enhanced synapse strength. Second, little is known about the kinetics of Arc disassembly from AMPA receptor containing endosomes, so Arc's presence in "new" dendrites could represent AMPA receptor containing endosomes that are being trafficked to "new" dendrites to support synapse strengthening. Finally, AMPA receptor subunits are mobile within the post-synaptic membrane, and they must be efficiently recycled in order to prevent their dispersion from post-synaptic sites (Petrini et al., 2009). Therefore, Arc could strengthen synapses on "new" dendrites by establishing AMPA receptor recycling at nascent synapses, which may explain BDNF's ability to increase spontaneous activity as determined with multi-electrode arrays.

Arc overexpression did not influence the number of VGlut1 pre-synaptic terminals or dendrite elongation. However, Arc loss of function did impair the process of BDNF-induced synapse and dendrite addition, which suggests that Arc is required for aspects of acute BDNF-induced plasticity at dendrites

and synapses. In conjunction with our live cell microscopy evidence that BDNF-induced Arc localizes to nascent dendrites, this evidence may indicate that Arc plays a direct role in the synaptic stabilization of nascent dendrites. In addition, this evidence may explain the phenomenon that sustained Arc expression is required for the late phase of BDNF-induced LTP at hippocampal synapses (Messaoudi et al., 2007). In these experiments, LTP was measured using extracellular field potential recordings, which is not capable of discriminating between synapse strengthening and the formation of new synapses. Therefore, it is possible that Arc enhances the efficacy of excitatory hippocampal pathways by translating the BDNF signal into increased excitatory synapse formation.

LRRTM1 as a BDNF Target Gene

We have presented evidence that the trans-synaptic adhesion molecule LRRTM1 is a BDNF target gene in vivo within the striatum and in vitro in primary cortical neurons. In situ hybridization and semi-quantitative RT-PCR have confirmed that LRRTM1 is expressed within the striatum and cortex in vivo in the adult mouse brain (Laurén et al., 2003). However, virtually nothing is known about the mechanisms that control LRRTM1 expression. Our results present some of the first insights into the regulatory program that governs LRRTM1 mRNA expression, although the prolonged time course indicates that the relationship between BDNF and LRRTM1 expression may be indirect. Recently, an intron within the LRRTM1 3' UTR has been discovered, which would make LRRTM1 a putative NMD substrate. Therefore, an alternative explanation for the indirectness could be that BDNF directly increases LRRTM1 transcription but that enhanced transcription is coupled to enhanced translation. In this scenario, LRRTM1 mRNAs would be synthesized at a higher rate but they would also be undergoing NMD-mediated decay at a higher rate as well. This explanation is supported by our analysis of LRRTM1-TimeStamp, which will be discussed below.

In response to acute BDNF stimulation, LRRTM1-TimeStamp expression increases and a fraction of LRRTM1-TimeStamp accumulates within dendrites apposed to VGlut1 positive pre-synaptic

structures. This observation leads to two conclusions. First, BDNF may regulate the translation of LRRTM1 in cortical neurons. Second, BDNF-induced LRRTM1 may directly participate in the process of BDNF-induced synapse formation. Similar to LRRTM1 transcription, little is known about the mechanisms that mediate LRRTM1 translation or LRRTM1 localization, so this result presents the first evidence that LRRTM1 abundance and subcellular distribution is influenced by extracellular factors.

BDNF governs aspects of excitatory synapse formation, but little is understood about the cellular mechanisms that dictate where a BDNF-induced synapse forms. BDNF stimulates the division of pre-synaptic vesicle pools, which presumably makes vesicles available for incorporation into nascent pre-synaptic terminals (Bamji et al., 2006). BDNF also stimulates the surface expression of glutamate receptors and the clustering of post-synaptic scaffolding molecules, which could prime the post-synaptic surface for functional contact with pre-synaptic axons (Caldeira et al., 2007a, 2007b). Since LRRTM1 clustering is sufficient to induce pre-synaptic differentiation (Linhoff et al., 2009), the BDNF-induced accumulation of LRRTM1 within dendrites could mark the physical location where other BDNF-induced synaptic proteins collect to form functional synapses. Assuming that the above speculation is correct, the next question becomes what dictates where BDNF-induced LRRTM1 accumulates within dendrites? As a transmembrane protein, LRRTM1 must be processed via the secretory pathway. Since dendrites are capable of local translation and dendrites harbor endoplasmic reticulum as well as Golgi outposts (Leal et al.; Ori-McKenney et al., 2012), an intriguing possibility is that LRRTM1 mRNA localizes to dendritic sites bestowed with the capacity to locally translate and secrete transmembrane proteins. Upon elevation of BDNF signaling, nascent synapses could form at these translational hotspots.

LRRTM1 and BDNF Display an Additive Interaction on Excitatory Synapse Numbers

I have presented evidence that LRRTM1 is a BDNF target gene and I have speculated that LRRTM1 may organize BDNF-induced synapses. However, functional experiments utilizing LRRTM1 overexpression and LRRTM1 shRNA do not indicate that LRRTM1 is necessary for BDNF-induced synapse

formation. If LRRTM1 functions downstream of BDNF in a linear pathway that promotes synapse formation, LRRTM1 overexpression should saturate the system and additional BDNF should promote no further increase in synapse number. Similarly, in a linear pathway LRRTM1 loss of function should prevent additional BDNF from increasing synapse numbers. However, the treatment of LRRTM1 overexpressing cells with BDNF resulted in an additive increase in excitatory synapses, while LRRTM1 loss of function did not prevent BDNF-induced synapse addition. An interpretation for each of these results will be discussed below.

LRRTM1 overexpression increases the strength of excitatory synapses by promoting the incorporation of AMPA receptor subunits (Soler-Llavina et al., 2013). BDNF signaling is potentiated by neuronal activity because neuronal activity increases the surface expression of the BDNF receptor TrkB (Nagappan and Lu, 2005). Therefore, one intriguing possibility to explain the additive interaction between BDNF and LRRTM1 during excitatory synapse formation is that LRRTM1 potentiates synapses in a cell-autonomous manner and thus makes LRRTM1 overexpressing neurons more sensitive to BDNF. In addition, since LRRTM1 and TrkB both share extracellular leucine-rich repeats, which can display homophillic interactions (Huang and Reichardt, 2003; de Wit et al., 2011), LRRTM1 could increase TrkB surface expression via a direct interaction at the post-synaptic membrane.

The process of trans-synaptic adhesion at synapses is highly redundant. This is evident from studies of the neuroligin knockout mouse, in which simultaneous deletion of all three neuroligins is not sufficient to disrupt the number of synapses as determined via morphological assays (Varoqueaux et al., 2006). Similarly, in cultured hippocampal neurons, simultaneous depletion of LRRTM1, LRRTM2, neuroligin-1 and neuroligin-3 was required to disrupt the baseline formation of excitatory synapses (Ko et al., 2011). Therefore, it is not surprising that the depletion of LRRTM1 on its own does not block BDNF-induced addition of excitatory synapses. I propose that the inability of LRRTM1 loss-of-function to display an interaction with BDNF likely reflects compensation from other post-synaptic adhesion

molecules. However, it is important to note that, although LRRTM1 is indispensable for the BDNF-induced formation of pre-synaptic VGlut1 vesicle clusters, I did not test the functional capacity of these synapses. Since LRRTM1 is required for LTP at hippocampal excitatory synapses, it is possible that BDNF-induced synapse formation proceeds in the absence of LRRTM1, but that these synapses are functionally and/or ultra-structurally compromised. Since the knockdown strategy that I developed was designed to specifically block the accumulation of BDNF-induced protein, it is also possible that pre-existing LRRTM1 is adequate for BDNF-induced excitatory synapse formation. Alternatively, since the LRRTM1 shRNA was only 70% effective, I cannot rule out the possibility that the BDNF-induced production of a limited amount of LRRTM1 is sufficient to mediate BDNF-induced excitatory synapse formation.

5.5 Summary

In this thesis I have explored BDNF's ability to modulate excitatory and inhibitory synaptic inputs. I developed an algorithm to quantify the number of excitatory and inhibitory pre-synaptic structures across the proximal arbor of individual neurons. In order to predict the functional consequences of individual distributions of excitatory and inhibitory pre-synaptic inputs, I developed a strategy to constrain computational models with morphological data. I then used this algorithm to characterize the functional consequences of BDNF-induced excitatory and inhibitory synapse formation throughout the proximal dendritic arbor. I determined that the spatial distribution of synaptic inputs that results from BDNF stimulation is intrinsically more excitable. Finally, I identified Arc and LRRTM1 as potential molecular intermediates between elevated BDNF signaling and excitatory synapse formation. I propose that these insights provide novel insight into the mechanisms that allow BDNF to shape the structure and function of cortical circuits.

References

Abidin, I., Eysel, U.T., Lessmann, V., and Mittmann, T. (2008). Impaired GABAergic inhibition in the visual cortex of brain-derived neurotrophic factor heterozygous knockout mice. J. Physiol. *586*, 1885–1901.

Adasme, T., Haeger, P., Paula-Lima, A.C., Espinoza, I., Casas-Alarcón, M.M., Carrasco, M.A., and Hidalgo, C. (2011). Involvement of ryanodine receptors in neurotrophin-induced hippocampal synaptic plasticity and spatial memory formation. Proc. Natl. Acad. Sci. *108*, 3029–3034.

Ahn, M., Beacham, D., Westenbroek, R.E., Scheuer, T., and Catterall, W.A. (2007). Regulation of Na(v)1.2 channels by brain-derived neurotrophic factor, TrkB, and associated Fyn kinase. J. Neurosci. Off. J. Soc. Neurosci. *27*, 11533–11542.

Alabi, A.A., and Tsien, R.W. (2012). Synaptic Vesicle Pools and Dynamics. Cold Spring Harb. Perspect. Biol. *4*, a013680.

Alder, J., Thakker-Varia, S., and Black, I.B. (2002). Transcriptional analysis in the brain: trophin-induced hippocampal synaptic plasticity. Neurochem. Res. *27*, 1079–1092.

Alder, J., Thakker-Varia, S., Bangasser, D.A., Kuroiwa, M., Plummer, M.R., Shors, T.J., and Black, I.B. (2003). Brain-derived neurotrophic factor-induced gene expression reveals novel actions of VGF in hippocampal synaptic plasticity. J. Neurosci. Off. J. Soc. Neurosci. *23*, 10800–10808.

Amaral, M.D., and Pozzo-Miller, L. (2007). TRPC3 channels are necessary for brain-derived neurotrophic factor to activate a nonselective cationic current and to induce dendritic spine formation. J. Neurosci. Off. J. Soc. Neurosci. *27*, 5179–5189.

Amaral, M.D., Chapleau, C.A., and Pozzo-Miller, L. (2007). Transient receptor potential channels as novel effectors of brain-derived neurotrophic factor signaling: Potential implications for Rett syndrome. Pharmacol. Ther. *113*, 394–409.

Amatrudo, J.M., Weaver, C.M., Crimins, J.L., Hof, P.R., Rosene, D.L., and Luebke, J.I. (2012). Influence of Highly Distinctive Structural Properties on the Excitability of Pyramidal Neurons in Monkey Visual and Prefrontal Cortices. J. Neurosci. *32*, 13644–13660.

Andersen, P. (1990). Synaptic integration in hippocampal CA1 pyramids. Prog. Brain Res. *83*, 215–222.

Anggono, V., and Huganir, R.L. (2012). Regulation of AMPA receptor trafficking and synaptic plasticity. Curr. Opin. Neurobiol. *22*, 461–469.

Attwell, D., and Gibb, A. (2005). Neuroenergetics and the kinetic design of excitatory synapses. Nat. Rev. Neurosci. *6*, 841–849.

Autry, A.E., and Monteggia, L.M. (2012). Brain-derived neurotrophic factor and neuropsychiatric disorders. Pharmacol. Rev. *64*, 238–258.

Balkowiec, A., and Katz, D.M. (2002). Cellular mechanisms regulating activity-dependent release of native brain-derived neurotrophic factor from hippocampal neurons. J. Neurosci. Off. J. Soc. Neurosci. *22*, 10399–10407.

Bamji, S.X., Rico, B., Kimes, N., and Reichardt, L.F. (2006). BDNF mobilizes synaptic vesicles and enhances synapse formation by disrupting cadherin–β-catenin interactions. J. Cell Biol. *174*, 289–299.

Banks, M.I., and Pearce, R.A. (2000). Kinetic Differences between Synaptic and Extrasynaptic GABAA Receptors in CA1 Pyramidal Cells. J. Neurosci. *20*, 937–948.

Baquet, Z.C., Gorski, J.A., and Jones, K.R. (2004). Early Striatal Dendrite Deficits followed by Neuron Loss with Advanced Age in the Absence of Anterograde Cortical Brain-Derived Neurotrophic Factor. J. Neurosci. *24*, 4250–4258.

Baquet, Z.C., Bickford, P.C., and Jones, K.R. (2005). Brain-derived neurotrophic factor is required for the establishment of the proper number of dopaminergic neurons in the substantia nigra pars compacta. J. Neurosci. Off. J. Soc. Neurosci. *25*, 6251–6259.

Barrow, S.L., Constable, J.R., Clark, E., El-Sabeawy, F., McAllister, A.K., and Washbourne, P. (2009). Neuroligin1: a cell adhesion molecule that recruits PSD-95 and NMDA receptors by distinct mechanisms during synaptogenesis. Neural Develop. *4*, 17.

Beck, H., and Yaari, Y. (2008). Plasticity of intrinsic neuronal properties in CNS disorders. Nat. Rev. Neurosci. *9*, 357–369.

Behabadi, B.F., Polsky, A., Jadi, M., Schiller, J., and Mel, B.W. (2012). Location-Dependent Excitatory Synaptic Interactions in Pyramidal Neuron Dendrites. PLoS Comput Biol *8*, e1002599.

Belelli, D., and Lambert, J.J. (2005). Neurosteroids: endogenous regulators of the GABAA receptor. Nat. Rev. Neurosci. *6*, 565–575.

Bertram, J.P., Rauch, M.F., Chang, K., and Lavik, E.B. (2010). Using polymer chemistry to modulate the delivery of neurotrophic factors from degradable microspheres: delivery of BDNF. Pharm. Res. *27*, 82–91.

Biederer, T., Sara, Y., Mozhayeva, M., Atasoy, D., Liu, X., Kavalali, E.T., and Südhof, T.C. (2002). SynCAM, a synaptic adhesion molecule that drives synapse assembly. Science *297*, 1525–1531.

Bleckert, A., Parker, E.D., Kang, Y., Pancaroglu, R., Soto, F., Lewis, R., Craig, A.M., and Wong, R.O.L. (2013). Spatial Relationships between GABAergic and Glutamatergic Synapses on the Dendrites of Distinct Types of Mouse Retinal Ganglion Cells across Development. PLoS ONE *8*, e69612.

Bolton, M.M., Pittman, A.J., and Lo, D.C. (2000). Brain-Derived Neurotrophic Factor Differentially Regulates Excitatory and Inhibitory Synaptic Transmission in Hippocampal Cultures. J. Neurosci. *20*, 3221–3232.

Bouron, A., Boisseau, S., De Waard, M., and Peris, L. (2006). Differential down-regulation of voltage-gated calcium channel currents by glutamate and BDNF in embryonic cortical neurons. Eur. J. Neurosci. *24*, 699–708.

Bower, J.M. (1998). The book of GENESIS: exploring realistic neural models with the GEneral NEural SImulation System (Santa Clara, Calif: TELOS).

Bramham, C.R., and Panja, D. (2013). BDNF regulation of synaptic structure, function, and plasticity. Neuropharmacology.

Bramham, C.R., Worley, P.F., Moore, M.J., and Guzowski, J.F. (2008). The immediate early gene arc/arg3.1: regulation, mechanisms, and function. J. Neurosci. Off. J. Soc. Neurosci. *28*, 11760–11767.

Brette, R., Rudolph, M., Carnevale, T., Hines, M., Beeman, D., Bower, J.M., Diesmann, M., Morrison, A., Goodman, P.H., Harris, F.C., Jr, et al. (2007). Simulation of networks of spiking neurons: a review of tools and strategies. J. Comput. Neurosci. *23*, 349–398.

Brown, K.M., Gillette, T.A., and Ascoli, G.A. (2008). Quantifying neuronal size: Summing up trees and splitting the branch difference. Semin. Cell Dev. Biol. *19*, 485–493.

Buckley, P.F., Pillai, A., and Howell, K.R. (2011). Brain-derived neurotrophic factor: findings in schizophrenia: Curr. Opin. Psychiatry *24*, 122–127.

Buddhala, C., Hsu, C.-C., and Wu, J.-Y. (2009). A novel mechanism for GABA synthesis and packaging into synaptic vesicles. Neurochem. Int. *55*, 9–12.

Bush, P.C., and Sejnowski, T.J. (1994). Effects of inhibition and dendritic saturation in simulated neocortical pyramidal cells. J. Neurophysiol. *71*, 2183–2193.

Butko, M.T., Savas, J.N., Friedman, B., Delahunty, C., Ebner, F., Yates, J.R., and Tsien, R.Y. (2013). In vivo quantitative proteomics of somatosensory cortical synapses shows which protein levels are modulated by sensory deprivation. Proc. Natl. Acad. Sci. *110*, E726–E735.

Caldeira, M.V., Melo, C.V., Pereira, D.B., Carvalho, R., Correia, S.S., Backos, D.S., Carvalho, A.L., Esteban, J.A., and Duarte, C.B. (2007a). Brain-derived neurotrophic factor regulates the expression and synaptic delivery of alpha-amino-3-hydroxy-5-methyl-4-isoxazole propionic acid receptor subunits in hippocampal neurons. J. Biol. Chem. *282*, 12619–12628.

Caldeira, M.V., Melo, C.V., Pereira, D.B., Carvalho, R.F., Carvalho, A.L., and Duarte, C.B. (2007b). BDNF regulates the expression and traffic of NMDA receptors in cultured hippocampal neurons. Mol. Cell. Neurosci. *35*, 208–219.

Canals, J.M., Pineda, J.R., Torres-Peraza, J.F., Bosch, M., Martín-Ibañez, R., Muñoz, M.T., Mengod, G., Ernfors, P., and Alberch, J. (2004). Brain-derived neurotrophic factor regulates the onset and severity of motor dysfunction associated with enkephalinergic neuronal degeneration in Huntington's disease. J. Neurosci. Off. J. Soc. Neurosci. *24*, 7727–7739.

Carmignoto, G., Pizzorusso, T., Tia, S., and Vicini, S. (1997). Brain-derived neurotrophic factor and nerve growth factor potentiate excitatory synaptic transmission in the rat visual cortex. J. Physiol. *498*, 153–164.

Carnevale, N.T., and Hines, M.L. (2006). The NEURON book (Cambridge: Cambridge University Press).

Carvalho, A.L., Caldeira, M.V., Santos, S.D., and Duarte, C.B. (2008). Role of the brain-derived neurotrophic factor at glutamatergic synapses. Br. J. Pharmacol. *153*, S310–S324.

Castillo, P.E. (2012). Presynaptic LTP and LTD of excitatory and inhibitory synapses. Cold Spring Harb. Perspect. Biol. *4*.

Chang, S., and De Camilli, P. (2001). Glutamate regulates actin-based motility in axonal filopodia. Nat. Neurosci. *4*, 787–793.

Chaudhry, F.A., Reimer, R.J., Bellocchio, E.E., Danbolt, N.C., Osen, K.K., Edwards, R.H., and Storm-Mathisen, J. (1998). The Vesicular GABA Transporter, VGAT, Localizes to Synaptic Vesicles in Sets of Glycinergic as Well as GABAergic Neurons. J. Neurosci. *18*, 9733–9750.

Chiu, C.Q., Lur, G., Morse, T.M., Carnevale, N.T., Ellis-Davies, G.C.R., and Higley, M.J. (2013). Compartmentalization of GABAergic Inhibition by Dendritic Spines. Science *340*, 759–762.

Chowdhury, S., Shepherd, J.D., Okuno, H., Lyford, G., Petralia, R.S., Plath, N., Kuhl, D., Huganir, R.L., and Worley, P.F. (2006). Arc/Arg3.1 interacts with the endocytic machinery to regulate AMPA receptor trafficking. Neuron *52*, 445–459.

Clarke, L.E., and Barres, B.A. (2013). Emerging roles of astrocytes in neural circuit development. Nat. Rev. Neurosci. *14*, 311–321.

Cline, H., and Haas, K. (2008). The regulation of dendritic arbor development and plasticity by glutamatergic synaptic input: a review of the synaptotrophic hypothesis. J. Physiol. *586*, 1509–1517.

Cohen-Cory, S., Kidane, A.H., Shirkey, N.J., and Marshak, S. (2010). Brain-derived neurotrophic factor and the development of structural neuronal connectivity. Dev. Neurobiol. *70*, 271–288.

Colombo, E., Cordiglieri, C., Melli, G., Newcombe, J., Krumbholz, M., Parada, L.F., Medico, E., Hohlfeld, R., Meinl, E., and Farina, C. (2012). Stimulation of the neurotrophin receptor TrkB on astrocytes drives nitric oxide production and neurodegeneration. J. Exp. Med. *209*, 521–535.

Connor, B., Young, D., Yan, Q., Faull, R.L., Synek, B., and Dragunow, M. (1997). Brain-derived neurotrophic factor is reduced in Alzheimer's disease. Brain Res. Mol. Brain Res. *49*, 71–81.

Contractor, A., Mulle, C., and Swanson, G.T. (2011). Kainate receptors coming of age: milestones of two decades of research. Trends Neurosci. *34*, 154–163.

Copits, B.A., and Swanson, G.T. (2012). Dancing partners at the synapse: auxiliary subunits that shape kainate receptor function. Nat. Rev. Neurosci. *13*, 675–686.

Craig, A.M., and Kang, Y. (2007). Neurexin-neuroligin signaling in synapse development. Curr. Opin. Neurobiol. *17*, 43–52.

Dean, C., Scholl, F.G., Choih, J., DeMaria, S., Berger, J., Isacoff, E., and Scheiffele, P. (2003). Neurexin mediates the assembly of presynaptic terminals. Nat. Neurosci. *6*, 708–716.

Dechant, G., and Barde, Y.-A. (2002). The neurotrophin receptor p75(NTR): novel functions and implications for diseases of the nervous system. Nat. Neurosci. *5*, 1131–1136.

DeFelipe, J. (2011). The evolution of the brain, the human nature of cortical circuits, and intellectual creativity. Front. Neuroanat. *5*, 29.

DeFelipe, J. (2013). Chapter 8 - Cajal and the discovery of a new artistic world: The neuronal forest. In Progress in Brain Research, D.W.Z. Stanley Finger, ed. (Elsevier), pp. 201–220.

Desai, N.S., Rutherford, L.C., and Turrigiano, G.G. (1999). BDNF Regulates the Intrinsic Excitability of Cortical Neurons. Learn. Mem. *6*, 284–291.

Dieni, S., Matsumoto, T., Dekkers, M., Rauskolb, S., Ionescu, M.S., Deogracias, R., Gundelfinger, E.D., Kojima, M., Nestel, S., Frotscher, M., et al. (2012). BDNF and its pro-peptide are stored in presynaptic dense core vesicles in brain neurons. J. Cell Biol. *196*, 775–788.

Dijkhuizen, P.A., and Ghosh, A. (2005). BDNF regulates primary dendrite formation in cortical neurons via the PI3-kinase and MAP kinase signaling pathways. J. Neurobiol. *62*, 278–288.

Duman, R.S., and Li, N. (2012). A neurotrophic hypothesis of depression: role of synaptogenesis in the actions of NMDA receptor antagonists. Philos. Trans. R. Soc. B Biol. Sci. *367*, 2475–2484.

Dynes, J.L., and Steward, O. (2012). Arc mRNA docks precisely at the base of individual dendritic spines indicating the existence of a specialized microdomain for synapse-specific mRNA translation. J. Comp. Neurol. *520*, 3105–3119.

Van Elburg, R.A.J., and van Ooyen, A. (2010). Impact of Dendritic Size and Dendritic Topology on Burst Firing in Pyramidal Cells. PLoS Comput Biol *6*, e1000781.

Elmariah, S.B., Crumling, M.A., Parsons, T.D., and Balice-Gordon, R.J. (2004). Postsynaptic TrkB-Mediated Signaling Modulates Excitatory and Inhibitory Neurotransmitter Receptor Clustering at Hippocampal Synapses. J. Neurosci. *24*, 2380–2393.

English, C.N., Vigers, A.J., and Jones, K.R. (2012). Genetic evidence that brain-derived neurotrophic factor mediates competitive interactions between individual cortical neurons. Proc. Natl. Acad. Sci. *109*, 19456–19461.

Fairless, R., Masius, H., Rohlmann, A., Heupel, K., Ahmad, M., Reissner, C., Dresbach, T., and Missler, M. (2008). Polarized Targeting of Neurexins to Synapses Is Regulated by their C-Terminal Sequences. J. Neurosci. *28*, 12969–12981.

Feldmeyer, D., Lübke, J., Silver, R.A., and Sakmann, B. (2002). Synaptic connections between layer 4 spiny neurone- layer 2/3 pyramidal cell pairs in juvenile rat barrel cortex: physiology and anatomy of interlaminar signalling within a cortical column. J. Physiol. *538*, 803–822.

Fenner, B.M. (2012). Truncated TrkB: beyond a dominant negative receptor. Cytokine Growth Factor Rev. *23*, 15–24.

Ferrante, M., Migliore, M., and Ascoli, G.A. (2013). Functional Impact of Dendritic Branch-Point Morphology. J. Neurosci. *33*, 2156–2165.

Ferrini, F., and De Koninck, Y. (2013). Microglia Control Neuronal Network Excitability via BDNF Signalling. Neural Plast. *2013*.

Francks, C., Maegawa, S., Laurén, J., Abrahams, B.S., Velayos-Baeza, A., Medland, S.E., Colella, S., Groszer, M., McAuley, E.Z., Caffrey, T.M., et al. (2007). LRRTM1 on chromosome 2p12 is a maternally suppressed gene that is associated paternally with handedness and schizophrenia. Mol. Psychiatry *12*, 1129–1139, 1057.

Friedman, H.V., Bresler, T., Garner, C.C., and Ziv, N.E. (2000). Assembly of new individual excitatory synapses: time course and temporal order of synaptic molecule recruitment. Neuron *27*, 57–69.

Fritschy, J.-M., Panzanelli, P., and Tyagarajan, S.K. (2012). Molecular and functional heterogeneity of GABAergic synapses. Cell. Mol. Life Sci. *69*, 2485–2499.

Gambazzi, L., Gokce, O., Seredenina, T., Katsyuba, E., Runne, H., Markram, H., Giugliano, M., and Luthi-Carter, R. (2010). Diminished Activity-Dependent Brain-Derived Neurotrophic Factor Expression Underlies Cortical Neuron Microcircuit Hypoconnectivity Resulting from Exposure to Mutant Huntingtin Fragments. J. Pharmacol. Exp. Ther. *335*, 13–22.

Gassmann, M., and Bettler, B. (2012). Regulation of neuronal GABAB receptor functions by subunit composition. Nat. Rev. Neurosci. *13*, 380–394.

Giannone, G., Mondin, M., Grillo-Bosch, D., Tessier, B., Saint-Michel, E., Czöndör, K., Sainlos, M., Choquet, D., and Thoumine, O. (2013). Neurexin-1β binding to neuroligin-1 triggers the preferential recruitment of PSD-95 versus gephyrin through tyrosine phosphorylation of neuroligin-1. Cell Rep. *3*, 1996–2007.

Giorgi, C., Yeo, G.W., Stone, M.E., Katz, D.B., Burge, C., Turrigiano, G., and Moore, M.J. (2007). The EJC factor eIF4AIII modulates synaptic strength and neuronal protein expression. Cell *130*, 179–191.

Glynn, M.W., and McAllister, A.K. (2006). Immunocytochemistry and quantification of protein colocalization in cultured neurons. Nat. Protoc. *1*, 1287–1296.

Gokce, O., Runne, H., Kuhn, A., and Luthi-Carter, R. (2009). Short-Term Striatal Gene Expression Responses to Brain-Derived Neurotrophic Factor Are Dependent on MEK and ERK Activation. PLoS ONE *4*, e5292.

Gomes, R.A., Hampton, C., El-Sabeawy, F., Sabo, S.L., and McAllister, A.K. (2006). The dynamic distribution of TrkB receptors before, during, and after synapse formation between cortical neurons. J. Neurosci. Off. J. Soc. Neurosci. *26*, 11487–11500.

Gorski, J.A., Balogh, S.A., Wehner, J.M., and Jones, K.R. (2003a). Learning deficits in forebrain-restricted brain-derived neurotrophic factor mutant mice. Neuroscience *121*, 341–354.

Gorski, J.A., Zeiler, S.R., Tamowski, S., and Jones, K.R. (2003b). Brain-Derived Neurotrophic Factor Is Required for the Maintenance of Cortical Dendrites. J. Neurosci. *23*, 6856–6865.

Gottmann, K., Mittmann, T., and Lessmann, V. (2009). BDNF signaling in the formation, maturation and plasticity of glutamatergic and GABAergic synapses. Exp. Brain Res. *199*, 203–234.

Graf, E.R., Zhang, X., Jin, S.-X., Linhoff, M.W., and Craig, A.M. (2004). Neurexins induce differentiation of GABA and glutamate postsynaptic specializations via neuroligins. Cell *119*, 1013–1026.

Greer, P.L., and Greenberg, M.E. (2008). From Synapse to Nucleus: Calcium-Dependent Gene Transcription in the Control of Synapse Development and Function. Neuron *59*, 846–860.

Grosshans, D.R., Clayton, D.A., Coultrap, S.J., and Browning, M.D. (2002). LTP leads to rapid surface expression of NMDA but not AMPA receptors in adult rat CA1. Nat. Neurosci. *5*, 27–33.

Gulledge, A.T., Kampa, B.M., and Stuart, G.J. (2005). Synaptic integration in dendritic trees. J. Neurobiol. *64*, 75–90.

Gulyás, A.I., Megías, M., Emri, Z., and Freund, T.F. (1999). Total Number and Ratio of Excitatory and Inhibitory Synapses Converging onto Single Interneurons of Different Types in the CA1 Area of the Rat Hippocampus. J. Neurosci. *19*, 10082–10097.

Guzowski, J.F., Lyford, G.L., Stevenson, G.D., Houston, F.P., McGaugh, J.L., Worley, P.F., and Barnes, C.A. (2000). Inhibition of activity-dependent arc protein expression in the rat hippocampus impairs the maintenance of long-term potentiation and the consolidation of long-term memory. J. Neurosci. Off. J. Soc. Neurosci. *20*, 3993–4001.

Hall, J., Thomas, K.L., and Everitt, B.J. (2000). Rapid and selective induction of BDNF expression in the hippocampus during contextual learning. Nat. Neurosci. *3*, 533–535.

Hariri, A.R., Goldberg, T.E., Mattay, V.S., Kolachana, B.S., Callicott, J.H., Egan, M.F., and Weinberger, D.R. (2003). Brain-derived neurotrophic factor val66met polymorphism affects human memory-related hippocampal activity and predicts memory performance. J. Neurosci. Off. J. Soc. Neurosci. *23*, 6690–6694.

Harnett, M.T., Makara, J.K., Spruston, N., Kath, W.L., and Magee, J.C. (2012). Synaptic amplification by dendritic spines enhances input cooperativity. Nature *491*, 599–602.

Harris, K.M., and Weinberg, R.J. (2012). Ultrastructure of Synapses in the Mammalian Brain. Cold Spring Harb. Perspect. Biol. *4*, a005587.

Hata, Y., Butz, S., and Südhof, T.C. (1996). CASK: a novel dlg/PSD95 homolog with an N-terminal calmodulin-dependent protein kinase domain identified by interaction with neurexins. J. Neurosci. Off. J. Soc. Neurosci. *16*, 2488–2494.

Häusser, M., and Roth, A. (1997). Estimating the time course of the excitatory synaptic conductance in neocortical pyramidal cells using a novel voltage jump method. J. Neurosci. Off. J. Soc. Neurosci. *17*, 7606–7625.

Helmstaedter, M., Sakmann, B., and Feldmeyer, D. (2009). The Relation between Dendritic Geometry, Electrical Excitability, and Axonal Projections of L2/3 Interneurons in Rat Barrel Cortex. Cereb. Cortex *19*, 938–950.

Henneberger, C., Kirischuk, S., and Grantyn, R. (2005). Brain-derived neurotrophic factor modulates GABAergic synaptic transmission by enhancing presynaptic glutamic acid decarboxylase 65 levels,

promoting asynchronous release and reducing the number of activated postsynaptic receptors. Neuroscience *135*, 749–763.

Herculano-Houzel, S. (2011). Not all brains are made the same: new views on brain scaling in evolution. Brain. Behav. Evol. *78*, 22–36.

Hiester, B.G. (2012). Determining the role of Wnt signaling during BDNF-induced cortical neuron growth and dendritic spine formation. Ph.D. University of Colorado at Boulder.

Hiester, B.G., Galati, D.F., Salinas, P.C., and Jones, K.R. (2013). Neurotrophin and Wnt signaling cooperatively regulate dendritic spine formation. Mol. Cell. Neurosci. *56*, 115–127.

Hines, M.L., and Carnevale, N.T. (1997). The NEURON simulation environment. Neural Comput. *9*, 1179–1209.

HODGKIN, A.L., and HUXLEY, A.F. (1952). A quantitative description of membrane current and its application to conduction and excitation in nerve. J. Physiol. *117*, 500–544.

Hong, E.J., McCord, A.E., and Greenberg, M.E. (2008). A biological function for the neuronal activity-dependent component of Bdnf transcription in the development of cortical inhibition. Neuron *60*, 610–624.

Hoopmann, P., Rizzoli, S.O., and Betz, W.J. (2012). Imaging synaptic vesicle recycling by staining and destaining vesicles with FM dyes. Cold Spring Harb. Protoc. *2012*, 77–83.

Horch, H.W., and Katz, L.C. (2002). BDNF release from single cells elicits local dendritic growth in nearby neurons. Nat. Neurosci. *5*, 1177–1184.

Huang, E.J., and Reichardt, L.F. (2003). Trk receptors: roles in neuronal signal transduction. Annu. Rev. Biochem. *72*, 609–642.

Huang, S.-H., Wang, J., Sui, W.-H., Chen, B., Zhang, X.-Y., Yan, J., Geng, Z., and Chen, Z.-Y. (2013). BDNF-dependent recycling facilitates TrkB translocation to postsynaptic density during LTP via a Rab11-dependent pathway. J. Neurosci. Off. J. Soc. Neurosci. *33*, 9214–9230.

Huang, Z.J., Kirkwood, A., Pizzorusso, T., Porciatti, V., Morales, B., Bear, M.F., Maffei, L., and Tonegawa, S. (1999). BDNF regulates the maturation of inhibition and the critical period of plasticity in mouse visual cortex. Cell *98*, 739–755.

Huettner, J.E., and Baughman, R.W. (1986). Primary culture of identified neurons from the visual cortex of postnatal rats. J. Neurosci. *6*, 3044–3060.

Irie, M., Hata, Y., Takeuchi, M., Ichtchenko, K., Toyoda, A., Hirao, K., Takai, Y., Rosahl, T.W., and Südhof, T.C. (1997). Binding of neuroligins to PSD-95. Science *277*, 1511–1515.

Jan, Y.-N., and Jan, L.Y. (2001). Dendrites. Genes Dev. *15*, 2627–2641.

Ji, Y., Lu, Y., Yang, F., Shen, W., Tang, T.T.-T., Feng, L., Duan, S., and Lu, B. (2010). Acute and gradual increases in BDNF concentration elicit distinct signaling and functions in neurons. Nat. Neurosci. *13*, 302–309.

Johnson, J., Tian, N., Caywood, M.S., Reimer, R.J., Edwards, R.H., and Copenhagen, D.R. (2003). Vesicular Neurotransmitter Transporter Expression in Developing Postnatal Rodent Retina: GABA and Glycine Precede Glutamate. J. Neurosci. *23*, 518–529.

Jones, K.R., Fariñas, I., Backus, C., and Reichardt, L.F. (1994). Targeted disruption of the BDNF gene perturbs brain and sensory neuron development but not motor neuron development. Cell *76*, 989–999.

Jong, A.P.H. de, Schmitz, S.K., Toonen, R.F.G., and Verhage, M. (2012). Dendritic position is a major determinant of presynaptic strength. J. Cell Biol. *197*, 327–337.

Jovanovic, J.N., Thomas, P., Kittler, J.T., Smart, T.G., and Moss, S.J. (2004). Brain-Derived Neurotrophic Factor Modulates Fast Synaptic Inhibition by Regulating GABAA Receptor Phosphorylation, Activity, and Cell-Surface Stability. J. Neurosci. *24*, 522–530.

Juge, N., Muroyama, A., Hiasa, M., Omote, H., and Moriyama, Y. (2009). Vesicular Inhibitory Amino Acid Transporter Is a Cl-/ -Aminobutyrate Co-transporter. J. Biol. Chem. *284*, 35073–35078.

Kang, H., and Schuman, E.M. (1995). Long-lasting neurotrophin-induced enhancement of synaptic transmission in the adult hippocampus. Science *267*, 1658–1662.

Kask, M., Pruunsild, P., and Timmusk, T. (2011). Bidirectional transcription from human LRRTM2/CTNNA1 and LRRTM1/CTNNA2 gene loci leads to expression of N-terminally truncated CTNNA1 and CTNNA2 isoforms. Biochem. Biophys. Res. Commun. *411*, 56–61.

Kawashima, T., Okuno, H., Nonaka, M., Adachi-Morishima, A., Kyo, N., Okamura, M., Takemoto-Kimura, S., Worley, P.F., and Bito, H. (2009). Synaptic activity-responsive element in the Arc/Arg3.1 promoter essential for synapse-to-nucleus signaling in activated neurons. Proc. Natl. Acad. Sci. U. S. A. *106*, 316–321.

Kettenmann, H., Kirchhoff, F., and Verkhratsky, A. (2013). Microglia: New Roles for the Synaptic Stripper. Neuron *77*, 10–18.

Klemann, C.J.H.M., and Roubos, E.W. (2011). The gray area between synapse structure and function-Gray's synapse types I and II revisited. Synapse *65*, 1222–1230.

Ko, J., Soler-Llavina, G.J., Fuccillo, M.V., Malenka, R.C., and Sudhof, T.C. (2011). Neuroligins/LRRTMs prevent activity- and Ca2+/calmodulin-dependent synapse elimination in cultured neurons. J. Cell Biol. *194*, 323–334.

Koch, C., and Segev, I. (1989). Methods in neuronal modeling: from synapses to networks (Cambridge, Mass.: MIT Press).

Koch, C., Poggio, T., and Torre, V. (1983). Nonlinear interactions in a dendritic tree: localization, timing, and role in information processing. Proc. Natl. Acad. Sci. *80*, 2799–2802.

Koehnke, J., Katsamba, P.S., Ahlsen, G., Bahna, F., Vendome, J., Honig, B., Shapiro, L., and Jin, X. (2010). Splice form dependence of beta-neurexin/neuroligin binding interactions. Neuron *67*, 61–74.

Koleske, A.J. (2013). Molecular mechanisms of dendrite stability. Nat. Rev. Neurosci. *14*, 536–550.

Komendantov, A.O., and Ascoli, G.A. (2009). Dendritic Excitability and Neuronal Morphology as Determinants of Synaptic Efficacy. J. Neurophysiol. *101*, 1847–1866.

Korte, M., Carroll, P., Wolf, E., Brem, G., Thoenen, H., and Bonhoeffer, T. (1995). Hippocampal long-term potentiation is impaired in mice lacking brain-derived neurotrophic factor. Proc. Natl. Acad. Sci. *92*, 8856–8860.

Korte, M., Griesbeck, O., Gravel, C., Carroll, P., Staiger, V., Thoenen, H., and Bonhoeffer, T. (1996). Virus-mediated gene transfer into hippocampal CA1 region restores long-term potentiation in brain-derived neurotrophic factor mutant mice. Proc. Natl. Acad. Sci. *93*, 12547–12552.

Krueger, D.D., Tuffy, L.P., Papadopoulos, T., and Brose, N. (2012). The role of neurexins and neuroligins in the formation, maturation, and function of vertebrate synapses. Curr. Opin. Neurobiol. *22*, 412–422.

Kwon, H.-B., Kozorovitskiy, Y., Oh, W.-J., Peixoto, R.T., Akhtar, N., Saulnier, J.L., Gu, C., and Sabatini, B.L. (2012). Neuroligin-1-dependent competition regulates cortical synaptogenesis and synapse number. Nat. Neurosci. *15*, 1667–1674.

Laurén, J., Airaksinen, M.S., Saarma, M., and Timmusk, T. õni. (2003). A novel gene family encoding leucine-rich repeat transmembrane proteins differentially expressed in the nervous system☆☆ Sequence data from this article have been deposited with the DDBJ/EMBL/GenBank Data Libraries under Accession Nos. AY182024 (human LRRTM1), AY182026 (human LRRTM2), AY182028 (human LRRTM3), AY182030 (human LRRTM4), AY182025 (mouse LRRTM1), AY182027 (mouse LRRTM2), AY182029 (mouse LRRTM3), and AY182031 (mouse LRRTM4). Genomics *81*, 411–421.

Lazo, O.M., Gonzalez, A., Ascaño, M., Kuruvilla, R., Couve, A., and Bronfman, F.C. (2013). BDNF Regulates Rab11-Mediated Recycling Endosome Dynamics to Induce Dendritic Branching. J. Neurosci. *33*, 6112–6122.

Leal, G., Comprido, D., and Duarte, C.B. BDNF-induced local protein synthesis and synaptic plasticity. Neuropharmacology.

Lesiak, A., Pelz, C., Ando, H., Zhu, M., Davare, M., Lambert, T.J., Hansen, K.F., Obrietan, K., Appleyard, S.M., Impey, S., et al. (2013). A Genome-Wide Screen of CREB Occupancy Identifies the RhoA Inhibitors Par6C and Rnd3 as Regulators of BDNF-Induced Synaptogenesis. PLoS ONE *8*, e64658.

Levine, E.S., Dreyfus, C.F., Black, I.B., and Plummer, M.R. (1995a). Brain-derived neurotrophic factor rapidly enhances synaptic transmission in hippocampal neurons via postsynaptic tyrosine kinase receptors. Proc. Natl. Acad. Sci. *92*, 8074–8077.

Levine, E.S., Dreyfus, C.F., Black, I.B., and Plummer, M.R. (1995b). Differential effects of NGF and BDNF on voltage-gated calcium currents in embryonic basal forebrain neurons. J. Neurosci. *15*, 3084–3091.

Lin, M.Z., Glenn, J.S., and Tsien, R.Y. (2008). A drug-controllable tag for visualizing newly synthesized proteins in cells and whole animals. Proc. Natl. Acad. Sci. *105*, 7744–7749.

Linhoff, M.W., Laurén, J., Cassidy, R.M., Dobie, F.A., Takahashi, H., Nygaard, H.B., Airaksinen, M.S., Strittmatter, S.M., and Craig, A.M. (2009). An unbiased expression screen for synaptogenic proteins identifies the LRRTM protein family as synaptic organizers. Neuron *61*, 734–749.

Liot, G., Zala, D., Pla, P., Mottet, G., Piel, M., and Saudou, F. (2013). Mutant Huntingtin alters retrograde transport of TrkB receptors in striatal dendrites. J. Neurosci. Off. J. Soc. Neurosci. *33*, 6298–6309.

Liu, G. (2004). Local structural balance and functional interaction of excitatory and inhibitory synapses in hippocampal dendrites. Nat. Neurosci. *7*, 373–379.

Liu, G., Gu, B., He, X.-P., Joshi, R.B., Wackerle, H.D., Rodriguiz, R.M., Wetsel, W.C., and McNamara, J.O. (2013). Transient inhibition of TrkB kinase after status epilepticus prevents development of temporal lobe epilepsy. Neuron *79*, 31–38.

Lohmann, C., Myhr, K.L., and Wong, R.O.L. (2002). Transmitter-evoked local calcium release stabilizes developing dendrites. Nature *418*, 177–181.

London, M., and Häusser, M. (2005). Dendritic Computation. Annu. Rev. Neurosci. *28*, 503–532.

Lu, B., Nagappan, G., Guan, X., Nathan, P.J., and Wren, P. (2013). BDNF-based synaptic repair as a disease-modifying strategy for neurodegenerative diseases. Nat. Rev. Neurosci. *14*, 401–416.

Lyons, M.R., and West, A.E. (2011). Mechanisms of specificity in neuronal activity-regulated gene transcription. Prog. Neurobiol. *94*, 259–295.

Magee, J.C. (2000). Dendritic integration of excitatory synaptic input. Nat. Rev. Neurosci. *1*, 181–190.

Magee, J.C., and Cook, E.P. (2000). Somatic EPSP amplitude is independent of synapse location in hippocampal pyramidal neurons. Nat. Neurosci. *3*, 895–903.

Le Magueresse, C., and Monyer, H. (2013). GABAergic Interneurons Shape the Functional Maturation of the Cortex. Neuron *77*, 388–405.

Mah, W., Ko, J., Nam, J., Han, K., Chung, W.S., and Kim, E. (2010). Selected SALM (synaptic adhesion-like molecule) family proteins regulate synapse formation. J. Neurosci. Off. J. Soc. Neurosci. *30*, 5559–5568.

Mainen, Z.F., and Sejnowski, T.J. (1996). Influence of dendritic structure on firing pattern in model neocortical neurons. Nature *382*, 363–366.

Maisonpierre, P.C., Belluscio, L., Friedman, B., Alderson, R.F., Wiegand, S.J., Furth, M.E., Lindsay, R.M., and Yancopoulos, G.D. (1990). NT-3, BDNF, and NGF in the developing rat nervous system: parallel as well as reciprocal patterns of expression. Neuron *5*, 501–509.

Man, H.-Y. (2011). GluA2-lacking, calcium-permeable AMPA receptors — inducers of plasticity? Curr. Opin. Neurobiol. *21*, 291–298.

Mantilla, C.B., Gransee, H.M., Zhan, W.-Z., and Sieck, G.C. (2013). Motoneuron BDNF/TrkB signaling enhances functional recovery after cervical spinal cord injury. Exp. Neurol. *247*, 101–109.

Marcello, E., Epis, R., Saraceno, C., and Di Luca, M. (2012). Synaptic dysfunction in Alzheimer's disease. Adv. Exp. Med. Biol. *970*, 573–601.

Markram, H., Toledo-Rodriguez, M., Wang, Y., Gupta, A., Silberberg, G., and Wu, C. (2004). Interneurons of the neocortical inhibitory system. Nat. Rev. Neurosci. *5*, 793–807.

Marsden, K.C., Beattie, J.B., Friedenthal, J., and Carroll, R.C. (2007). NMDA Receptor Activation Potentiates Inhibitory Transmission through GABA Receptor-Associated Protein-Dependent Exocytosis of GABAA Receptors. J. Neurosci. *27*, 14326–14337.

Marty, S., Wehrlé, R., and Sotelo, C. (2000). Neuronal Activity and Brain-Derived Neurotrophic Factor Regulate the Density of Inhibitory Synapses in Organotypic Slice Cultures of Postnatal Hippocampus. J. Neurosci. *20*, 8087–8095.

Matsuda, N., Lu, H., Fukata, Y., Noritake, J., Gao, H., Mukherjee, S., Nemoto, T., Fukata, M., and Poo, M.-M. (2009). Differential activity-dependent secretion of brain-derived neurotrophic factor from axon and dendrite. J. Neurosci. Off. J. Soc. Neurosci. *29*, 14185–14198.

McAllister, A.K. (2007). Dynamic Aspects of CNS Synapse Formation. Annu. Rev. Neurosci. *30*, 425–450.

McAllister, A.K., Lo, D.C., and Katz, L.C. (1995). Neurotrophins regulate dendritic growth in developing visual cortex. Neuron *15*, 791–803.

McAllister, A.K., Katz, L.C., and Lo, D.C. (1996). Neurotrophin regulation of cortical dendritic growth requires activity. Neuron *17*, 1057–1064.

Megías, M., Emri, Z., Freund, T.., and Gulyás, A.. (2001). Total number and distribution of inhibitory and excitatory synapses on hippocampal CA1 pyramidal cells. Neuroscience *102*, 527–540.

Melo, C.V., Mele, M., Curcio, M., Comprido, D., Silva, C.G., and Duarte, C.B. (2013). BDNF Regulates the Expression and Distribution of Vesicular Glutamate Transporters in Cultured Hippocampal Neurons. PLoS ONE *8*, e53793.

Mérot, Y., Rétaux, S., and Heng, J.I.-T. (2009). Molecular mechanisms of projection neuron production and maturation in the developing cerebral cortex. Semin. Cell Dev. Biol. *20*, 726–734.

Messaoudi, E., Kanhema, T., Soulé, J., Tiron, A., Dagyte, G., Silva, B. da, and Bramham, C.R. (2007). Sustained Arc/Arg3.1 Synthesis Controls Long-Term Potentiation Consolidation through Regulation of Local Actin Polymerization in the Dentate Gyrus In Vivo. J. Neurosci. *27*, 10445–10455.

Meunier, C., and Lamotte d'Incamps, B. (2008). Extending cable theory to heterogeneous dendrites. Neural Comput. *20*, 1732–1775.

Miles, R., Tóth, K., Gulyás, A.I., Hájos, N., and Freund, T.F. (1996). Differences between Somatic and Dendritic Inhibition in the Hippocampus. Neuron *16*, 815–823.

Minichiello, L. (2009). TrkB signalling pathways in LTP and learning. Nat. Rev. Neurosci. *10*, 850–860.

Missler, M., Zhang, W., Rohlmann, A., Kattenstroth, G., Hammer, R.E., Gottmann, K., and Südhof, T.C. (2003). Alpha-neurexins couple Ca2+ channels to synaptic vesicle exocytosis. Nature *423*, 939–948.

Mizuno, M., Yamada, K., Olariu, A., Nawa, H., and Nabeshima, T. (2000). Involvement of brain-derived neurotrophic factor in spatial memory formation and maintenance in a radial arm maze test in rats. J. Neurosci. Off. J. Soc. Neurosci. *20*, 7116–7121.

Mo, C.-H., Gu, M., and Koch, C. (2004). A learning rule for local synaptic interactions between excitation and shunting inhibition. Neural Comput. *16*, 2507–2532.

Mogi, M., Togari, A., Kondo, T., Mizuno, Y., Komure, O., Kuno, S., Ichinose, H., and Nagatsu, T. (1999). Brain-derived growth factor and nerve growth factor concentrations are decreased in the substantia nigra in Parkinson's disease. Neurosci. Lett. *270*, 45–48.

Molina-Holgado, F., Doherty, P., and Williams, G. (2008). Tandem repeat peptide strategy for the design of neurotrophic factor mimetics. CNS Neurol. Disord. Drug Targets *7*, 110–119.

Nagahara, A.H., and Tuszynski, M.H. (2011). Potential therapeutic uses of BDNF in neurological and psychiatric disorders. Nat. Rev. Drug Discov. *10*, 209–219.

Nagahara, A.H., Merrill, D.A., Coppola, G., Tsukada, S., Schroeder, B.E., Shaked, G.M., Wang, L., Blesch, A., Kim, A., Conner, J.M., et al. (2009). Neuroprotective effects of brain-derived neurotrophic factor in rodent and primate models of Alzheimer's disease. Nat. Med. *15*, 331–337.

Nagappan, G., and Lu, B. (2005). Activity-dependent modulation of the BDNF receptor TrkB: mechanisms and implications. Trends Neurosci. *28*, 464–471.

Nettleton, J.S., and Spain, W.J. (2000). Linear to Supralinear Summation of AMPA-Mediated EPSPs in Neocortical Pyramidal Neurons. J. Neurophysiol. *83*, 3310–3322.

Niswender, C.M., and Conn, P.J. (2010). Metabotropic glutamate receptors: physiology, pharmacology, and disease. Annu. Rev. Pharmacol. Toxicol. *50*, 295–322.

Ohira, K. (2005). A Truncated Tropo-Myosine-Related Kinase B Receptor, T1, Regulates Glial Cell Morphology via Rho GDP Dissociation Inhibitor 1. J. Neurosci. *25*, 1343–1353.

Ollion, J., Cochennec, J., Loll, F., Escudé, C., and Boudier, T. (2013). TANGO: A Generic Tool for High-throughput 3D Image Analysis for Studying Nuclear Organization. Bioinformatics.

Omote, H., Miyaji, T., Juge, N., and Moriyama, Y. (2011). Vesicular neurotransmitter transporter: bioenergetics and regulation of glutamate transport. Biochemistry (Mosc.) *50*, 5558–5565.

Orefice, L.L., Waterhouse, E.G., Partridge, J.G., Lalchandani, R.R., Vicini, S., and Xu, B. (2013). Distinct Roles for Somatically and Dendritically Synthesized Brain-Derived Neurotrophic Factor in Morphogenesis of Dendritic Spines. J. Neurosci. *33*, 11618–11632.

Ori-McKenney, K.M., Jan, L.Y., and Jan, Y.-N. (2012). Golgi outposts shape dendrite morphology by functioning as sites of acentrosomal microtubule nucleation in neurons. Neuron *76*, 921–930.

Paoletti, P., Bellone, C., and Zhou, Q. (2013). NMDA receptor subunit diversity: impact on receptor properties, synaptic plasticity and disease. Nat. Rev. Neurosci. *14*, 383–400.

Paradis, S., Harrar, D.B., Lin, Y., Koon, A.C., Hauser, J.L., Griffith, E.C., Zhu, L., Brass, L.F., Chen, C., and Greenberg, M.E. (2007). An RNAi-Based Approach Identifies Molecules Required for Glutamatergic and GABAergic Synapse Development. Neuron *53*, 217–232.

Park, H., and Poo, M. (2013). Neurotrophin regulation of neural circuit development and function. Nat. Rev. Neurosci. *14*, 7–23.

Patterson, S.L., Abel, T., Deuel, T.A.., Martin, K.C., Rose, J.C., and Kandel, E.R. (1996). Recombinant BDNF Rescues Deficits in Basal Synaptic Transmission and Hippocampal LTP in BDNF Knockout Mice. Neuron *16*, 1137–1145.

Peebles, C.L., Yoo, J., Thwin, M.T., Palop, J.J., Noebels, J.L., and Finkbeiner, S. (2010). Arc regulates spine morphology and maintains network stability in vivo. Proc. Natl. Acad. Sci. *107*, 18173–18178.

Petrini, E.M., Lu, J., Cognet, L., Lounis, B., Ehlers, M.D., and Choquet, D. (2009). Endocytic Trafficking and Recycling Maintain a Pool of Mobile Surface AMPA Receptors Required for Synaptic Potentiation. Neuron *63*, 92–105.

Pezawas, L., Verchinski, B.A., Mattay, V.S., Callicott, J.H., Kolachana, B.S., Straub, R.E., Egan, M.F., Meyer-Lindenberg, A., and Weinberger, D.R. (2004). The brain-derived neurotrophic factor val66met polymorphism and variation in human cortical morphology. J. Neurosci. Off. J. Soc. Neurosci. *24*, 10099–10102.

Picconi, B., Passino, E., Sgobio, C., Bonsi, P., Barone, I., Ghiglieri, V., Pisani, A., Bernardi, G., Ammassari-Teule, M., and Calabresi, P. (2006). Plastic and behavioral abnormalities in experimental Huntington's disease: A crucial role for cholinergic interneurons. Neurobiol. Dis. *22*, 143–152.

Picconi, B., Piccoli, G., and Calabresi, P. (2012). Synaptic dysfunction in Parkinson's disease. Adv. Exp. Med. Biol. *970*, 553–572.

Pilakka-Kanthikeel, S., Atluri, V.S.R., Sagar, V., Saxena, S.K., and Nair, M. (2013). Targeted brain derived neurotropic factors (BDNF) delivery across the blood-brain barrier for neuro-protection using magnetic nano carriers: an in-vitro study. PloS One *8*, e62241.

Plath, N., Ohana, O., Dammermann, B., Errington, M.L., Schmitz, D., Gross, C., Mao, X., Engelsberg, A., Mahlke, C., Welzl, H., et al. (2006). Arc/Arg3.1 is essential for the consolidation of synaptic plasticity and memories. Neuron *52*, 437–444.

Plotkin, J.L., Shen, W., Rafalovich, I., Sebel, L.E., Day, M., Chan, C.S., and Surmeier, D.J. (2013). Regulation of dendritic calcium release in striatal spiny projection neurons. J. Neurophysiol. jn.00422.2013.

Poulopoulos, A., Aramuni, G., Meyer, G., Soykan, T., Hoon, M., Papadopoulos, T., Zhang, M., Paarmann, I., Fuchs, C., Harvey, K., et al. (2009). Neuroligin 2 drives postsynaptic assembly at perisomatic inhibitory synapses through gephyrin and collybistin. Neuron *63*, 628–642.

Prescott, S.A., and Koninck, Y.D. (2003). Gain control of firing rate by shunting inhibition: Roles of synaptic noise and dendritic saturation. Proc. Natl. Acad. Sci. *100*, 2076–2081.

Pruunsild, P., Kazantseva, A., Aid, T., Palm, K., and Timmusk, T. (2007). Dissecting the human BDNF locus: Bidirectional transcription, complex splicing, and multiple promoters. Genomics *90*, 397–406.

Purves, D., Augustine, G.J., Fitzpatrick, D., Katz, L.C., LaMantia, A.-S., McNamara, J.O., and Williams, S.M. (2001). Spinal Cord Circuitry and Locomotion.

Qian, N., and Sejnowski, T.J. (1990). When is an inhibitory synapse effective? Proc. Natl. Acad. Sci. *87*, 8145–8149.

Qu, J., and Myhr, K.L. (2011). The Morphology and Intrinsic Excitability of Developing Mouse Retinal Ganglion Cells. PLoS ONE *6*, e21777.

Rajkowska, G., Hughes, J., Stockmeier, C.A., Javier Miguel-Hidalgo, J., and Maciag, D. (2013). Coverage of blood vessels by astrocytic endfeet is reduced in major depressive disorder. Biol. Psychiatry *73*, 613–621.

Rall, W. (1969). Distributions of potential in cylindrical coordinates and time constants for a membrane cylinder. Biophys. J. *9*, 1509–1541.

Reichelt, A.C., Rodgers, R.J., and Clapcote, S.J. (2012). The role of neurexins in schizophrenia and autistic spectrum disorder. Neuropharmacology *62*, 1519–1526.

Reissner, C., Runkel, F., and Missler, M. (2013). Neurexins. Genome Biol. *14*, 213.

Rizzoli, S.O., and Betz, W.J. (2005). Synaptic vesicle pools. Nat. Rev. Neurosci. *6*, 57–69.

Roth Modeling synapses.

Roxin, A., Brunel, N., Hansel, D., Mongillo, G., and Vreeswijk, C. van (2011). On the Distribution of Firing Rates in Networks of Cortical Neurons. J. Neurosci. *31*, 16217–16226.

Rutherford, L.C., DeWan, A., Lauer, H.M., and Turrigiano, G.G. (1997). Brain-Derived Neurotrophic Factor Mediates the Activity-Dependent Regulation of Inhibition in Neocortical Cultures. J. Neurosci. *17*, 4527–4535.

Rutherford, L.C., Nelson, S.B., and Turrigiano, G.G. (1998). BDNF Has Opposite Effects on the Quantal Amplitude of Pyramidal Neuron and Interneuron Excitatory Synapses. Neuron *21*, 521–530.

Saliba, R.S., Kretschmannova, K., and Moss, S.J. (2012). Activity-dependent phosphorylation of GABAA receptors regulates receptor insertion and tonic current. EMBO J. *31*, 2937–2951.

Sanchez, A.L., Matthews, B.J., Meynard, M.M., Hu, B., Javed, S., and Cohen Cory, S. (2006). BDNF increases synapse density in dendrites of developing tectal neurons in vivo. Dev. Camb. Engl. *133*, 2477–2486.

Scharfman, H.E. (1997). Hyperexcitability in Combined Entorhinal/Hippocampal Slices of Adult Rat After Exposure to Brain-Derived Neurotrophic Factor. J. Neurophysiol. *78*, 1082–1095.

Scheiffele, P., Fan, J., Choih, J., Fetter, R., and Serafini, T. (2000). Neuroligin expressed in nonneuronal cells triggers presynaptic development in contacting axons. Cell *101*, 657–669.

Schikorski, T., and Stevens, C.F. (1997). Quantitative Ultrastructural Analysis of Hippocampal Excitatory Synapses. J. Neurosci. *17*, 5858–5867.

Schmitz, S.K., Hjorth, J.J.J., Joemai, R.M.S., Wijntjes, R., Eijgenraam, S., de Bruijn, P., Georgiou, C., de Jong, A.P.H., van Ooyen, A., Verhage, M., et al. (2011). Automated analysis of neuronal morphology, synapse number and synaptic recruitment. J. Neurosci. Methods *195*, 185–193.

Schratt, G.M., Nigh, E.A., Chen, W.G., Hu, L., and Greenberg, M.E. (2004). BDNF regulates the translation of a select group of mRNAs by a mammalian target of rapamycin-phosphatidylinositol 3-kinase-dependent pathway during neuronal development. J. Neurosci. Off. J. Soc. Neurosci. *24*, 7366–7377.

Segev, I., and London, M. (2000). Untangling dendrites with quantitative models. Science *290*, 744–750.

Sheng, M., and Hoogenraad, C.C. (2007). The Postsynaptic Architecture of Excitatory Synapses: A More Quantitative View. Annu. Rev. Biochem. *76*, 823–847.

Shepherd, J.D., Rumbaugh, G., Wu, J., Chowdhury, S., Plath, N., Kuhl, D., Huganir, R.L., and Worley, P.F. (2006). Arc/Arg3.1 Mediates Homeostatic Synaptic Scaling of AMPA Receptors. Neuron *52*, 475–484.

Sherwood, N.T., and Lo, D.C. (1999). Long-Term Enhancement of Central Synaptic Transmission by Chronic Brain-Derived Neurotrophic Factor Treatment. J. Neurosci. *19*, 7025–7036.

Siddiqui, T.J., Pancaroglu, R., Kang, Y., Rooyakkers, A., and Craig, A.M. (2010). LRRTMs and neuroligins bind neurexins with a differential code to cooperate in glutamate synapse development. J. Neurosci. Off. J. Soc. Neurosci. *30*, 7495–7506.

Sigel, E., and Steinmann, M.E. (2012). Structure, Function, and Modulation of GABAA Receptors. J. Biol. Chem. *287*, 40224–40231.

Simons, M., and Lyons, D.A. (2013). Axonal selection and myelin sheath generation in the central nervous system. Curr. Opin. Cell Biol. *25*, 512–519.

Singh, B., Henneberger, C., Betances, D., Arevalo, M.A., Rodríguez-Tébar, A., Meier, J.C., and Grantyn, R. (2006). Altered Balance of Glutamatergic/GABAergic Synaptic Input and Associated Changes in Dendrite Morphology after BDNF Expression in BDNF-Deficient Hippocampal Neurons. J. Neurosci. *26*, 7189–7200.

Smith, S.L., Smith, I.T., Branco, T., and Häusser, M. (2013). Dendritic spikes enhance stimulus selectivity in cortical neurons in vivo. Nature.

Snider, W.D., and Lichtman, J.W. (1996). Are Neurotrophins Synaptotrophins? Mol. Cell. Neurosci. *7*, 433–442.

Soler-Llavina, G.J., Arstikaitis, P., Morishita, W., Ahmad, M., Südhof, T.C., and Malenka, R.C. (2013). Leucine-rich repeat transmembrane proteins are essential for maintenance of long-term potentiation. Neuron *79*, 439–446.

Soto, F., Bleckert, A., Lewis, R., Kang, Y., Kerschensteiner, D., Craig, A.M., and Wong, R.O. (2011). Coordinated increase in inhibitory and excitatory synapses onto retinal ganglion cells during development. Neural Develop. *6*, 31.

Spruston, N. (2008). Pyramidal neurons: dendritic structure and synaptic integration. Nat. Rev. Neurosci. *9*, 206–221.

Strand, A.D., Baquet, Z.C., Aragaki, A.K., Holmans, P., Yang, L., Cleren, C., Beal, M.F., Jones, L., Kooperberg, C., Olson, J.M., et al. (2007). Expression Profiling of Huntington's Disease Models Suggests That Brain-Derived Neurotrophic Factor Depletion Plays a Major Role in Striatal Degeneration. J. Neurosci. *27*, 11758–11768.

Südhof, T.C. (2008). Neuroligins and neurexins link synaptic function to cognitive disease. Nature *455*, 903–911.

Südhof, T.C. (2012). The Presynaptic Active Zone. Neuron *75*, 11–25.

Tabuchi, K., Blundell, J., Etherton, M.R., Hammer, R.E., Liu, X., Powell, C.M., and Sudhof, T.C. (2007). A Neuroligin-3 Mutation Implicated in Autism Increases Inhibitory Synaptic Transmission in Mice. Science *318*, 71–76.

Takamori, S. (2006). VGLUTs: "Exciting" times for glutamatergic research? Neurosci. Res. *55*, 343–351.

Takamori, S., Holt, M., Stenius, K., Lemke, E.A., Grønborg, M., Riedel, D., Urlaub, H., Schenck, S., Brügger, B., and Ringler, P. (2006). Molecular Anatomy of a Trafficking Organelle. Cell *127*, 831–846.

Takashima, N., Odaka, Y.S., Sakoori, K., Akagi, T., Hashikawa, T., Morimura, N., Yamada, K., and Aruga, J. (2011). Impaired Cognitive Function and Altered Hippocampal Synapse Morphology in Mice Lacking Lrrtm1, a Gene Associated with Schizophrenia. PLoS ONE *6*, e22716.

Tanaka, J., Horiike, Y., Matsuzaki, M., Miyazaki, T., Ellis-Davies, G.C.R., and Kasai, H. (2008). Protein Synthesis and Neurotrophin-Dependent Structural Plasticity of Single Dendritic Spines. Science *319*, 1683–1687.

Tanaka, T., Saito, H., and Matsuki, N. (1997). Inhibition of GABAA Synaptic Responses by Brain-Derived Neurotrophic Factor (BDNF) in Rat Hippocampus. J. Neurosci. *17*, 2959–2966.

Taniguchi, N., Takada, N., Kimura, F., and Tsumoto, T. (2000). Actions of brain-derived neurotrophic factor on evoked and spontaneous EPSCs dissociate with maturation of neurones cultured from rat visual cortex. J. Physiol. *527*, 579–592.

Taniguchi, N., Shinoda, Y., Takei, N., Nawa, H., Ogura, A., and Tominaga-Yoshino, K. (2006). Possible involvement of BDNF release in long-lasting synapse formation induced by repetitive PKA activation. Neurosci. Lett. *406*, 38–42.

Tongiorgi, E. (2008). Activity-dependent expression of brain-derived neurotrophic factor in dendrites: facts and open questions. Neurosci. Res. *61*, 335–346.

Traynelis, S.F., Wollmuth, L.P., McBain, C.J., Menniti, F.S., Vance, K.M., Ogden, K.K., Hansen, K.B., Yuan, H., Myers, S.J., and Dingledine, R. (2010). Glutamate Receptor Ion Channels: Structure, Regulation, and Function. Pharmacol. Rev. *62*, 405–496.

Tsukahara, T., Takeda, M., Shimohama, S., Ohara, O., and Hashimoto, N. (1995). Effects of brain-derived neurotrophic factor on 1-methyl-4-phenyl-1,2,3,6-tetrahydropyridine-induced parkinsonism in monkeys. Neurosurgery *37*, 733–739; discussion 739–741.

Turrigiano, G. (2011). Too Many Cooks? Intrinsic and Synaptic Homeostatic Mechanisms in Cortical Circuit Refinement. Annu. Rev. Neurosci. *34*, 89–103.

Turrigiano, G.G. (2008). The self-tuning neuron: synaptic scaling of excitatory synapses. Cell *135*, 422–435.

Turrigiano, G.G., Leslie, K.R., Desai, N.S., Rutherford, L.C., and Nelson, S.B. (1998). Activity-dependent scaling of quantal amplitude in neocortical neurons. Nature *391*, 892–896.

Tyler, W.J., and Pozzo-Miller, L.D. (2001). BDNF enhances quantal neurotransmitter release and increases the number of docked vesicles at the active zones of hippocampal excitatory synapses. J. Neurosci. Off. J. Soc. Neurosci. *21*, 4249–4258.

Vaka, S.R.K., Murthy, S.N., Balaji, A., and Repka, M.A. (2012). Delivery of brain-derived neurotrophic factor via nose-to-brain pathway. Pharm. Res. *29*, 441–447.

Varoqueaux, F., Aramuni, G., Rawson, R.L., Mohrmann, R., Missler, M., Gottmann, K., Zhang, W., Südhof, T.C., and Brose, N. (2006). Neuroligins determine synapse maturation and function. Neuron *51*, 741–754.

Vaughn, J.E. (1989). Fine structure of synaptogenesis in the vertebrate central nervous system. Synap. N. Y. N *3*, 255–285.

Vicario-Abejón, C., Collin, C., McKay, R.D.G., and Segal, M. (1998). Neurotrophins Induce Formation of Functional Excitatory and Inhibitory Synapses between Cultured Hippocampal Neurons. J. Neurosci. *18*, 7256–7271.

Vigers, A.J., Amin, D.S., Talley-Farnham, T., Gorski, J.A., Xu, B., and Jones, K.R. (2012). Sustained expression of brain-derived neurotrophic factor is required for maintenance of dendritic spines and normal behavior. Neuroscience *212*, 1–18.

Voikar, V., Kulesskaya, N., Laakso, T., Lauren, J., Strittmatter, S.M., and Airaksinen, M.S. (2013). LRRTM1-deficient mice show a rare phenotype of avoiding small enclosures--a tentative mouse model for claustrophobia-like behaviour. Behav. Brain Res. *238*, 69–78.

Wagenaar, D.A., Pine, J., and Potter, S.M. (2006). An extremely rich repertoire of bursting patterns during the development of cortical cultures. BMC Neurosci. *7*, 11.

Waterhouse, E.G., and Xu, B. (2013). The skinny on brain-derived neurotrophic factor: evidence from animal models to GWAS. J. Mol. Med. Berl. Ger.

Waters, J., Schaefer, A., and Sakmann, B. (2005). Backpropagating action potentials in neurones: measurement, mechanisms and potential functions. Prog. Biophys. Mol. Biol. *87*, 145–170.

Weaver, C.M., and Wearne, S.L. (2008). Neuronal Firing Sensitivity to Morphologic and Active Membrane Parameters. PLoS Comput Biol *4*, e11.

Wetmore, C., Olson, L., and Bean, A.J. (1994). Regulation of brain-derived neurotrophic factor (BDNF) expression and release from hippocampal neurons is mediated by non-NMDA type glutamate receptors. J. Neurosci. *14*, 1688–1700.

Wibrand, K., Messaoudi, E., Håvik, B., Steenslid, V., Løvlie, R., Steen, V.M., and Bramham, C.R. (2006). Identification of genes co-upregulated with Arc during BDNF-induced long-term potentiation in adult rat dentate gyrus in vivo. Eur. J. Neurosci. *23*, 1501–1511.

Williams, S.R. (2002). Dependence of EPSP Efficacy on Synapse Location in Neocortical Pyramidal Neurons. Science *295*, 1907–1910.

Wilson, N.R., Kang, J., Hueske, E.V., Leung, T., Varoqui, H., Murnick, J.G., Erickson, J.D., and Liu, G. (2005). Presynaptic Regulation of Quantal Size by the Vesicular Glutamate Transporter VGLUT1. J. Neurosci. *25*, 6221–6234.

Wilson Horch, H., Krüttgen, A., Portbury, S.D., and Katz, L.C. (1999). Destabilization of Cortical Dendrites and Spines by BDNF. Neuron *23*, 353–364.

De Wit, J., Sylwestrak, E., O'Sullivan, M.L., Otto, S., Tiglio, K., Savas, J.N., Yates, J.R., 3rd, Comoletti, D., Taylor, P., and Ghosh, A. (2009). LRRTM2 interacts with Neurexin1 and regulates excitatory synapse formation. Neuron *64*, 799–806.

De Wit, J., Hong, W., Luo, L., and Ghosh, A. (2011). Role of Leucine-Rich Repeat Proteins in the Development and Function of Neural Circuits. Annu. Rev. Cell Dev. Biol. *27*, 697–729.

Wong, A.W., Xiao, J., Kemper, D., Kilpatrick, T.J., and Murray, S.S. (2013). Oligodendroglial Expression of TrkB Independently Regulates Myelination and Progenitor Cell Proliferation. J. Neurosci. *33*, 4947–4957.

Woo, J., Kwon, S.-K., Nam, J., Choi, S., Takahashi, H., Krueger, D., Park, J., Lee, Y., Bae, J.Y., Lee, D., et al. (2013). The adhesion protein IgSF9b is coupled to neuroligin 2 via S-SCAM to promote inhibitory synapse development. J. Cell Biol. *201*, 929–944.

Wuchter, J., Beuter, S., Treindl, F., Herrmann, T., Zeck, G., Templin, M.F., and Volkmer, H. (2012). A Comprehensive Small Interfering RNA Screen Identifies Signaling Pathways Required for Gephyrin Clustering. J. Neurosci. *32*, 14821–14834.

Yamada, M.K., Nakanishi, K., Ohba, S., Nakamura, T., Ikegaya, Y., Nishiyama, N., and Matsuki, N. (2002). Brain-Derived Neurotrophic Factor Promotes the Maturation of GABAergic Mechanisms in Cultured Hippocampal Neurons. J. Neurosci. *22*, 7580–7585.

Yang, Y., and Calakos, N. (2013). Presynaptic long-term plasticity. Front. Synaptic Neurosci. *5*, 8.

Yang, J., Siao, C.-J., Nagappan, G., Marinic, T., Jing, D., McGrath, K., Chen, Z.-Y., Mark, W., Tessarollo, L., Lee, F.S., et al. (2009). Neuronal release of proBDNF. Nat. Neurosci. *12*, 113–115.

Yin, Y., Edelman, G.M., and Vanderklish, P.W. (2002). The brain-derived neurotrophic factor enhances synthesis of Arc in synaptoneurosomes. Proc. Natl. Acad. Sci. *99*, 2368–2373.

Yoshii, A., and Constantine-Paton, M. (2007). BDNF induces transport of PSD-95 to dendrites through PI3K-AKT signaling after NMDA receptor activation. Nat. Neurosci. *10*, 702–711.

Yoshii, A., and Constantine-Paton, M. (2010). Postsynaptic BDNF-TrkB signaling in synapse maturation, plasticity, and disease. Dev. Neurobiol. *70*, 304–322.

Yuste, R., and Bonhoeffer, T. (2004). Genesis of dendritic spines: insights from ultrastructural and imaging studies. Nat. Rev. Neurosci. *5*, 24–34.

Zhou, B., Cai, Q., Xie, Y., and Sheng, Z.-H. (2012). Snapin recruits dynein to BDNF-TrkB signaling endosomes for retrograde axonal transport and is essential for dendrite growth of cortical neurons. Cell Rep. *2*, 42–51.

Zito, K., Scheuss, V., Knott, G., Hill, T., and Svoboda, K. (2009). Rapid functional maturation of nascent dendritic spines. Neuron *61*, 247–258.

Ziv, N.E., and Smith, S.J. (1996). Evidence for a role of dendritic filopodia in synaptogenesis and spine formation. Neuron *17*, 91–102.

Zuccato, C., Ciammola, A., Rigamonti, D., Leavitt, B.R., Goffredo, D., Conti, L., MacDonald, M.E., Friedlander, R.M., Silani, V., Hayden, M.R., et al. (2001). Loss of huntingtin-mediated BDNF gene transcription in Huntington's disease. Science *293*, 493–498.